

Air Force Institute of Technology

AFIT Scholar

Theses and Dissertations

Student Graduate Works

9-2007

Finite Element Analysis of Lamb Waves Acting within a Thin Aluminum Plate

SeJin Han

Follow this and additional works at: <https://scholar.afit.edu/etd>



Part of the [Aerospace Engineering Commons](#)

Recommended Citation

Han, SeJin, "Finite Element Analysis of Lamb Waves Acting within a Thin Aluminum Plate" (2007). *Theses and Dissertations*. 2978.

<https://scholar.afit.edu/etd/2978>

This Thesis is brought to you for free and open access by the Student Graduate Works at AFIT Scholar. It has been accepted for inclusion in Theses and Dissertations by an authorized administrator of AFIT Scholar. For more information, please contact AFIT.ENWL.Repository@us.af.mil.



**FINITE ELEMENT ANALYSIS OF LAMB WAVES
ACTING WITHIN A THIN ALUMINUM PLATE**

THESIS

SeJin Han, Captain, ROKA

AFIT/GAE/ENY/07-S02

**DEPARTMENT OF THE AIR FORCE
AIR UNIVERSITY**

AIR FORCE INSTITUTE OF TECHNOLOGY

Wright-Patterson Air Force Base, Ohio

APPROVED FOR PUBLIC RELEASE; DISTRIBUTION UNLIMITED

The views expressed in this thesis are those of the author and do not reflect the official policy or position of the United States Air Force, Department of Defense, or the United States Government.

AFIT/GAE/ENY/07-S02

**FINITE ELEMENT ANALYSIS OF LAMB WAVES
ACTING WITHIN A THIN ALUMINUM PLATE**

THESIS

Presented to the Faculty

Department of Aeronautical and Astronautical Engineering

Graduate School of Engineering and Management

Air Force Institute of Technology

Air University

Air Education and Training Command

In Partial Fulfillment of the Requirements for the
Degree of Master of Science in Aeronautical Engineering

SeJin Han, BS

Captain, ROKA

September 2007

APPROVED FOR PUBLIC RELEASE; DISTRIBUTION UNLIMITED

**FINITE ELEMENT ANALYSIS OF LAMB WAVES
ACTING WITHIN A THIN ALUMINUM PLATE**

SeJin Han, BS

Captain, ROKA

Approved:

Dr. Anthony N. Palazotto
Chairman

Date

Dr. Charles Leakeas
Committee Member

Date

Maj. Eric Swenson
Committee Member

Date

Abstract

Structural health monitoring (SHM) is an emerging technology that can be used to identify, locate and quantify structural damages before failure. Among SHM techniques, Lamb waves have become widely used since they can cover large areas from one single location. Due to the development of various structural simulation programs, there is increasing interest in whether SHM data obtained from the simulation can be verified by experimentation.

The objective of this thesis is to determine Lamb wave responses using SHM models in ABAQUS CAE (a Finite Element Analysis (FEA) program). These results are then compared to experimental results and theoretical predictions under isothermal and thermal gradient conditions in order to assess the sensitivity of piezo-generated Lamb wave propagation. Simulations of isothermal tests are conducted over a temperature range of 0-190°F with 100kHz and 300kHz excitation signal frequencies. The changes in temperature-dependent material properties are correlated to measurable differences in the response signal's waveform and propagation speed. An analysis of the simulated signal response data demonstrated that elevated temperatures delay wave propagation, although the delays are minimal at the temperatures tested in this study. In addition, a varying temperature gradient ranging from 75°F to 281°F is experimentally developed prior to actuating a pulse. It is observed that a plate bow occurred which indicated a thermal stress build up in the specimen through the thickness prior to a steady state condition. This condition is numerically evaluated and, at specific initial times, varying through the thickness stress that is due to gradual thermal flow is analyzed. Asymmetric thermal stress through the thickness of the thin specimen could possibly create geometric instability due to the development of a bending moment.

Acknowledgements

I would like to thank Dr. Anthony Palazotto for his endless support and dedication in the role of my thesis advisor over the past two years. I have learned many things from him, not least of which is a scholarly attitude. I would also like to acknowledge the members of my committee Dr. Charles Leakeas and Major Eric Swenson, for their valuable insight and feedback. I would also like to thank Steven Olson, Jennifer Andrews, and Robert Brockman for their continual assistance and support and Mark Derriso for his sponsorship. Finally, I thank my mother, my lovely son, and all of my American friends. Their existence and expectations gave me the motivation and impowerment to proceed.

Table of Contents

	Page
ABSTRACT	V
ACKNOWLEDGEMENTS	VI
LIST OF FIGURES	X
LIST OF TABLES	XIII
LIST OF SYMBOLS	XIV
CHAPTER 1 INTRODUCTION	1
1.1 MOTIVATION: STRUCTURAL HEALTH MONITORING	1
<i>1.1.1 Active and Passive SHM</i>	<i>1</i>
<i>1.1.2 Vibration Approach versus Wave Propagation Approach</i>	<i>2</i>
<i>1.1.3 Pitch-Catch and Pulse-Echo Techniques</i>	<i>2</i>
1.2 PIEZOELECTRIC TRANSDUCER	3
1.3 ELASTIC WAVES	4
1.4 PREVIOUS STUDIES	6
<i>1.4.1 Lamb Waves for the Long Range Inspection</i>	<i>6</i>
<i>1.4.2 Lamb Wave Propagation</i>	<i>6</i>
<i>1.4.3 Lamb Wave Scanning Approach</i>	<i>6</i>
<i>1.4.4 Defect Detection Using Guided Waves</i>	<i>7</i>
<i>1.4.5 Efficient Lamb Modes for Detecting Defects</i>	<i>7</i>
<i>1.4.6 Detection of Kissing Bonds by Lamb Waves</i>	<i>7</i>
<i>1.4.7 Temperature Influences on Wave Propagation</i>	<i>7</i>
1.5 RESEARCH OBJECTIVE	8
CHAPTER 2 THEORY	9

2.1 ELASTIC WAVE PROPAGATION	9
2.2 LAMB WAVE IN THE FREE PLATE	11
2.2.1 <i>Solution of the Free Plate Problem by the Method of Potential</i>	12
2.3 PHASE VELOCITY(c_p) AND GROUP VELOCITY(c_g)	19
2.4 LAMB WAVE MODES	22
2.5 THERMAL THEORY	25
2.5.1 <i>Thermal Stress and Expansion</i>	25
2.5.2 <i>Relationship between Temperature and the Wave Phase and Group Velocities</i>	32
CHAPTER 3 MODEL DEVELOPMENT	33
3.1 MODELING	33
3.1.1 <i>Modeling of Specimen I for Isothermal Testing</i>	33
3.1.2 <i>Modeling of Specimen III for Thermal Gradient Testing</i>	34
3.2 MATERIAL PROPERTIES OF 2024-T3 ALUMINUM	38
3.3 DETERMINING ELEMENT EDGE LENGTH (L_e) OF FE MODELS	41
3.4 CALCULATING TIME STEP (Δt)	42
3.5 FIVE AND A HALF CYCLE HANNIN-WINDOW EXCITATION SIGNAL	43
3.6 DETERMINING THE SENSOR RESULTS	47
3.7 CONVERGENCE STUDY	51
CHAPTER 4 RESULTS AND DISCUSSION	52
4.1 ISOTHERMAL TESTING OF THE SPECIMEN I	52
4.1.1 S_0 Response at 100 kHz	52

4.1.2 S_0 Response at 300kHz	60
4.2 THERMAL GRADIENT TESTING OF THE SPECIMEN III	65
4.2.1 S_0 Response Comparison	65
4.2.2 Thermal Stress and Bowing Phenomenon	72
CHAPTER 5 SUMMARY & CONCLUSIONS	80
APPENDIX A: ISOTHERMAL SIMULATION WITHIN ABAQUS CAE	83
APPENDIX B: THERMAL GRADIENT SIMULATION WITHIN ABAQUS CAE	100
APPENDIX C: MATLAB® CODE	128
APPENDIX D: SAMPLES OF THE DATA FILES	139
BIBLIOGRAPHY	143
VITA	145

List of Figures

	Page
FIGURE 1: TRANSVERSE AND LONGITUDINAL WAVES(4).....	10
FIGURE 2: FREE PLATE GEOMETRY.....	11
FIGURE 3: SYMMETRIC AND ASYMMETRIC PARTICLE MOTION ACROSS THE PLATE THICKNESS(10).....	17
FIGURE 4: THEORETICAL GROUP VELOCITY DISPERSION CURVES FOR AN ALUMINUM PLATE(4).....	24
FIGURE 5: LAMB WAVE MODES OF THE RESPONSE.....	24
FIGURE 6: THERMAL STRESS GENERATION DUE TO NONUNIFORM HEATING(25)....	26
FIGURE 7: NONUNIFORM HEATING IN 1-D MODEL.....	26
FIGURE 8: NONUNIFORM HEATING IN 2-D MODEL.....	27
FIGURE 9: DIFFERENT TEMPERATURE OF THE TWO SEGMENTS IN THE MODEL.....	30
FIGURE 10: THERMAL STRESS FIELD, (a) : σ_x , (b) : σ_y THROUGH THE THICKNESS	30
FIGURE 11: PLOT OF σ_x THROUGH THE THICKNESS.....	31
FIGURE 12: PLOT OF σ_y THROUGH THE THICKNESS.....	31
FIGURE 13: ALUMINUM MODULUS OF ELASTICITY VARYING WITH TEMPERATURE	32
FIGURE 14: SCHEMATIC OF THE ALUMINUM SHEET SPECIMEN FOR ISOTHERMAL TESTING.....	34
FIGURE 15: SCHEMATIC OF THE ALUMINUM SHEET SPECIMEN FOR THERMAL GRADIENT TESTING.....	35
FIGURE 16: INFRARED IMAGE(4).....	36

FIGURE 17: SPECIMEN III THERMAL GRADIENT PROFILES USING 10 THERMOCOUPLES.....	37
FIGURE 18: MIL-HDBK-5J(7).....	39
FIGURE 19: 5 ½ CYCLE HANNING-WINDOW EXCITATION SIGNALS AT 100kHz.....	45
FIGURE 20: 5 ½ CYCLE HANNING-WINDOW EXCITATION SIGNALS AT 200kHz.....	45
FIGURE 21: 5 ½ CYCLE HANNING-WINDOW EXCITATION SIGNALS AT 300kHz.....	46
FIGURE 22: 5 ½ CYCLE HANNING-WINDOW EXCITATION SIGNALS AT 500kHz.....	46
FIGURE 23 : MODELING OF THE ACTUATING AND SENSING TRANSDUCERS IN ABAQUS CAE.....	50
FIGURE 24 : COMPARISON OF S_0 RESPONSE IN CONVERGENCE STUDY.....	51
FIGURE 25 : THE EXISTENCE OF THE MAGNETIC NOISE(4).....	54
FIGURE 26: SPECIMEN I S_0 RESPONSE AT 100kHz (0°F).....	55
FIGURE 27: SPECIMEN I S_0 RESPONSE AT 100kHz (25°F).....	56
FIGURE 28: SPECIMEN I S_0 RESPONSE AT 100kHz (50°F)	56
FIGURE 29: SPECIMEN I S_0 RESPONSE AT 100kHz (75°F).....	57
FIGURE 30: SPECIMEN I S_0 RESPONSE AT 100kHz (100°F)	57
FIGURE 31: SPECIMEN I S_0 RESPONSE AT 100kHz (125°F)	58
FIGURE 32: SPECIMEN I S_0 RESPONSE AT 100kHz (150°F)	58
FIGURE 33: SPECIMEN I S_0 RESPONSE AT 100kHz (175°F)	59
FIGURE 34: SPECIMEN I S_0 RESPONSE AT 100kHz (190°F)	59
FIGURE 35: SPECIMEN I S_0 RESPONSE AT 300kHz (0°F)	62
FIGURE 36: SPECIMEN I S_0 RESPONSE AT 300kHz (50°F)	62
FIGURE 37: SPECIMEN I S_0 RESPONSE AT 300kHz (100°F)	63

FIGURE 38: SPECIMEN I S_0 RESPONSE AT 300kHz (125°F)	63
FIGURE 39: SPECIMEN I S_0 RESPONSE AT 300kHz (150°F)	64
FIGURE 40: SPECIMEN I S_0 RESPONSE AT 300kHz (175°F)	64
FIGURE 41: SPECIMEN I S_0 RESPONSE AT 300kHz (190°F)	65
FIGURE 42: SPECIMEN III S_0 RESPONSE COMPARISON(RM vs TG 1) AT 200kHz.....	68
FIGURE 43: SPECIMEN III S_0 RESPONSE COMPARISON(RM vs TG 2) AT 200kHz.....	68
FIGURE 44: SPECIMEN III S_0 RESPONSE COMPARISON(RM vs TG 3) AT 200kHz.....	69
FIGURE 45: SPECIMEN III S_0 RESPONSE COMPARISON(RM vs TG 1) AT 300kHz.....	69
FIGURE 46: SPECIMEN III S_0 RESPONSE COMPARISON(RM vs TG 2) AT 300kHz.....	70
FIGURE 47: SPECIMEN III S_0 RESPONSE COMPARISON(RM vs TG 3) AT 300kHz.....	70
FIGURE 48: SPECIMEN III S_0 RESPONSE COMPARISON(RM vs TG 1) AT 500kHz.....	71
FIGURE 49: SPECIMEN III S_0 RESPONSE COMPARISON(RM vs TG 2) AT 500kHz.....	71
FIGURE 50: SPECIMEN III S_0 RESPONSE COMPARISON(RM vs TG 3) AT 500kHz.....	72
FIGURE 51: HEAT TRANSFER FROM THE HEATING POINTS.....	74
FIGURE 52: TEMPERATURE FUNCTION AT THE HEATING POINTS.....	74
FIGURE 53: HEAT TRANSFER FROM THE ONE HEATING POINT THROUGH THE TIME	77
FIGURE 54: THERMAL STRESS FIELD, (a) : σ_x , (b) : σ_y THROUGH THE THICKNESS	78
FIGURE 55: PLOT OF σ_x THROUGH THE THICKNESS.....	79
FIGURE 56: PLOT OF σ_y THROUGH THE THICKNESS.....	79

List of Tables

	Page
TABLE 1: DIMENSION OF THE ALUMINUM SHEET SPECIMEN FOR ISOTHERMAL TESTING.....	34
TABLE 2: DIMENSION OF THE ALUMINUM SHEET SPECIMEN FOR THERMAL GRADIENT TESTING.....	35
TABLE 3: SPECIMEN III THERMAL GRADIENT PROFILES.....	37
TABLE 4: UNIT CONVERSIONS OF THE BASIC 2024-T3 ALUMINUM PROPERTIES.....	39
TABLE 5: TEMPERATURE DEPENDENT PROPERTIES OF THE 2024-T3 ALUMINUM....	40
TABLE 6: DURATION OF 5.5 CYCLE HANNING-WINDOW EXCITATION SIGNALS.....	44
TABLE 7: FORMATION OF THE EXPERIMENTAL DATA FILE.....	49
TABLE 8: FORMATION OF THE SIMULATED DATA FILE.....	49
TABLE 9: DATA FOR CONVERGENCE STUDY.....	51
TABLE 10: SPECIMEN I TOA OF S_0 RESPONSE AT 100kHz.....	55
TABLE 11: SPECIMEN I TOA OF S_0 RESPONSE AT 300kHz.....	61
TABLE 12: SPECIMEN III TOA OF S_0 RESPONSE.....	67

List of Symbols

Symbol	Explanation
A	Amplitude
A_i	Asymmetric modes
c_g	Group velocity (m/s)
c_L	Longitudinal wave speed (m/s)
c_p	Phase velocity (m/s)
C_p	Specific Heat ($mm^2 / sec^2 \cdot ^\circ C$)
c_T	Transverse wave speed (m/s)
d	Thickness of the plate (mm or in)
E	Young's Modulus, Elastic Modulus (N / mm^2 or psi)
f	Frequency (Hz)
f_i	Applied force (N)
G	Shear Modulus (N / mm^2 or psi)
h	A half thickness of the plate (mm or in)
k	Circular wave number
\tilde{k}	Thermal conductivity ($N / sec \cdot ^\circ C$)
L_e	Element edge length (mm or in)
M	Plane wave Modulus (N / mm^2 or psi)
n_j	Unit normal
p	Parameter

P_i Phase
 q Parameter
 r Radius of a piezoelectric transducer (mm or in)
 S_i Symmetric modes
 t Time (sec)
 T Temperature ($^{\circ}\text{F}$ or $^{\circ}\text{C}$)
 t_i Traction component
 \tilde{T} Period (sec)
 Δt Step time (ns)
 u_i Displacement vector ($u_x = u, u_y = v, u_z = w$)
 x Cartesian coordinate (mm or in)
 y Cartesian coordinate (mm or in)
 z Cartesian coordinate (mm or in)
 α Thermal expansion coefficient ($1/^{\circ}\text{C}$)
 δ_{ij} Kronecker Delta
 ε_{ij} Strain
 λ Lame' constant
 $\tilde{\lambda}$ Wavelength (mm or in)
 μ Lame' constant
 ν Poisson's ratio
 ρ Density ($N \cdot \text{sec}^2 / \text{mm}^4$)
 σ_{ij} Stress (N / mm^2)

ϕ Scalar potential
 Φ Unknown function
 ψ Vector potential
 Ψ Unknown function
 ω Angular frequency

FINITE ELEMENT ANALYSIS OF LAMB WAVES ACTING WITHIN A THIN ALUMINUM PLATE

Chapter 1 Introduction

1.1 Motivation: Structural Health Monitoring

Structural Health Monitoring(SHM) is an emerging technology that can be used to identify, locate and quantify damage in a structural member or system before failure occurs. SHM addresses an urgent need of our aging aircraft infrastructure. The United States spends many billions of dollars every year on the maintenance of plant equipment and facilities. Maintenance and repairs represent about a quarter of the commercial aircraft operating costs. Much of the civilian and military aircraft fleets have exceeded their design life. Some of NASA's space shuttles are more than 20 years old. The mounting costs of maintaining the aging infrastructure can be addressed through SHM systems that reduce scheduled and unscheduled repairs while increasing safety and reliability(10). Therefore, using SHM techniques have a benefit of reducing cost, increasing availability, and maintaining safety of current and future air vehicle systems(22). This chapter discusses several methods that have been incorporated over the past decade in monitoring structural damage. It also describes the features of the use of Lamb waves in SHM.

1.1.1 Active and Passive SHM

There are two types of SHM techniques. These are active and passive techniques. An active technique uses sensors to interrogate the structure in order to detect damage presence, extent, and intensity. Active sensors act upon the structure in much the same way that conventional nondestructive evaluation(NDE) transducers do. Active sensors interact directly with the structure and find its state of health and reliability. However, passive SHM infers the state of the structure using passive sensors(loading, stress, environmental conditions, performance indicators, acoustic

emission from cracks, etc.) that are monitored over time and fed back into a structural model.

Passive SHM only ‘listens’ to the structure but does not interact with it(10).

In this thesis, the active SHM technique is used. The actuator is used to excite the structure while a sensor is used to monitor, collect, and process the response in an effort to provide a prognosis of its condition.

1.1.2 Vibration Approach versus Wave Propagation Approach

A global vibration approach can be used to determine the location and nature of a defect in the structure by detecting a difference in the dynamical behavior of the structure. Changes in the frequency response functions(FRF) of a structure due to the presence of damage indicate the presence of damage. However, when the defects are small compared to the dimensions of the structure, it is not easy to distinguish the differences in the vibration response since they are small. The differences may sometimes be below the noise level. Even though, techniques have been developed to amplify the differences and eliminate noise, effectiveness of using the vibration approach in detecting small defects in complex structures remains uncertain at present. However, the vibration approach is useful to detect widespread or extensive damage(20).

The wave propagation approach is a conventional NDE methodology that has long been used to detect and characterize damage. Unlike the vibration approach, the wave approach is useful to detect and characterize small and hidden defects since the wave length is smaller than the defects(20).

1.1.3 Pitch-Catch and Pulse-Echo Techniques

Ultrasonic NDE techniques are based on the propagation and reflection of elastic waves, with the assumption that damage in the structure alters the behavior of the waves. Typical ultrasonic methods include pitch-catch and pulse-echo techniques.

For pitch-catch techniques, elastic waves are generated using an actuating transducer at one location on the structure, and the response is recorded using a sensing transducer at a different

location. Damage is detected by examining the response. The severity of the damage can be estimated based on the wave attenuation or dispersion. However, to locate the damage, various pairs of pitch-catch transducers may be required.

For pulse-echo techniques, the same transducer used to create the elastic waves is used to measure the response after the transducer has finished exciting the structure. Damage is detected by investigating echoes in the measured response due to wave reflections off damaged regions. The time of flight(TOF) can be used to locate the damage and the amplitude of the reflected signal can be used to assess the severity of the damage(22).

1.2 Piezoelectric Transducer

In the past decade, there has been increasing interest in the fields of sensors that employ ultrasonic Lamb waves. Lamb waves can be excited and detected by a variety of methods. The wedge method is probably the most well known in which a prism or wedge is employed to convert bulk waves into Lamb waves. These conventional ultrasonic NDE techniques, wedge, or comb transducers, have three disadvantages(i.e., They have weak coupling with the structure through a fluid, they are resonant narrowband devices by themselves, and they excite and sense the response indirectly.). Other transduction techniques have also been reported in the literature, including optical methods, electromagnetic acoustic transducers(EMATs), capacitance transducers, and air-coupled transducers. The major advantage of the non-contact techniques lies in the elimination of the coupling materials, which is undesirable or impossible in applications such as the testing of hot metals, or structures where the surface contamination produced by a coupling fluid cannot be tolerated. Recent work using lasers for both generation and detection is potentially very attractive. This laser ultrasonic technique has the advantage of being non-contact and scanned easily and rapidly over the surface of an object, though the required equipment is bulky and expensive and has mainly been used in the laboratory rather than in industrial testing applications. At present, in the majority of standard ultrasonic testing, piezoelectric transducers

remain the most utilized for guided wave excitations, since the manufacture and use of these transducers are well understood, they can overcome the above disadvantages of the conventional transducers, and additionally, the piezoelectric transducers are relatively cheap and light weight(12).

In this thesis, piezoelectric transducers are used for both actuating and sensing Lamb waves. Thin disks made from ceramic material PZT(Piezoceramic Lead Zirconate Titanate) are used as the piezoelectric transducers. When transducers are attached to a test specimen for SHM, a transducer that sends out a wave is commonly referred to as an actuator, while a transducer that receives a wave is referred to as a sensor. Piezoelectric transducers are polarized such that a voltage differential applied across the thickness of the disk causes the radius of the disk to contract or expand. The radial displacement creates an elastic wave within the host material that propagates through a medium and eventually strains a sensor. A gain property relates strain to voltage, thus the resulting compression and expansion of the sensing transducer generate voltage differentials which are recorded as voltage amplitudes over time(4). Formation of the received data is introduced in Table 7 & 8 and Appendix D.

1.3 Elastic Waves

Elastic waves are a primary method of defect detection implemented in the field of SHM. These waves occur as a result of the restoring forces between particles when the material is elastically displaced. When elastic waves are excited in a medium, they transmit changes in stress and velocity inside the material(18). This change in stress and velocity influence the quantitative wave characteristics. These are the frequency, period, phase, wavelength, wave speed, wave number, and amplitude of particle displacement.

Elastic waves consist of either bulk waves or guided waves. Bulk waves travel within the interior of a material away from any boundaries and exhibit a finite number of wave modes. However, guided waves travel on the surface of a material or through the thickness of thin

materials and exhibit an infinite number of wave modes because the waves are dispersive (i.e., the wave speed is a function of frequency). These waves obey the same set of governing equations except guided waves are only affected by boundary conditions. In reality, there is no physical material that doesn't have boundary conditions. Therefore, to find surface or through the thickness damage the guided waves is considered.

Guided waves consist of Rayleigh or Lamb waves. These waves are generated from the coupling between longitudinal and vertical shear waves that are reflected and refracted at the free surfaces of a material. Rayleigh waves are free waves on the surface of a semi-infinite solid. The traction forces must vanish on the surface and the wave amplitude decays into the depth of the solid. Lamb waves are waves of plane strain that occur in a free plate. The traction forces must vanish on both the upper and lower surfaces of the plate. Due to these different characteristics, Rayleigh waves are useful for damage detection of surface cracks in thick structures and Lamb waves are useful for damage detection in plate and shell structures(23).

Guided Lamb Waves

Lamb waves (a.k.a. guided plate waves) are a type of ultrasonic wave that remains guided between two parallel free surfaces, such as the upper and lower surfaces of a plate or shell(10). The initial analysis of elastic wave propagation was carried out in the late 19th and early 20th centuries. Lamb wave theory was first introduced by Horace Lamb in 1917(16). However, the first use of Lamb waves in SHM was introduced by Worlton in 1957(27). More specific theory on Lamb waves is introduced in Chapter 2.

Advantages and Disadvantages of Lamb Waves in SHM

One way to achieve structural interrogation is through ultrasonic waves. Among ultrasonic waves, Lamb waves are particularly advantageous since they can propagate over large distances in plates and shells(13). Active SHM systems using interrogative Lamb waves would be able to cover large areas from one single location. Such systems would be cost-effective and efficient.

Another advantage is that Lamb waves provide through-the-thickness interrogation which allows us to detect internal defects in thin materials(26).

However, there are several disadvantages in using Lamb waves in SHM. These disadvantages are generally due to wave behavior. Dispersive characteristics of Lamb waves and existence of multiple waveforms in single frequency waves are the disadvantages(22). To analyze the response in SHM, these dispersive phenomena should be understood. These characteristics are discussed in Chapter 2.

1.4 Previous Studies

The following summarizes the previous studies dealing with SHM using Lamb wave technology.

1.4.1 Lamb Waves for the Long Range Inspection

Cawley and Alleyne(5) found that Lamb waves can propagate long distances and it is useful for the inspection of large areas. As mentioned before, it allows the development of a cost-effective system. To apply this method successfully, proper excitation of a single mode at a frequency located in a near non-dispersive region is needed. The proper non-dispersive region for a given structure is introduced in Section 2.4.

1.4.2 Lamb Wave Propagation

Derriso et al.(8) studied simple Lamb wave propagation. In their study piezoelectric transducers were used as an actuator and a sensor. Knowing the propagation distance of Lamb waves and the TOF(time of flight), the group velocities of the received signal were calculated and experimental group velocity dispersion curves were generated and compared to theoretical group velocity dispersion curves.

1.4.3 Lamb Wave Scanning Approach

Kundu et al.(15) used Lamb waves for scanning internal defects for composite materials. They used the pitch-catch technique with an immersed actuator and sensor. The pitch-catch

technique is introduced in Section 1.1.3. Their scanning technique is effective in detecting internal defects such as missing fibers and fiber breakage.

1.4.4 Defect Detection using Guided Waves

Lowe et al.(19) investigated the sensitivity of Lamb waves for defects. They also tried to relate proper wave modes to the defect size and strength of wave reflections. Various defects with different sizes and forms were discussed in this research. Lamb modes are discussed in Section 2.4.

1.4.5 Efficient Lamb Modes for Detecting Defects

Ghosh et al.(9) tried to find efficient Lamb modes for particular types of material defects. They propagated Lamb waves in large plates and computed stress fields inside the plate.

1.4.6 Detection of Kissing Bonds by Lamb Waves

Kundu et al.(14) studied the effectiveness of using Lamb waves for the detection of kissing bonds. The kissing bonds are defined as closed cracks under compressive normal stresses. They used A_1 Lamb mode(asymmetric waves to be described subsequently), which proved sensitive to cause excitations in the interface of the crack's surfaces.

1.4.7 Temperature Influences on Wave Propagation

Grisso et al.(11) simulated the effects of a varying temperature on damage detection under the impedance-based SHM approach. Different temperatures change the material properties including the modulus of elasticity and density. Since the wave speed, which is used to determine the location of the defects, depends on the properties, different temperatures affect the localization of structural defects. In their study, the elastic modulus seemed to be significant for changing the wave speed, on the other hand, density was not significant. These relations are shown in Section 2.5.2.

1.5 Research Objective

The objective of this thesis is to determine Lamb wave responses using SHM models in ABAQUS CAE(a Finite Element Analysis(FEA) program). These FEA analytical results are then compared to experimental results and theoretical predictions under isothermal and thermal gradient conditions in order to assess the sensitivity of piezo-generated Lamb wave propagation. Since Andrews(4) theoretically and experimentally dealt with the same conditions present in this thesis, her theoretical and experimental results are used as a comparison.

Simulations of isothermal tests using specimen I (The numbering of the specimen is chosen in Reference(4)) are conducted over a temperature range of 0-190°F with 100kHz and 300kHz excitation signal frequencies. In this test, differences in the response signal's waveform and propagation speed that are due to the changes in temperature-dependent material properties are considered.

Simulations of thermal gradient tests using specimen III are conducted using varying temperature gradients ranging from 75°F to 281°F with 200kHz, 300kHz, and 500kHz excitation signal frequencies. In the experiment, that was conducted by Andrews(4); it was observed that a plate bowed which indicates a thermal stress build up in the specimen in the thickness direction prior to a steady state condition. This condition is numerically evaluated and, at specific times, varying through the thickness stress that is due to gradual thermal flow is analyzed. Also differences in the response signal's waveform and propagation speed that are due to the changes in temperature-dependent material properties are considered.

Chapter 2 Theory

2.1 Elastic Wave Propagation

A wave mode is defined as the manner of particle oscillation during wave propagation. In a solid material, particles can oscillate in four primary modes: as longitudinal waves, shear(transverse) waves, surface waves, and in thin materials as plate waves. These waves occur as a result of the material elastically displacing. Particles are displaced from their equilibrium positions and as a result internal (electrostatic) restoring forces between particles combined with their inertias generate oscillatory motions which can also be referred to as elastic waves.

When shear waves occur, a structure's particles can move in two directions, both of which are perpendicular to the line of propagation. One wave can occur within the plane of the plate, horizontal shear waves, and vertical shear waves can propagate normal to the plate (through the thickness). In contrast, longitudinal waves oscillate in the direction of wave propagation. In this thesis, plate waves are used in the experiments. Plate waves are "complex vibrational waves that travel through the entire thickness of a material" and are commonly referred to as guided Lamb waves. These waves result from the conversion between transverse(T) and longitudinal(L) modes(4).

Since Lamb waves are waves of plane strain that occur in a free plate, only displacements through the thickness(y-direction) and in the direction of wave propagation (x-direction) are taken into consideration. Displacements in the x-direction correspond to longitudinal waves and displacements in the y-direction correspond to vertical shear waves. If the z-direction are considered in Lamb wave propagation, the resulting waves in this direction will be referred to as horizontal shear waves. Similar to vertical shear waves, horizontal shear waves propagate perpendicular to longitudinal waves(4). Figure 1 depicts particle motion in transverse and longitudinal waves. The black lines are the direction of particle motion and the red arrows are the direction of wave propagation(4).

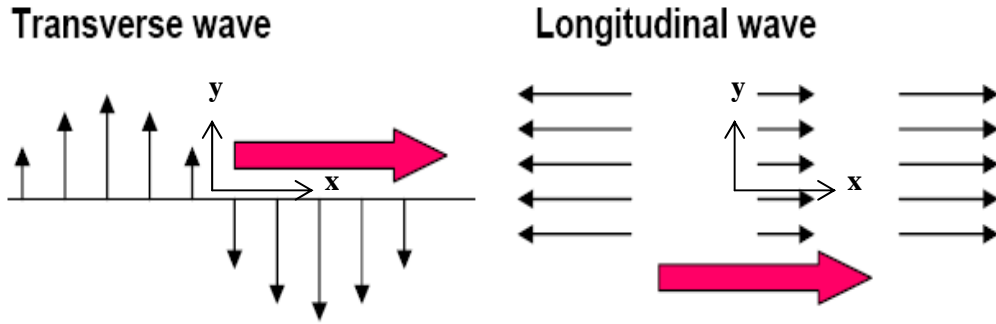


Figure 1: Transverse and Longitudinal Waves(4)

Wave propagation is dependent on the density (ρ) and elastic properties of a medium.

The longitudinal wave speed is characterized by the Young's modulus (E) as follows(4):

$$c_L = \sqrt{\frac{E}{\rho}} \quad 2.1.1$$

Similarly, the transverse(shear) wave speed is characterized by the shear modulus (G) as follows(4):

$$c_T = \sqrt{\frac{G}{\rho}} \quad 2.1.2$$

Since the modulus values for an isotropic material which is used for the free plate are constant in all directions, the previous longitudinal and transverse wave speed equations can be replaced with the Lamé constants (λ and μ). Additionally, the modulus originally used for longitudinal wave speeds has been modified. When the lateral dimension of a medium, that is, of the wave propagating direction, are much greater than the wavelength, which is the case in this problem, the modulus is sometimes referred to as the plane wave Modulus(M)(25). The plane wave modulus is equivalent to $\lambda + 2\mu$ and the shear modulus is equivalent to μ (24:199). The new equations for the longitudinal and transverse wave speeds, along with the plane wave modulus, are as follows(25):

$$c_L = \sqrt{\frac{M}{\rho}} = \sqrt{\frac{\lambda + 2\mu}{\rho}} \quad 2.1.3$$

$$M = \frac{E(1-\nu)}{(1-\nu-2\nu^2)} \quad 2.1.4$$

$$c_T = \sqrt{\frac{G}{\rho}} = \sqrt{\frac{\mu}{\rho}} \quad 2.1.5$$

Where ν is Poisson's ratio. The dependence of the Lamé constants on E and Poisson's ratio, ν , is displayed in the following equations(25):

$$\mu = G = \frac{E}{2(1+\nu)} \quad 2.1.6$$

$$\lambda = \frac{E\nu}{(1+\nu)(1-2\nu)} \quad 2.1.7$$

Recall that as guided waves, Lamb waves are dispersive. At this point, the longitudinal and transverse waves are non-dispersive since their wave speeds are only a function of material properties, not frequency. The dispersive equations(the Rayleigh-Lamb frequency relations) are introduced in the following section.

2.2 Lamb Wave in the Free Plate

In this section, theories and equations, which are corresponding to the Lamb wave propagation in free plate are introduced. Figure 2 shows the free plate which is used in this thesis.

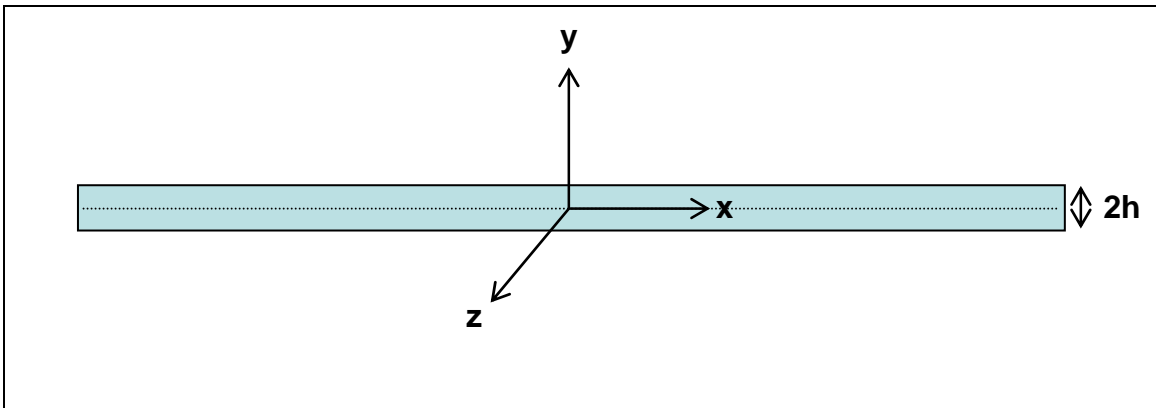


Figure 2: Free Plate Geometry

In order to understand Lamb wave behavior in the free plate, the governing equations need to be considered. First, recall basic elasticity equations using Cartesian tensor notation(23):

$$\sigma_{ij,j} + \rho f_i = \rho \ddot{u}_i \quad \text{yields 3 equations of motion}(i = x, y, z) \quad 2.2.1$$

$$\varepsilon_{ij} = \frac{1}{2}(u_{i,j} + u_{j,i}) \quad \text{6 independent strain displacement equations} \quad 2.2.2$$

$$\sigma_{ij} = \lambda \varepsilon_{kk} \delta_{ij} + 2\mu \varepsilon_{ij} \quad \text{6 independent constitutive equations(isotropic materials)} \quad 2.2.3$$

Equation 2.2.1 and 2.2.2 are valid for any continuous medium and equation 2.2.3 is only valid for isotropic materials. After eliminating the stress and strain terms from equations 2.2.1, 2.2.2 and 2.2.3, the following equations of motion can be derived(23):

$$\mu u_{i,jj} + (\lambda + \mu) u_{j,ji} + \rho f_i = \rho \ddot{u}_i \quad 2.2.4$$

where the Lamé constants are μ and λ , u is displacement, and f is an applied force. Additionally, the subscripts i and j equal x , y , or z . Equation 2.2.4 contains only the particle displacement and describes the governing partial differential equations for displacement. The free plate problem is governed by the equations of motion(equation 2.2.4) and requires the surface traction boundary conditions(23):

$$t_i = \sigma_{ji} n_j \quad 2.2.5$$

The three traction components t_i are prescribed on the boundary with unit normal n (2:56). The surface at the coordinates $y = h$ and $y = -h$ are considered traction free.

2.2.1 Solution of the Free Plate Problem by the Method of Potential

When ultrasonic excitation occurs at some point in the plate, ultrasonic energy from the excitation region encounters the upper and lower bounding surfaces of the plate resulting in mode conversion(L wave to T wave, and vice versa). After some travel in the plate, superposition causes the formation of “wave packets” or what are commonly called guided wave modes in the plate. Based on entry angle and frequency used, how many different modes can be produced in

the plate can be predicted. In what follows, the solution of the free plate problem(i.e., displacement potentials techniques) is introduced.

In the absence of body forces, equation 2.2.4 become as follows(2:65):

$$\mu u_{i,jj} + (\lambda + \mu)u_{j,ji} = \rho \ddot{u}_i \quad 2.2.6$$

In vector notation, equation 2.2.6 can be written as(2:65):

$$\mu \nabla^2 u + (\lambda + \mu) \nabla \nabla \cdot u = \rho \ddot{u} \quad 2.2.7$$

Consider a decomposition of the displacement vector of the form(2:65):

$$u = \nabla \phi + \nabla \wedge \psi \quad 2.2.8$$

where u is a displacement vector, ϕ is a scalar potential, and ψ is a vector potential. Equation is expressed using the Helmholtz decomposition of a vector(2:88). For this plane strain problem, the following conditions hold(2:221):

$$u_z = w \equiv 0, \quad \frac{\partial}{\partial z} (\) \equiv 0 \quad 2.2.9$$

Equation 2.2.8 then reduces to(2:221):

$$u_x = u = \frac{\partial \phi}{\partial x} + \frac{\partial \psi}{\partial y} \quad 2.2.10$$

$$u_y = v = \frac{\partial \phi}{\partial y} - \frac{\partial \psi}{\partial x} \quad 2.2.11$$

For simplicity of notation, the subscript z has been omitted from ψ in equations 2.2.10 and 2.2.11. The relevant components of the stress tensor follow from Hooke's law as(2:221):

$$\sigma_{yx} = \mu \left(\frac{\partial u_y}{\partial x} + \frac{\partial u_x}{\partial y} \right) = \mu \left(2 \frac{\partial^2 \phi}{\partial x \partial y} - \frac{\partial^2 \psi}{\partial x^2} + \frac{\partial^2 \psi}{\partial y^2} \right) \quad 2.2.12$$

$$\sigma_{yy} = \lambda \left(\frac{\partial u_x}{\partial x} + \frac{\partial u_y}{\partial y} \right) + 2\mu \frac{\partial u_y}{\partial y} = \lambda \left(\frac{\partial^2 \phi}{\partial x^2} + \frac{\partial^2 \phi}{\partial y^2} \right) + 2\mu \left(\frac{\partial^2 \phi}{\partial y^2} - \frac{\partial^2 \psi}{\partial x \partial y} \right) \quad 2.2.13$$

Substitution of equation 2.2.8 into equation 2.2.7 yields(2:65):

$$\mu \nabla^2 [\nabla \phi + \nabla \wedge \psi] + (\lambda + \mu) \nabla \nabla \cdot [\nabla \phi + \nabla \wedge \psi] = \rho \frac{\partial^2}{\partial t^2} [\nabla \phi + \nabla \wedge \psi] \quad 2.2.14$$

Since $\nabla \cdot \nabla \phi = \nabla^2 \phi$ and $\nabla \cdot \nabla \wedge \psi = 0$, equation 2.2.14 is rearranged(2:65):

$$\nabla [(\lambda + 2\mu) \nabla^2 \phi - \rho \ddot{\phi}] + \nabla \wedge [\mu \nabla^2 \psi - \rho \ddot{\psi}] = 0 \quad 2.2.15$$

Clearly, equation 2.2.8 satisfies the equation of motion if(2:65):

$$\nabla^2 \phi = \frac{1}{c_L^2} \ddot{\phi} \quad 2.2.16$$

$$\nabla^2 \psi = \frac{1}{c_T^2} \ddot{\psi} \quad 2.2.17$$

where(2:68):

$$\nabla^2 = \frac{\partial^2}{\partial x^2} + \frac{\partial^2}{\partial y^2} + \frac{\partial^2}{\partial z^2} \quad 2.2.18$$

For plane strain equation 2.2.16 and 2.2.17 can be written as follows(23):

$$\frac{\partial^2 \phi}{\partial x^2} + \frac{\partial^2 \phi}{\partial y^2} = \frac{1}{c_L^2} \frac{\partial^2 \phi}{\partial t^2}, \text{ governing longitudinal waves} \quad 2.2.19$$

$$\frac{\partial^2 \psi}{\partial x^2} + \frac{\partial^2 \psi}{\partial y^2} = \frac{1}{c_T^2} \frac{\partial^2 \psi}{\partial t^2}, \text{ governing shear waves} \quad 2.2.20$$

where c_L and c_T are the longitudinal and transverse wave speed in the material, respectively.

Since the time dependence is assumed harmonic in the form $e^{-i\omega t}$, the general solutions to

equation 2.2.19 and 2.2.20(i.e., ϕ and ψ) can be found to take the form(23):

$$\phi = \Phi(y) \exp(ikx - \omega t) \quad 2.2.21$$

$$\psi = \Psi(y) \exp(ikx - \omega t) \quad 2.2.22$$

where ω is the circular frequency of the external pulse applied to the surface and k is a parameter to be determined called the wave number numerically equal to ω/c_p and c_p is the phase velocity to be discussed subsequently. These solutions represent traveling waves in the x-direction and standing waves in the y-direction. This is evident from the fact that there is only an unknown “static” function of y for the y dependency(23). Substitution of these solutions into equations 2.2.19 and 2.2.20 yields equations governing the unknown functions Φ and Ψ . The solutions to these equations are(23):

$$\Phi(y) = A_1 \sin(py) + A_2 \cos(py) \quad 2.2.23$$

$$\Psi(y) = B_1 \sin(qy) + B_2 \cos(qy) \quad 2.2.24$$

where $A_1, A_2, B_1,$ and B_2 are arbitrary constants which can be found from the boundary conditions. The unknown amplitude constants A and B denote longitudinal and shear waves, and subscripts 1 and 2 indicate propagation in the outward and inward directions with respect to the plate, respectively. The parameters p and q can be expressed in terms of the angular frequency(ω), the circular wavenumber(k), and the longitudinal and transverse wave speeds(c_L and c_T)(23:104-107):

$$p^2 = \left(\frac{\omega}{c_L}\right)^2 - k^2 \quad 2.2.25$$

$$q^2 = \left(\frac{\omega}{c_T}\right)^2 - k^2 \quad 2.2.26$$

With these results, the displacements and stresses can be obtained directly from equation 2.2.10 - 2.2.13. Omitting the term $\exp[i(kx - \omega t)]$ in all expressions, the results are as follows(23):

$$u_x = \left[ik\Phi + \frac{d\Psi}{dy} \right] \quad 2.2.27$$

$$u_y = \left[\frac{d\Phi}{dy} - ik\Psi \right] \quad 2.2.28$$

which produces the stress components in the unabridged form.

$$\sigma_{yy} = \left[\lambda \left(-k^2\Phi + \frac{d^2\Phi}{dy^2} \right) + 2\mu \left(\frac{d^2\Phi}{dy^2} - ik \frac{d\Psi}{dy} \right) \right] \quad 2.2.29$$

$$\sigma_{yx} = \mu \left(2ik \frac{d\Phi}{dy} + k^2\Psi + \frac{d^2\Psi}{dy^2} \right) \quad 2.2.30$$

Since the field variables involve sines and cosines with argument y , which are odd(or even for cosines) functions about $y=0$, the solution is split into two sets of modes(i.e., symmetric and asymmetric modes). Specifically, for displacement in the x-direction, the motion will be symmetric with respect to the midplane of the plate if u_x contains cosines but will be asymmetric if u_x contains sines. The opposite is true for displacements in the y-direction. Thus, the modes of wave propagation in the plate are split into two systems(23):

Symmetric modes:

$$\Phi = A_2 \cos(py)$$

$$\Psi = B_1 \sin(qy)$$

$$u = u_x = ikA_2 \cos(py) + qB_1 \cos(qy)$$

$$v = u_y = -pA_2 \sin(py) - ikB_1 \sin(qy) \quad 2.2.31$$

$$\sigma_{yx} = \mu \left[-2ikpA_2 \sin(py) + (k^2 - q^2)B_1 \sin(qy) \right]$$

$$\sigma_{yy} = -\lambda(k^2 + p^2)A_2 \cos(py) - 2\mu \left[p^2 A_2 \cos(py) + ikqB_1 \cos(qy) \right]$$

Asymmetric modes:

$$\Phi = A_1 \sin(py)$$

$$\Psi = B_2 \cos(qy)$$

$$u = u_x = ikA_1 \sin(py) - qB_2 \sin(qy)$$

$$v = u_y = pA_1 \cos(py) - ikB_2 \cos(qy) \quad 2.2.32$$

$$\sigma_{yx} = \mu \left[2ikpA_1 \cos(py) + (k^2 - q^2)B_2 \cos(qy) \right]$$

$$\sigma_{yy} = -\lambda(k^2 + p^2)A_1 \sin(py) - 2\mu \left[p^2 A_1 \sin(py) - ikqB_2 \sin(qy) \right]$$

For the symmetric modes, the wave structure across the thickness of the plate is symmetric for u and asymmetric for v . On the other hand, for asymmetric modes, the wave structure across the thickness is symmetric for v and asymmetric for u . Figure 3 shows the symmetric and asymmetric particle motion across the plate thickness.

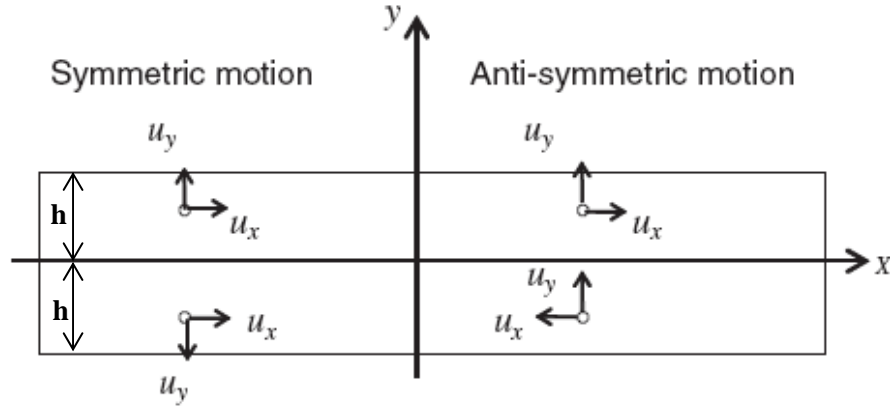


Figure 3: Symmetric and Asymmetric particle motion across the plate thickness(10)

The constants $A_1, A_2, B_1,$ and B_2 are still unknown. They can be determined by applying the traction-free boundary condition for a free plate(23):

$$\sigma_{yx} = \sigma_{yy} \equiv 0 \quad \text{at } y = \pm d/2 = \pm h \quad 2.2.33$$

in the case of plane strain. The resulting displacement, stress, and strain fields depend upon the type of mode. However, applying the boundary conditions will give a homogeneous system of two equations for the appropriate two constants A_2, B_1 for the symmetric case and A_1, B_2 for the

asymmetric case. For homogeneous equations the determinant of the coefficient matrix vanish in order to ensure solutions other than the trivial one. From equation 2.2.33(23):

$$\frac{(k^2 - q^2) \sin(qh)}{2ikp(\sin(ph))} = \frac{-2\mu ikq(\cos(qh))}{(\lambda k^2 + \lambda p^2 + 2\mu p^2) \cos(ph)} \quad \text{for the symmetric modes} \quad 2.2.34$$

$$\frac{(k^2 - q^2) \sin(ph)}{2ikp(\sin(qh))} = \frac{-2\mu ikq(\cos(ph))}{(\lambda k^2 + \lambda p^2 + 2\mu p^2) \cos(qh)} \quad \text{for the asymmetric modes} \quad 2.2.35$$

After some rearranging, equation 2.2.34 is rewritten as(23):

$$\frac{\tan(qh)}{\tan(ph)} = \frac{4k^2 qp\mu}{(\lambda k^2 + \lambda p^2 + 2\mu p^2)(k^2 - q^2)} \quad \text{for the symmetric modes} \quad 2.2.36$$

The denominator on the RHS of equation 2.2.36 can be simplified by using the wave velocities and the definitions of p and q from equation 2.2.25 and 2.2.26. Using equation 2.1.3 to simplify(23):

$$\lambda = c_L^2 \rho - 2\mu \quad 2.2.37$$

Then RHS of equation 2.2.36 will be as follows(23):

$$\begin{aligned} \lambda k^2 + \lambda p^2 + 2\mu p^2 &= \lambda(k^2 + p^2) + 2\mu p^2 \\ &= (c_L^2 \rho - 2\mu)(k^2 + p^2) + 2\mu p^2 = \rho c_L^2(k^2 + p^2) - 2\mu k^2 \end{aligned} \quad 2.2.38$$

Equation 2.2.38 can be rewritten by using equation 2.2.25, 2.2.26 and 2.1.5(23):

$$\begin{aligned} \lambda k^2 + \lambda p^2 + 2\mu p^2 &= \rho \omega^2 - 2\rho c_T^2 k^2 \\ &= \rho c_T^2 \left[\left(\frac{\omega}{c_T} \right)^2 - 2k^2 \right] = \rho c_T^2 (q^2 - k^2) = \mu (q^2 - k^2) \end{aligned} \quad 2.2.39$$

Substituting equation 2.2.39 into an initial form of the dispersion equation 2.2.35, a dispersion equation for symmetric modes is written as(23):

$$\frac{\tan(qh)}{\tan(ph)} = -\frac{4k^2 pq}{(q^2 - k^2)^2} \quad \text{for the symmetric modes} \quad 2.2.40$$

Also, a dispersion equation for asymmetric modes can be shown using equation 2.2.35 by similar procedures as above(23):

$$\frac{\tan(qh)}{\tan(ph)} = -\frac{(q^2 - k^2)^2}{4k^2 pq} \quad \text{for the asymmetric modes} \quad 2.2.41$$

For a given ω and derived k , the displacements can be determined from equation 2.2.31. These equations are known as the Rayleigh-Lamb frequency relations and they can be used to determine the velocity at which a wave of a particular frequency will propagate within the plate. Equations of this nature are known as dispersion relations.

2.3 Phase Velocity(c_p) and Group Velocity(c_g)

There are multiple solutions to equation 2.2.40 and 2.2.41. Since the Lamb waves are dispersive, for each solution, the wave speed, or phase velocity, is a function of frequency. These individual waves interact and the resulting wave propagates at a group velocity which may be different from the individual phase velocities(22). Numerical methods for calculating phase and group velocity dispersion curves are outlined by Rose(23) to solve equation 2.2.40 and 2.2.41.

In this section, the basic concept of the phase velocity and the group velocity is introduced. The phase velocity is the velocity at which a wave of a single frequency propagates. Since the period(\tilde{T}) of the signal is the time in which the signal travels the length of a single wave, the wavelength($\tilde{\lambda}$) divided by the period will be the phase velocity(17):

$$c_p = \frac{\tilde{\lambda}}{\tilde{T}} \quad 2.3.1$$

Since the frequency(f) is the number of repetitions of the signal per second, the period(repetition interval) can be expressed using the frequency(17):

$$\tilde{T} = \frac{1}{f} \quad 2.3.2$$

Using equation 2.3.2, the phase velocity in equation 2.3.1 can be expressed as follows(4):

$$c_p = f \tilde{\lambda} \quad 2.3.3$$

Circular frequency(ω) is expressed as follows(17):

$$\omega = 2\pi f \quad 2.3.4$$

Additionally, the circular wave number(k) is expressed as follows(4):

$$k = \frac{2\pi}{\tilde{\lambda}} \quad 2.3.5$$

Substituting the frequency(f) from equation 2.3.4 and the wavelength($\tilde{\lambda}$) from equation 2.3.5 to the equation 2.3.3 generates new phase velocity equation as follows(4):

$$c_p = \frac{\omega}{k} \quad 2.3.6$$

The group velocity is the propagation velocity of a wave packet. A wave packet is a group of waves that travel together with similar but distinct frequencies and varying wave speeds. As an example, consider an excitation signal that has energy over a range of frequencies. When this excitation pulse is transmitted in a specimen, the propagating wave is actually comprised of several component waves of varying frequencies and phase speeds. If these waves of varying phase speeds are superimposed then the speed of the resulting wave is the group velocity. The group velocity is also referred to as the signal velocity or the velocity at which the energy of a wave packet is conveyed through a structure(4). The group velocity can be defined using a classical approach. Consider a cosine wave with components which compose the wave packet(23:12):

$$u = A \cos(k_i x - \omega_i t) \quad 2.3.7$$

At some time increment $t = t_0 + dt$, the changes in phase of any individual component can be represented as follows(23):

$$dP_i = \{k_i(x_0 + dx) - \omega_i(t_0 + dt)\} - \{k_i x_0 - \omega_0 t\} = k_i dx - \omega_i dt \quad 2.3.8$$

In order for the wave packet to be maintained, the change in phase for all components should be the same as follows(23):

$$dP_j - dP_i = 0 \quad 2.3.9$$

With regard to the phase angle $kx - \omega t$, equation 2.3.9 will be as follows(23):

$$\underbrace{(k_j - k_i)}_{dk} dx - \underbrace{(\omega_j - \omega_i)}_{d\omega} dt = 0 \quad 2.3.10$$

From equation 2.3.10, the group velocity can be expressed as follows(23):

$$\frac{dx}{dt} = \frac{d\omega}{dk} = c_g \Rightarrow \frac{\partial \omega}{\partial k} \quad 2.3.11$$

Where c_g is the group velocity, ω is the circular frequency and k is the circular wave number.

The group velocity also can be related to the phase velocity by substituting k from equation 2.3.6 to equation 2.3.11 as follows(23):

$$c_g = d\omega \left[d \left(\frac{\omega}{c_p} \right) \right]^{-1} = d\omega \left[\frac{d\omega}{c_p} - \omega \frac{dc_p}{c_p^2} \right]^{-1} = c_p^2 \left[c_p - \omega \frac{dc_p}{d\omega} \right]^{-1} \quad 2.3.12$$

Using equation 2.3.4, the group velocity can be written as(23):

$$c_g = c_p^2 \left[c_p - (fd) \frac{dc_p}{d(fd)} \right]^{-1} \quad 2.3.13$$

When the phase velocity or wave speed is independent of frequency, the phase velocity is equivalent to the group velocity. However, in dispersive mediums the phase velocity is dependent on frequency. When the wave speed decreases with frequency, the group velocity is less than the phase velocity. Conversely, when the wave speed increases with frequency the group velocity is greater than the phase velocity. In a dispersive medium, a wave packet generally propagates at a group velocity slower than the phase speed of the original excitation signal(4).

2.4 Lamb Wave Modes

The first goal of this thesis is getting the Lamb wave response from the excitation signal. If the free plate is excited, the excitation will generate the plate waves(guided Lamb waves). As mentioned before, the plate waves are composed of couplings between x and y directed elastic displacements of particles. The x-direction displacement of the particle is called the longitudinal wave and the y-direction displacement of the particle is called the transverse wave. Since, for Lamb waves, the angular frequency is not directly proportional to the wavenumber, dispersion occurs and the waves become distorted as they propagate. Therefore, Lamb waves have various Lamb wave modes. The Lamb wave modes can be categorized by two modes(i.e., symmetric(S_i) and asymmetric(A_i) modes). As shown in Figure 3, motion of the particles is symmetric to the midplane of the plate in symmetric Lamb wave modes. Conversely, motion of the particles is asymmetric to the midplane of the plate in asymmetric Lamb wave modes.

In the received guided Lamb wave response, multiple symmetric and asymmetric Lamb wave modes can exist. The number of coexisting wave modes goes up as the frequency-thickness product increases, as seen in Figure 4. Since the existence of many modes in the response makes the analysis difficult, isolating fundamental modes(i.e., S_0 and A_0) from other modes(i.e., S_1, S_2, S_3, A_1, A_2 and $A_3 \dots$) is recommended. If one wants to trace a particular mode, don't forget, this is very important in studying SHM. To do this, the frequency-thickness product(fd) will be kept below 1.8 MHz-mm. For this frequency-thickness product(fd), the group velocity of the S_0 mode is faster than the group velocity of the A_0 mode. So the S_0 mode is easier to analyze since the A_0 mode can be mixed with reflected waves as shown in Figure 5. Thus, in this thesis, the S_0 mode is analyzed in the response signal.

Also, the thickness of the specimen (free plate) and the frequency of the excitation signal are decided by the restriction of the frequency-thickness product (fd). Using frequencies under 500 kHz and plate thickness of one and 0.6 mm satisfy the isolating criteria (i.e., $fd < 1.8$ MHz-mm).

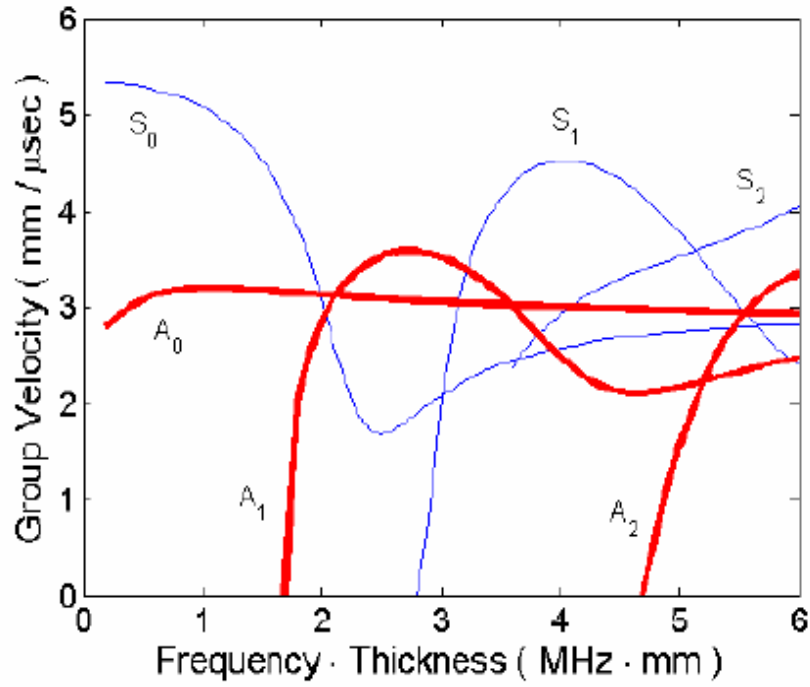


Figure 4: Theoretical Group Velocity Dispersion Curves for an Aluminum Plate(4)

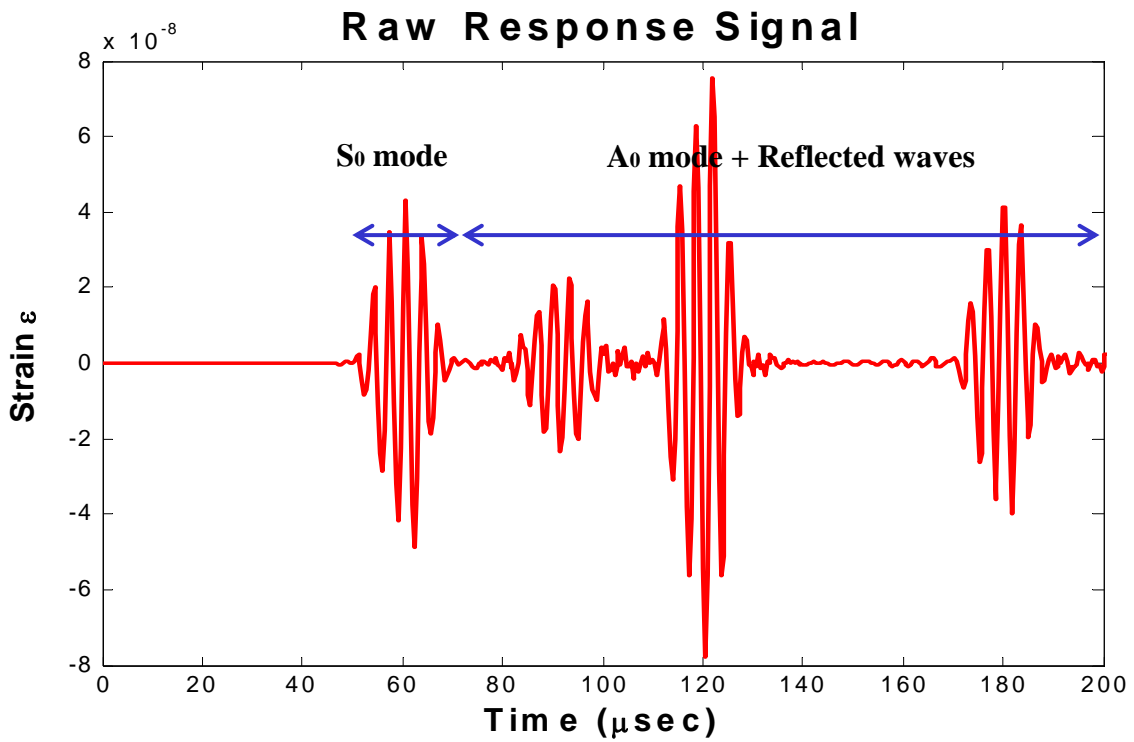


Figure 5: Lamb wave modes of the response

2.5 Thermal Theory

2.5.1 Thermal Stress and Expansion

The purpose of this section is to evaluate a thermal stress due to a thermal gradient imposed on the plate. As mentioned previously, bowing occurs in the experimental study. First, the simple solution to the thermal gradient is to take the temperature to vary along the longitudinal direction of the plate. This is similar to Timoshenko's(25) thermal elastic solution. The bowing phenomenon will be discussed through this section and Section 4.2.2.

The Timoshenko's(25) basic thermal stress theory that is due to a thermal gradient is introduced. One of the causes of stress in a body is non-uniform heating. With rising temperature, the elements of a body expand. However, such an expansion generally can not proceed freely in a continuous body because thermal stresses are set up.

If the specimen(free plate) is non-uniformly heated, as shown in Figure 6 (a), so that the temperature T is a function of the longitudinal coordinate x only, being uniform across any given cross section, then each vertical thin segment of the plate has different amounts of vertical expansion due to the different temperature. However, the vertical expansion can not occur since each vertical segment is attached to one another. This restricted vertical expansion acts as a compressive stress(25):

$$\sigma_y = -\alpha ET \quad 2.5.1$$

at the edges of the each segment. Where α is the thermal expansion coefficient, E is the Young's Modulus, and T is the temperature. The segments fit together as in the unheated plate. To arrive at the thermal stress we must superpose on Figure 6 (a) the stress due to the application of equal and opposite forces(i.e., tension of intensity αET) along the edge of the segment. A normal stress on a straight boundary produces a like normal stress parallel to and at the boundary. Hence, the tension αET produces a tensile stress(αET) in the x -direction considering the equilibrium equations(25). The compressive and tensile stress curves are shown in Figure 6 (b). Near the

edges the prevailing stress is σ_x , a tensile stress of magnitude αET when T is positive, and near the middle the prevailing stress is σ_y , a compressive stress of magnitude αET when T is positive.

The maximum stresses are of magnitude αET_{\max} (25).

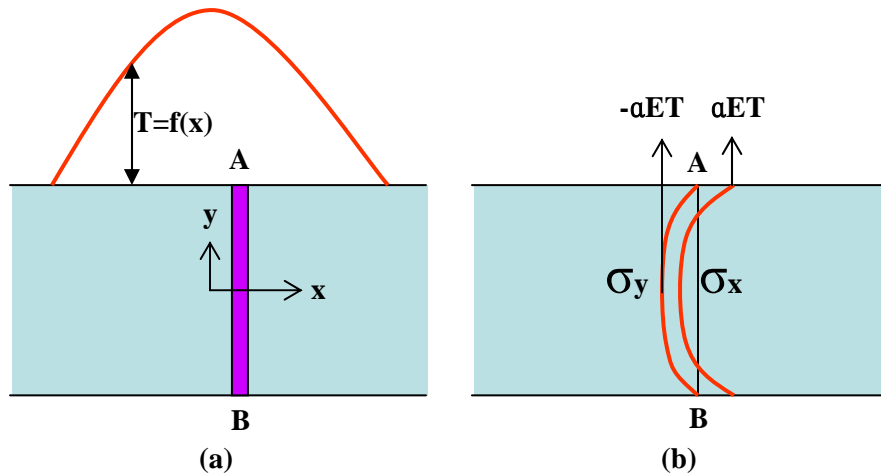


Figure 6: Thermal stress generation due to nonuniform heating(25)

To help understand the relation between thermal expansion and thermal stress, 1-D and 2-D models are introduced as examples. Figure 7 shows the 1-D model which is composed of three elements(i.e., A, B and C). When each element has a different temperature as shown in Figure 7, element A & C have strains of $\alpha T2$ and element B has a strain of $\alpha T1$ in x-direction. In this case, a thermal stress can not be generated since there is no restriction to the expansion that is brought by non-uniform heating in the x-direction. The model is free to expand in x-direction.

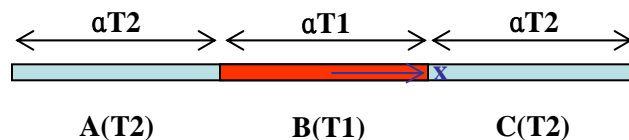


Figure 7: Nonuniform heating in 1-D model

Figure 8 shows the 2-D model which is composed of six elements (i.e., A, B, C, D, E and F). Each element has a different temperature as shown in Figure 8. When expansion in the x-direction is considered as shown in Figure 8 (a), elements A, B and C versus elements D, E and F are compared. Strain of the elements A, B and C is the sum of the αT_1 , αT_2 and αT_1 , and elements D, E and F have the same strain as the neighbor elements. Therefore, there is no restriction of the expansion in the x-direction since they both expand the same amount of distance in the x-direction. As a result, the expansion in the x-direction does not cause a thermal stress. However, when expansion in y-direction is considered as shown in Figure 8 (b), elements A and D versus elements B and E, and elements B and E versus elements C and F are compared. Strains of the elements A and D, and C and F are the sum of the αT_2 and αT_2 .

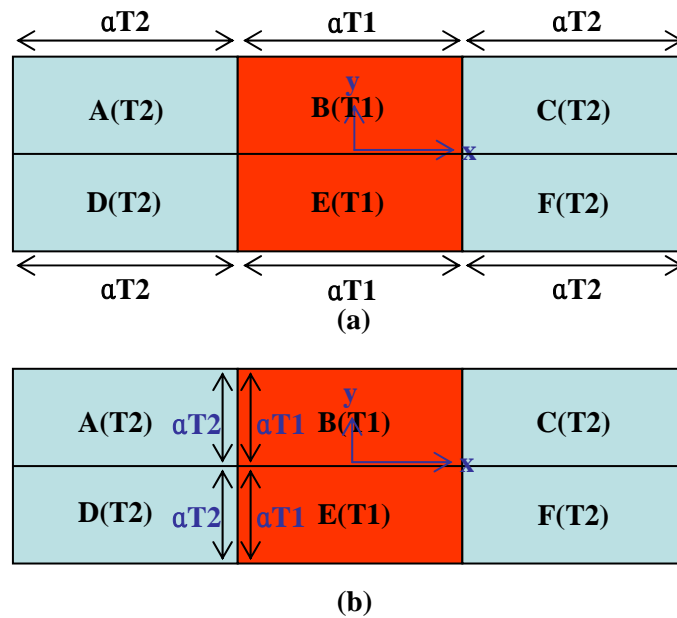


Figure 8: Nonuniform heating in 2-D model

However, a strain of elements B and E is the sum of αT_1 and αT_1 . As mentioned before, different expansions in the continuous medium can not happen since the neighboring elements of the each element act as boundary conditions. As a result, this restriction in the y-direction that is brought

by the boundary conditions at both right and left sides of the B and E elements generates the thermal stress in the model.

Simulation of the Timoshenko(25) Theory

In this section, a thermal gradient model using Timoshenko(25) theory is simulated to verify his thermal stress theory and compare against the thermal stress field of this thesis in Section 4.2.2. The same dimension and element size of specimen III is used for the simulation. The dimensions can be seen in Table 2 while the element size is 0.1mm. Figure 9 shows two segments of the model and these two segments have different temperatures. Each segment in the model has a different uniform temperature and the different temperatures are expressed using different colors. Since the temperature is uniform through the thickness and the temperatures are only varying in the x-direction each segment can be considered as a thin segment A-B in the Figure 6 (a).

During the simulation, a thermal stress field is generated due to the different temperatures of each segment. Figure 10 (a) shows the σ_x stress contours through the thickness, and the stress field values are plotted in Figure 11 with the thickness coordinate shown along the horizontal axis. Figure 10 (b) shows the σ_y stress field through the thickness and the stress field is plotted in Figure 12. In these figures, a few phenomena are observed. First, the symmetric σ_x and σ_y stresses are observed through the thickness. These stress fields look like the stress fields in Figure 6 (b), near the edges the prevailing stress is tensile σ_x , and near the middle the prevailing stress is compressive σ_y . This indicates, in the thermal gradient model that is built using Timoshenko(25) theory, bowing can not occur since the entire model has a symmetric stress field in x and y-direction(i.e., no bending moment). The symmetric stress field in the x-direction is generated since the thermal gradient is symmetric through the x-direction. In order to explain the bowing phenomenon in the thermal gradient test using specimen III a different modeling method

needs to be built. A new modeling technique and the bowing phenomenon are introduced in Section 4.2.2. Second, the thermal stress is focused around the intersection of the two different temperature segments. Since each length of the segment is fairly long, unlike Timoshenko(25) model which is shown in Figure 6 (a), as distance moves far away from the intersection the expansion of the element is less restricted by the neighboring elements. Because the neighbor elements have the same temperature. Thus, one will see a difference in stress as compared with Timoshenko(25), at the top and bottom surfaces($\sigma_y \neq 0$ as Timoshenko indicates). This simulation satisfied the objectives, therefore further simulation for making an exact same stress field like Timoshenko(25) is not conducted.

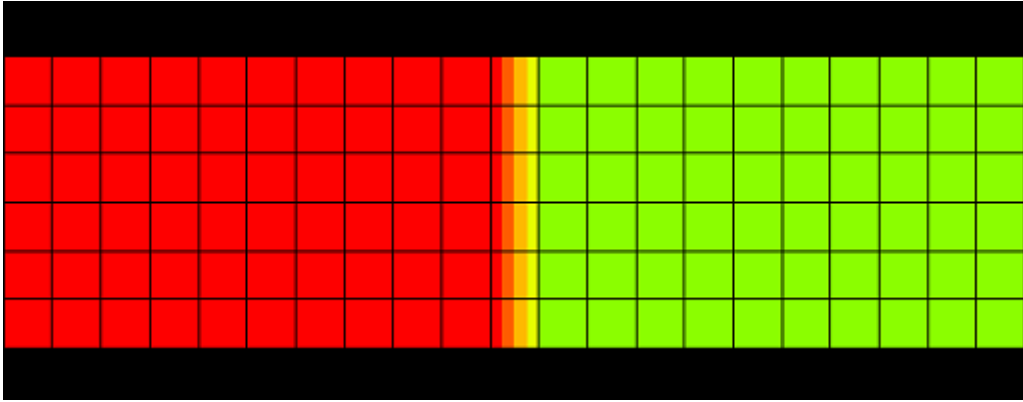
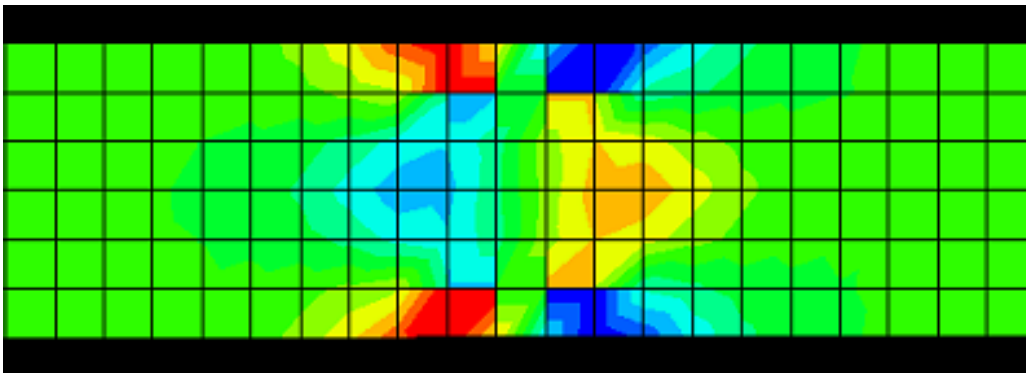
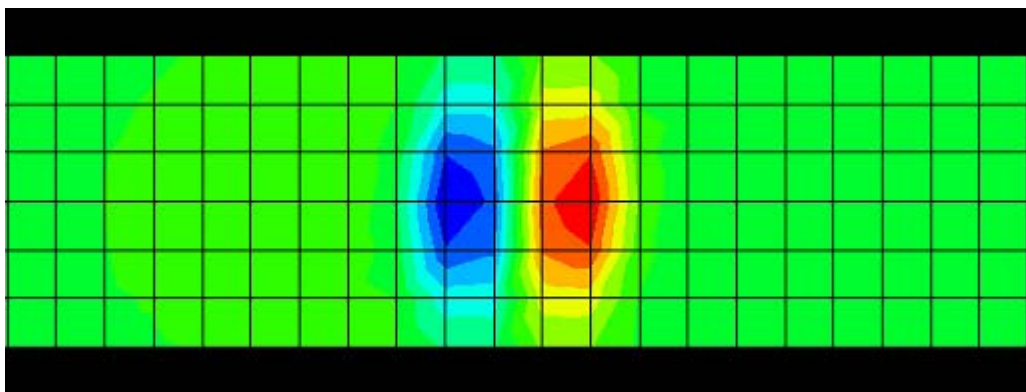


Figure 9: Different temperature of the two segments in the model



(a)



(b)

Figure 10: Thermal stress field, (a) : σ_x , (b) : σ_y through the thickness

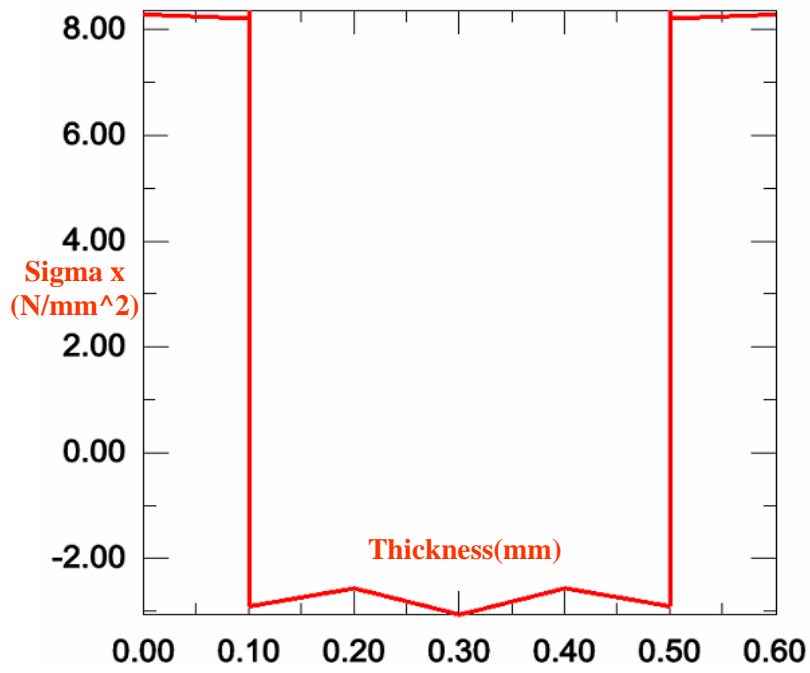


Figure 11: Plot of σ_x through the thickness

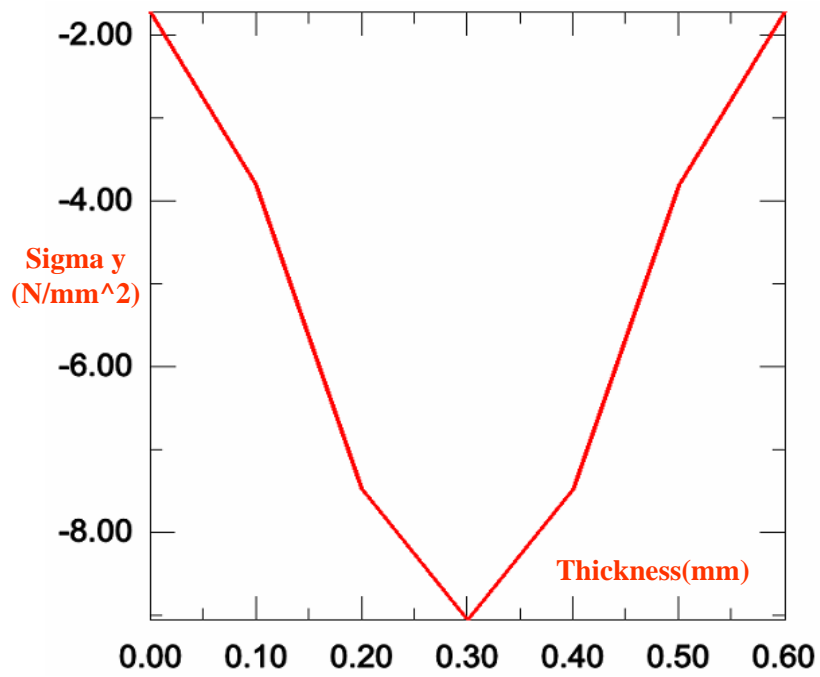


Figure 12: Plot of σ_y through the thickness

2.5.2 Relationship between Temperature and the Wave Phase and Group Velocities

Elevated temperatures decrease the material strength(i.e., Young's Modulus) of an aluminum specimen and reduce the phase and group velocities of traveling waves because the equations of wave speeds are dependent on the material properties. Figure 13(based on an interpolation of values taken from MIL-HDBK-5(7)) shows the relations between the Young's Modulus and the temperature. Numerical data of this curve is shown in Table 5.

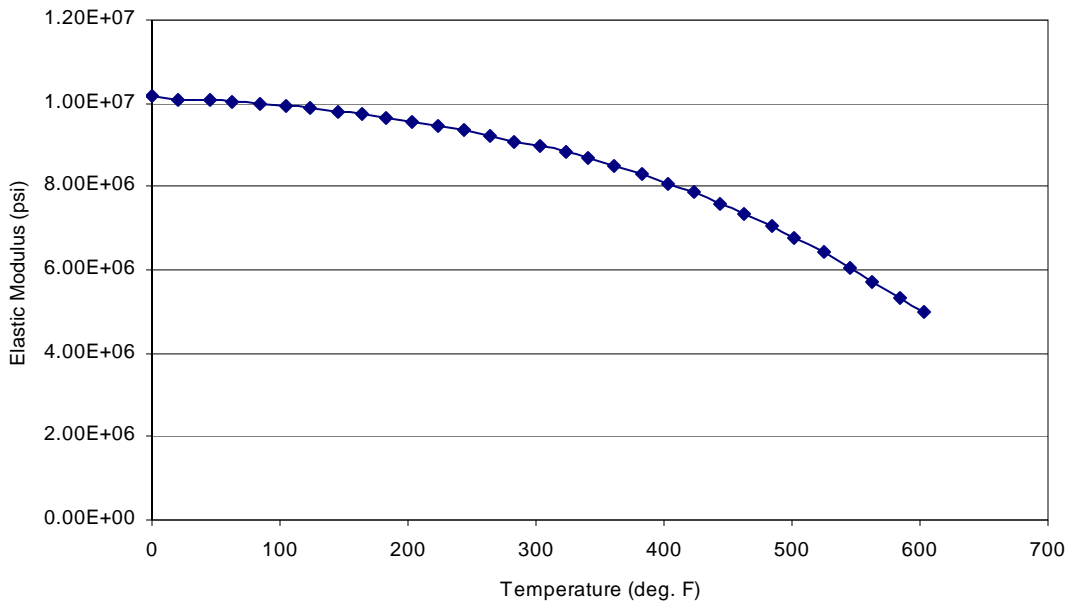


Figure 13: Aluminum Modulus of Elasticity Varying with Temperature

Chapter 3 Model Development

Chapter 3 introduces finite element(FE) model development. Chapter 3.1 presents the Finite Element(FE) modeling of the two specimens that are used for isothermal and thermal gradient tests respectively. Chapter 3.2 presents material properties which are used for the specimens. Chapter 3.3 and 3.4 present element edge length of the model and time step which are used when the specimen is developed in ABAQUS CAE. Chapter 3.5 presents excitation signals which are used for the experiment, ABAQUS simulation, and Matlab theoretical prediction. Chapter 3.6 presents how to determine the received response from simulation. Chapter 3.7 presents convergence study to verify the model development which is developed in this chapter.

3.1 Modeling

3.1.1 Modeling of Specimen I for Isothermal Testing

For the isothermal tests, we use a relatively small specimen as compared to the thermal gradient test since the Micro-Climate Oven, which can produce pre-determined temperatures for the isothermal testing, has size restrictions. Figure 14 shows a schematic of the aluminum sheet specimen used for the simulation of the isothermal test and Table 1 shows its dimensions.

Piezoelectric transducers are used for both the actuator and sensor for the Lamb wave propagation study. These transducers are centered along the width of the plate and placed along the length.

The length of the propagation distance allows time for changes in the signal to occur.

In order to use ABAQUS CAE, the specimen is converted to a 2D plane strain model(z -direction is infinite) as shown in Appendix A. The ideal model for Lamb wave propagation is a thin plate with boundary conditions that eliminate wave reflection. Even though it is impossible to make such the ideal model in real life, our specimen is still adequate because it is sufficiently wide to get the S_0 response before any interruptions from the reflected waves occur.

Table 1: Dimension of the aluminum sheet specimen for isothermal testing

Specimen	Length (mm)	Width (mm)	Thickness (mm)	Propagation Distance (mm)
I	475.9	247.7	1.015	158

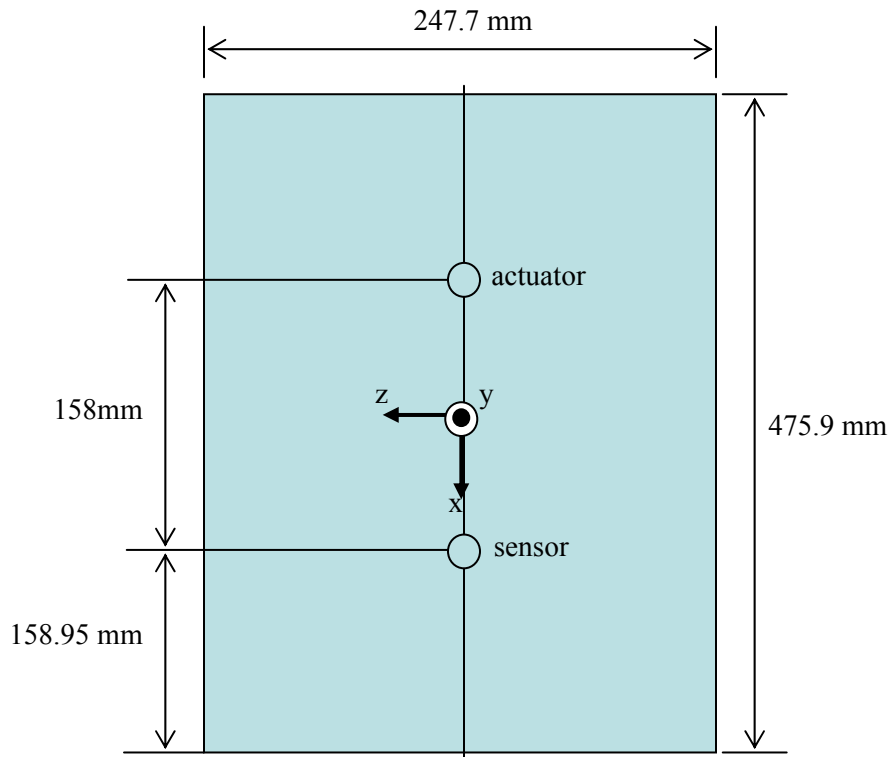


Figure 14: Schematic of the aluminum sheet specimen for isothermal testing

3.1.2 Modeling of Specimen III for Thermal Gradient Testing

Figure 15 and Table 2 show a schematic of the aluminum sheet specimen used for the simulation of the thermal gradient test with its dimensions. In the experiment, for producing a

symmetric thermal gradient condition between actuator and sensor, a 14inch PROTHERM 40 Series Infrared Heater is placed in the middle of the plate.

For the thermal gradient testing a relatively large specimen, as compared to the isothermal test, is used. The use of the larger specimen assures that the transducers are close to room temperature while the center of the specimen is heated to temperatures exceeding 200°F. Additionally, the larger specimen also provides sufficient propagation distance making it easier to analyze the time delay due to the thermal gradient region.

Table 2: Dimension of the aluminum sheet specimen for thermal gradient testing

Specimen	Length (mm)	Width (mm)	Thickness (mm)	Propagation Distance (mm)
III	1217	645.0	0.6345	512

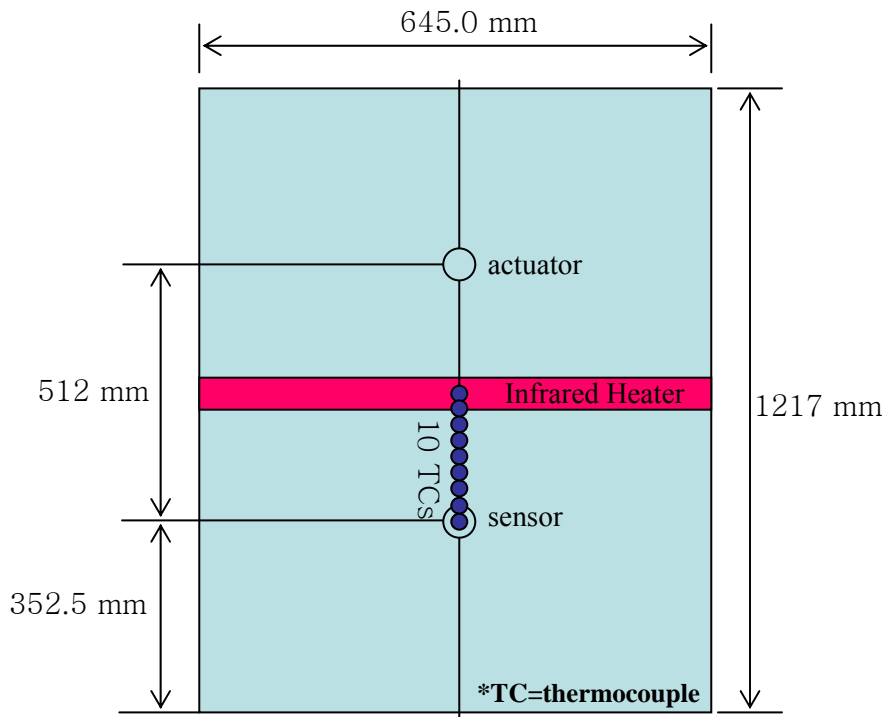


Figure 15: Schematic of the aluminum sheet specimen for thermal gradient testing

In the first thermal gradient experiment, 5 thermocouples(TCs) and a FLIR ThermoCAM P Series Infrared Camera PM695 are used to verify the symmetric thermal gradient field and to check the agreement of the temperature measurement between them. Since results from these experiments show that the thermal gradient is symmetric, capturing the thermal data for at least half of the gradient during testing is sufficient to characterize the entire gradient. In the second thermal gradient experiment, 10 thermocouples(TCs) are used for half of the propagation path of the model as shown in Figure 15(4).

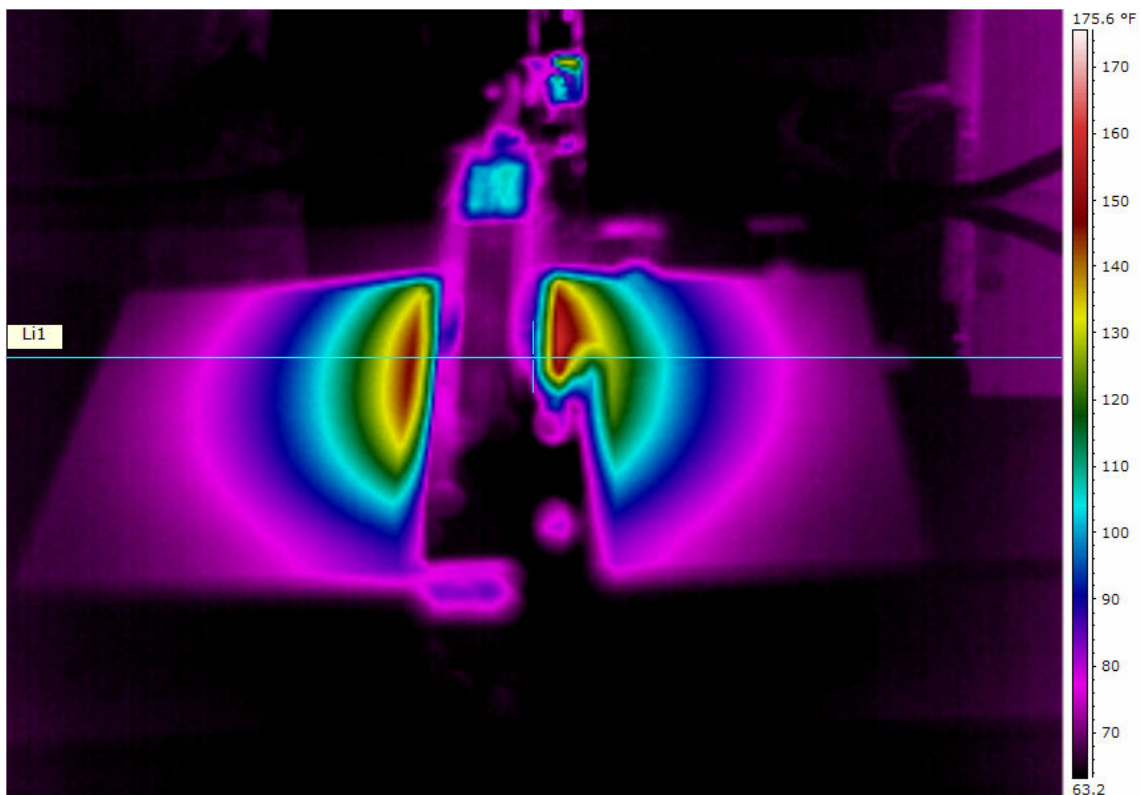


Figure 16: Infrared Image(4)

An image is captured by the Infrared Camera as shown in Figure 16. Since the heat lamp is placed approximately an inch above the center of the plate, in an effort to minimize radiation flow due to the air, the lamp is captured in the images and is the reason why the center of the images appears lower in temperature. In actuality, the midpoint of the plate is the hottest region. The horizontal line depicted in the figure is used to identify the centerline along the specimen since

this line coincides with the propagation path during Lamb wave testing. The temperature range of the gradients depicted in the infrared images is depicted by the color scheme displayed in the legend to the right of the figure(4).

The three thermal gradient data(i.e., TG 1, TG 2, and TG 3) are captured using ten thermocouples in the experiment after an equilibrium condition is reached as shown in Table 3. The 2-D profile is shown in Figure 17.

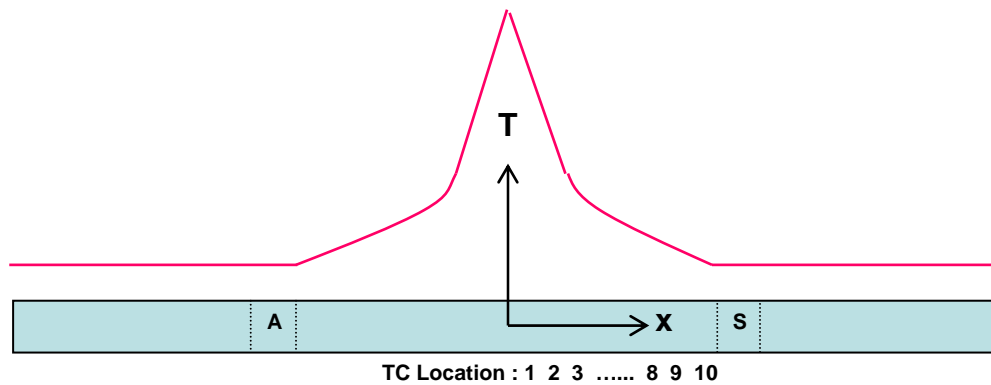


Figure 17: Specimen III Thermal Gradient Profiles Using 10 Thermocouples

Table 3: Specimen III Thermal Gradient Profiles

		Thermocouple Number									
		1	2	3	4	5	6	7	8	9	10
Location(mm)		0	24	47	77	106	136	166	196	226	256
Temp (°F)	RM	75									
	TG 1	281	220	148	123	107	98	91	88	75	75
	TG 2	239	189	142	122	107	99	91	89	75	75
	TG 3	184	153	123	110	100	96	89	88	75	75

3.2 Material Properties of 2024-T3 Aluminum

In this thesis, we assume the properties of the two specimens are the same as 2024-T3 aluminum which is an isotropic material. Temperature dependent properties of the 2024-T3 aluminum are given in Table 5. The Shear Modulus(G) is calculated from Young's Modulus in equation 2.1.6. Table 4 shows unit conversions of the basic 2024-T3 aluminum properties which are used in this study.

To obtain results under a thermal gradient condition, the following thermal properties are needed(i.e., thermal conductivity, specific heat, and thermal expansion coefficient). These properties are referenced in MIL-HDBK-5J(7) which is shown in Figure 18.

This analysis referred to is a heat transfer 2-D analysis with in ABAQUS. For the actual theory behind this series of computations one should look at the ABAQUS theory manual(1).

Table 4: Unit conversions of the basic 2024-T3 aluminum properties

Elastic Modulus(E)	$E = 68.95 \text{ GPa} = 68.95 \times 10^9 \text{ N/m}^2 = 68,947.6 \text{ N/mm}^2 = 9.99 \times 10^6 \text{ psi}$
Shear Modulus(G)	$G = 25.92 \text{ Gpa} = 25.92 \times 10^9 \text{ N/m}^2 = 25,920 \text{ N/mm}^2$
Poisson's ratio (ν)	$\nu = 0.33$
Density (ρ)	$\rho = 2.768 \text{ g/cm}^3 = 2767.8 \text{ kg/m}^3 = 2.7678E-9 \text{ N}\cdot\text{s}^2/\text{mm}^4$
Thermal Conductivity(\tilde{k})	$k = 121 \text{ w/m}\cdot^\circ\text{C} = 121 \text{ N}\cdot\text{m}/\text{sec}\cdot\text{m}\cdot^\circ\text{C} = 121 \text{ N}/\text{sec}\cdot^\circ\text{C}$
Specific Heat(C_p)	$C_p = 0.963 \text{ kJ/kg}\cdot^\circ\text{C} = 963 \text{ N}\cdot\text{m}/\text{kg}\cdot^\circ\text{C} = 963 \text{ E6mm}^2/\text{sec}^2\cdot^\circ\text{C}$
Thermal Expansion coefficient(α)	$\alpha = 22.7E-6 \frac{1}{^\circ\text{C}}$

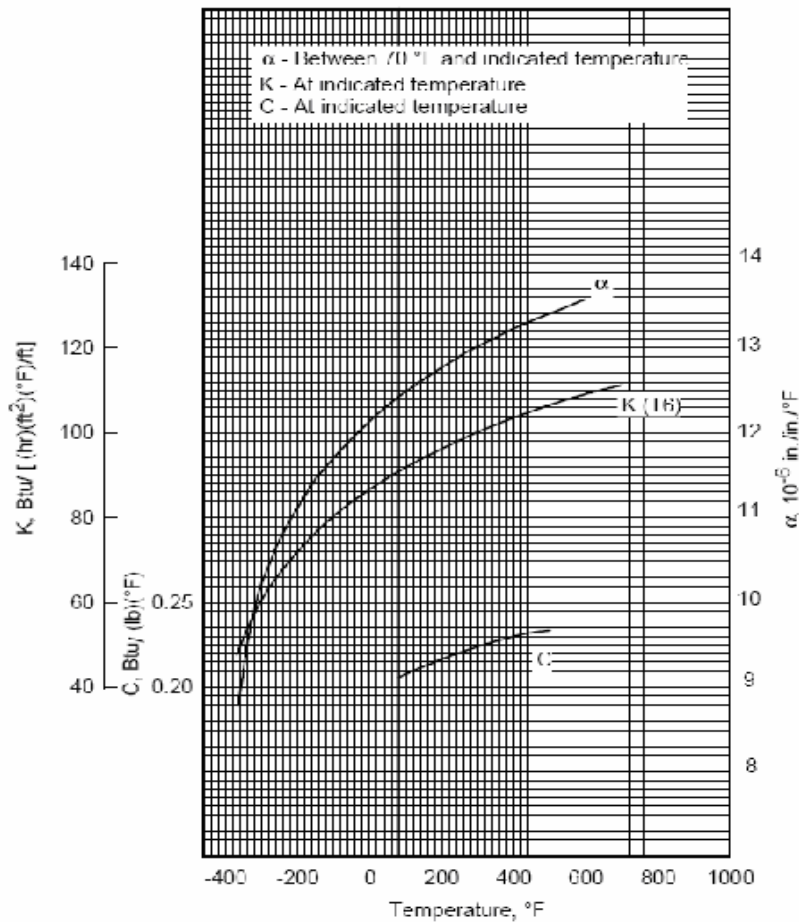


Figure 18: MIL-HDBK-5J(7)

Table 5: Temperature dependent properties of the 2024-T3 aluminum

Temperature(T)		Young`s Modulus(E)		Poisson`s ratio(ν)
degree °F	degree °C	psi	N / mm^2	
0.155642	-17.691310	10173528.9624726	70146.52293	0.33
20.0389	-6.645056	10097828.9624726	69624.57112	
45.6031	7.557278	10072528.9624726	69450.12752	
62.6459	17.025500	10022028.9624726	69101.92982	
84.6858	29.269889	9982728.96247261	68830.95616	
104.4110	40.228333	9924298.9624726	68428.08108	
124.1370	51.187222	9880458.96247261	68125.80410	
145.5060	63.058889	9792778.96247261	67521.25015	
163.5880	73.104444	9734318.96247261	67118.16822	
183.3130	84.062778	9646638.96247261	66513.61427	
203.0390	95.021667	9558958.96247261	65909.06032	
222.7640	105.980000	9471278.96247261	65304.50637	
244.1330	117.851667	9354368.96247261	64498.41145	
263.8590	128.810556	9237458.96247261	63692.31653	
283.5840	139.768889	9091318.9624726	62684.68064	
303.3100	150.727778	8959798.9624726	61777.84972	
323.0350	161.686111	8828268.96247261	60870.94984	
341.1170	171.731667	8667518.96247261	59762.57795	
360.8420	182.690000	8492158.96247261	58553.47005	
382.2120	194.562222	8287558.96247261	57142.75223	
403.5810	206.433889	8068358.9624726	55631.36735	
423.3060	217.392222	7849148.96247261	54119.91352	
443.0320	228.351111	7586098.96247261	52306.18272	
462.7570	239.309444	7323058.9624726	50492.52086	
484.1260	251.181111	7060008.9624726	48678.79006	
502.2080	261.226667	6767738.96247261	46663.58724	
525.2210	274.011667	6417008.96247261	44245.30249	
544.9470	284.970556	6051658.96247261	41726.21277	
563.0280	295.015556	5715548.96247261	39408.73298	
584.3980	306.887778	5335588.96247261	36788.90726	
602.4790	316.932778	4999468.96247261	34471.35851	

3.3 Determining Element Edge Length (L_e) of FE Models

The lowest phase velocity (i.e., transverse wave speed), and hence the shortest wavelength sets the maximum permissible grid spacing that must be chosen so that spatial aliasing due to the finite element discretization does not occur(3). The size of the elements are chosen in a manner so that the propagating waves are spatially resolved(21). To do this, more than 10 nodes per wavelength is adequate(3).

In this study, a minimum element edge length of 0.1mm is used for modeling of the two specimens. To decide on a proper element size the following procedure is incorporated. First, the transverse wave speed (c_T) is calculated using equation 2.1.5.

$$c_T = \sqrt{\frac{\mu}{\rho}} = \sqrt{\frac{G}{\rho}} = \sqrt{\frac{25.92 \times 10^9 \text{ N/m}^2}{2767.8 \text{ kg/m}^3}} = 3060.2 \text{ m/s} \quad \text{from 2.1.5}$$

Simulations have been performed up to frequencies of 2 MHz. This maximum frequency is from the restriction of the frequency-thickness product of the specimen as discussed in Section 2.4.

Using this maximum frequency of 2 MHz and the transverse wave speed (c_T), the smallest wavelength (λ_{\min}) is calculated(3):

$$f_{\max} = 2 \text{ MHz} = 2 \times 10^6 \text{ Hz} = 2 \times 10^6 \text{ cycles/s}$$

$$\lambda_{\min} = \frac{c_T}{f_{\max}} = \frac{3060.2 \text{ m/s}}{2 \times 10^6 \text{ cycle/s}} = 0.0015301 \text{ m} = 1.5301 \text{ mm} \quad 3.3.1$$

From the above results, the typical element edge length (L_e) and the minimum element edge length (L_{\min}) can be calculated(3):

$$L_e < \frac{\lambda_{\min}}{10} = 0.15301 \text{ mm} \quad 3.3.2$$

This relation ensures that there are at least 10 elements across the smallest wavelength of interest. Rounding down the value of L_e to a value of 0.1mm ensures that an integer number of elements

can be placed along the length and the thickness of the plate in the finite element model. Thus, the minimum element edge length used becomes:

$$L_{\min} = 0.1 \text{ mm} \quad 3.3.3$$

As mentioned above, this study uses models with a typical element edge length of 0.1mm, so it satisfies the criteria that is given from equation 3.3.2, and this value is used in the Mesh Module in ABAQUS CAE.

3.4 Calculating Time Step (Δt)

Choosing an adequate integration time step(Δt) is very important for the accuracy of the solution. In general, the accuracy of the model can be increased with increasingly smaller integration time steps. With time steps that are too long, the high frequency components are not resolved accurately enough. On the other hand, too small time steps are a waste of calculation time. Therefore, a compromise must be found. For this study, 20 points per cycle of the highest frequency results in the compromise. This gives accurate solutions in an efficient manner(21). This rule is expressed in equation 3.4.2.

In this study, a time step(Δt) of 5ns is used for modeling the two specimens. In order to decide on a proper time step, the following procedure is performed. To calculate the time step(Δt), first the Lamé' constants (μ, λ) need to be calculated from equation 2.1.6 and equation 2.1.7 respectively:

$$\mu = \frac{E}{2(1+\nu)} = G(\text{shear modulus}) = 25.92 \text{ GPa} = 25.92 \times 10^9 \text{ N/m}^2 \quad \text{from 2.1.6}$$

$$\lambda = \frac{E\nu}{(1+\nu)(1-2\nu)} = \frac{(68.95 \times 10^9 \text{ N/m}^2)(0.33)}{(1.33)(0.34)} = 50.3173 \times 10^9 \text{ N/m}^2 \quad \text{from 2.1.7}$$

Using the results of the Lamé' constants (μ, λ) above, the longitudinal wave speed (c_L) can be calculated from equation 2.1.3:

$$c_L = \sqrt{\frac{\lambda + 2\mu}{\rho}} = \sqrt{\frac{(50.3173 \times 10^9 \text{ N/m}^2) + 2(25.92 \times 10^9 \text{ N/m}^2)}{2767.8 \text{ kg/m}^3}} = 6075.3 \text{ m/s}$$

The time step (Δt) has two criterion from equation 3.4.1 and equation 3.4.2. Equation 3.4.1 is the CFL condition(named for Courant, Friedrichs, and Lewy). This condition prevents a longitudinal wave from traveling completely through an element during a single time step(6:413). Equation 3.4.2 is the criteria given by Moser(21). Using the previous results(i.e., the minimum element edge length (L_{\min}) and the maximum frequency of 2 MHz), both criterion can be calculated(6:413)(21):

$$\Delta t < \frac{L_{\min}}{c_L} = \frac{0.1 \text{ mm}}{6075.3 \times 10^3 \text{ mm/s}} = 1.646 \times 10^{-8} \text{ s} = 16.46 \text{ ns} \quad 3.4.1$$

$$\Delta t < \frac{1}{20f_{\max}} = \frac{1}{20 \times 2 \times 10^6 \text{ cycles/s}} = 2.5 \times 10^{-8} \text{ s} = 25 \text{ ns} \quad 3.4.2$$

Equation 3.4.2 ensures that there are at least 20 time steps during the cycle of a wave at the highest frequency. The 5.0 nsec time step($\Delta t = 5 \text{ ns}$) meets these criterion and this value is used in the Step Module in ABAQUS CAE.

3.5 Five and a Half Cycle Hanning-Window Excitation Signal

The five and a half cycle Hanning-window excitation signal is used in this study because it has the following advantages. First, it reduces the energy at frequencies other than the excitation or ‘center’ frequency. Second, since the signal is based on a limited cycle sinusoidal tone burst, the undesired reflections between packets are reduced thereby allowing for TOA calculations. Figures 19 - 22 provide 5 ½ cycle Hanning-window excitation signals at 100, 200, 300, and 500kHz. In the figures, ‘Sim’ is short form of ‘Simulation’ and ‘Exp’ is short form of ‘Experimental’. The addition of the half cycle, to an integer number of cycles, provides a distinct peak in the excitation signal and provides its symmetry. Since the frequency content is narrow relative to the center frequency this is considered a narrow-band signal.

The time duration is the time a 5 ½ cycle excitation signal travels from the actuator into the medium from the outer edge of the actuator. The duration can be calculated in following equation(4):

$$\text{(number of cycles)}/f \quad 3.5.1$$

Table 6 contains the duration of 5 ½ cycle Hanning-window excitation signal which is used in this thesis. The length($\tilde{\lambda}$) of one cycle is determined from the theoretical phase velocity(c_p) and signal frequency(f)(4):

$$c_p = f \tilde{\lambda} \quad 3.5.2$$

And length of 5 ½ cycle Hanning-window excitation can be calculated by(4):

$$\text{(number of cycles)* } \tilde{\lambda} \quad 3.5.3$$

Table 6: Duration of 5.5 Cycle Hanning-window Excitation Signals

Frequency(kHz)	100	200	300	500
Duration(μ sec)	55.00	27.50	18.33	11.00

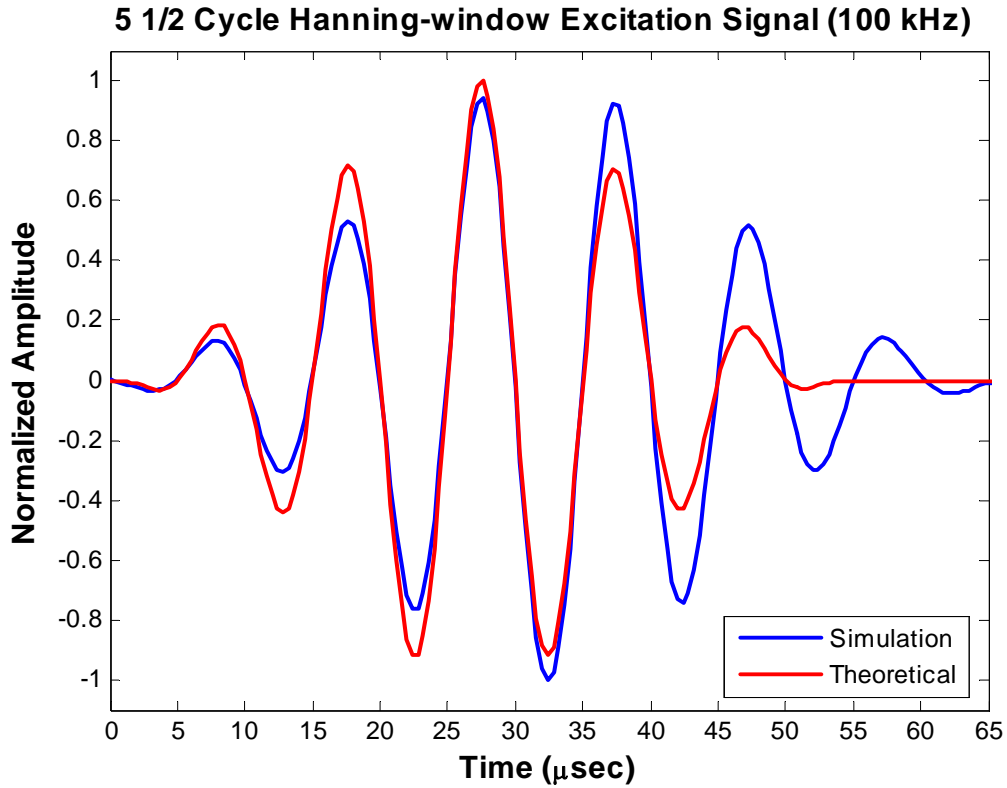


Figure 19: 5 1/2 cycle Hanning-window excitation signals at 100kHz

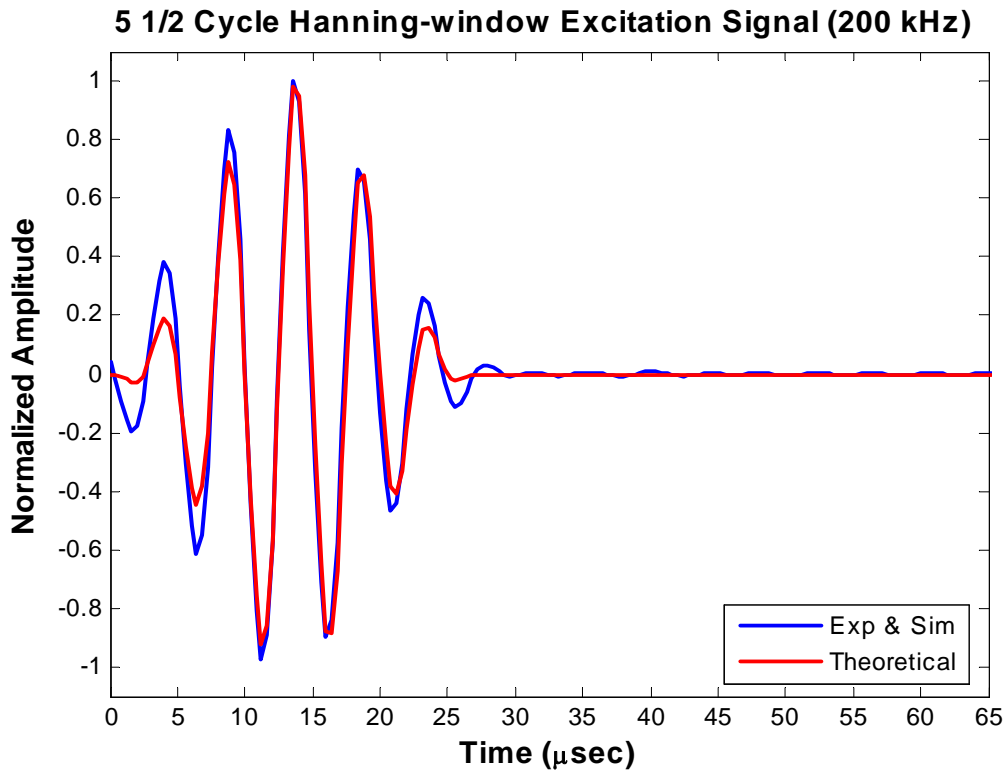


Figure 20: 5 1/2 cycle Hanning-window excitation signals at 200kHz

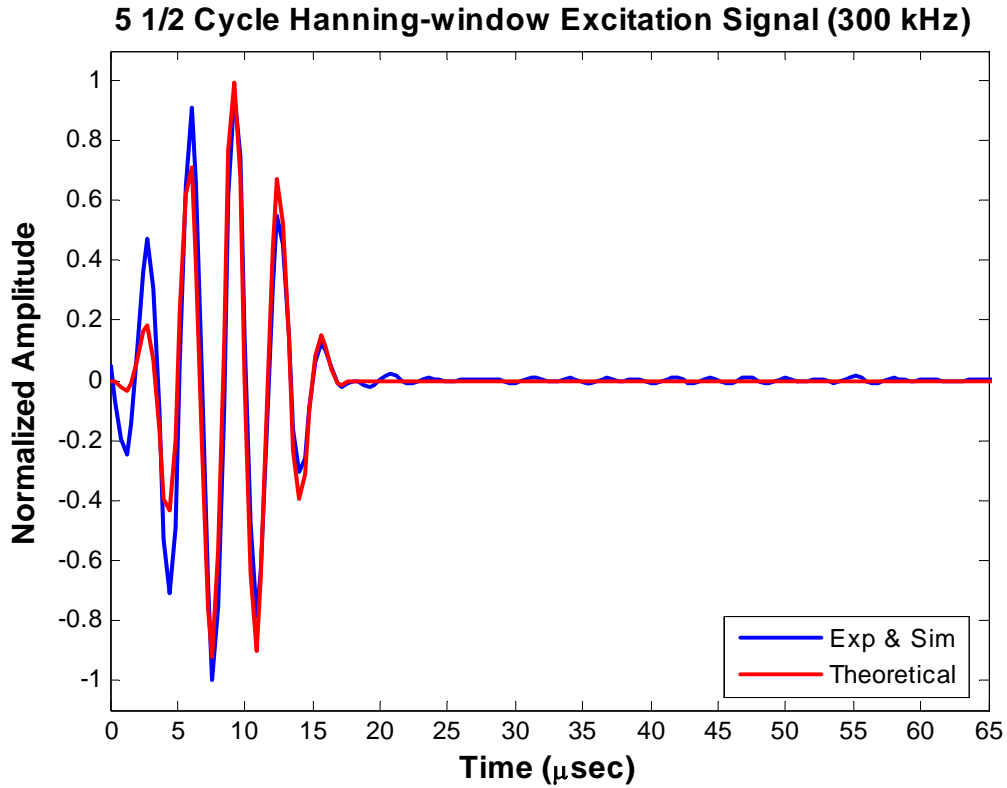


Figure 21: 5 1/2 cycle Hanning-window excitation signals at 300kHz

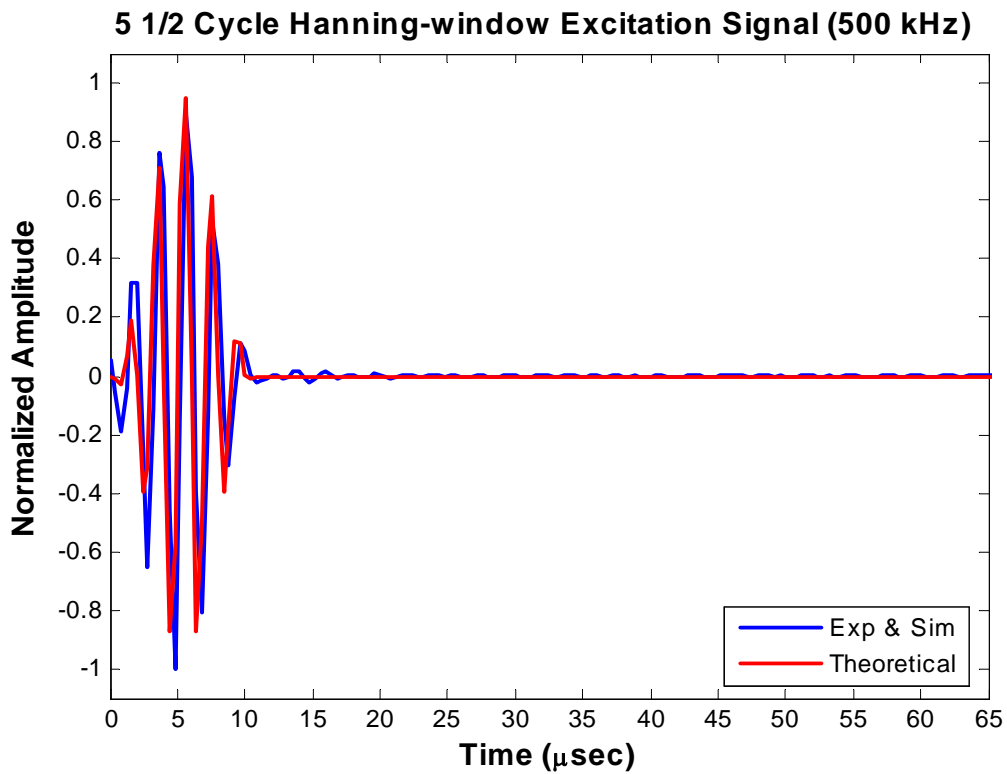


Figure 22: 5 1/2 cycle Hanning-window excitation signals at 500kHz

3.6 Determining the Sensor Results

In this thesis, three responses(i.e., experimental, simulation, theoretical results) are compared. The experimental response and theoretical response are already provided by a previous researcher Andrews(4) who was dealing with same conditions of SPECIMEN I & III in AFRL. For a proper comparison, the different forms of the three response data must be considered.

First, the experimental responses are generated by the following procedures. If an input voltage makes an excitation(i.e., expansion and contraction of the actuator which is bonded to the plate), the excitation generates Lamb waves through the plate. The Lamb wave causes changes of distances between the center(mid-point) and edges of the sensor. These distance changes generate a strain voltage in the sensing piezo-electric transducer and then the strain voltage is recorded in the third row of the experimental data file. Table 7 and 8 show the formation of the experimental and simulated data file, respectively. Actual samples of the experimental and simulated data files are in Appendix D.

Second, the simulation response can be calculated from the displacements on the center and edge of the sensor. The displacements can be obtained from the output requested in ABAQUS CAE. Since the response voltage of the experiment come from the strain between the center and edge of the sensor, these displacements must be converted to strains in order to compare with experimentation. Figure 23 shows the modeling of the actuating and sensing transducers in ABAQUS CAE. The actuating transducer is shown in Figure 23 (a). Since the excitation signal needs to be applied at the edges of the actuator, the edges are modeled using two vertical lines through the thickness. The excitation signals which are applied at the edges are depicted with arrows on top surface of the model. Figure 23 (b) shows mesh elements which are seeded using a 0.1mm element length(L_e). Since the thickness of the Specimen I is 1mm, 10 elements are observed through the thickness. The sensing transducer is shown in Figure 23 (c). Since the edges and mid-point of the sensor are needed in order to calculate the strain of the sensor, the edges and

mid-point are modeled using three vertical lines through the thickness. These three points on the top surface of the model are called the three sensing points(i.e., i, i+1, i+2). If the displacements of the each sensing point are u_i , u_{i+1} , and u_{i+2} , respectively, the displacements can be converted to strain in following equation:

$$\text{right part strain of the sensor using forward differencing} = \frac{u_{i+2} - u_{i+1}}{r} \quad 3.6.1$$

$$\text{left part strain of the sensor using backward differencing} = \frac{u_{i+1} - u_i}{r} \quad 3.6.2$$

average strain of the sensor using central differencing =

$$\frac{1}{2} \left\{ \frac{u_{i+2} - u_{i+1}}{r} + \frac{u_{i+1} - u_i}{r} \right\} = \frac{u_{i+2} - u_i}{2r} \quad 3.6.3$$

A parameter r is defined as the radius of the transducer. The equations 3.6.1 and 3.6.2 indicate the strain of the half sensor(i.e., between the center and edge). The average strain(i.e., total strain of the sensor) is calculated from equation 3.6.3 for node i+1.

Third, the theoretical responses are generated given the solutions to the Rayleigh-Lamb frequency equations which are introduced in Chap 2. To compare the theoretical responses with others, the time delay between experimental, simulation, and theoretical excitation signals must be considered.

Finally, all three responses are compared in Chap 4. Before any comparison can be performed a proper data conversion must be conducted since each response has a different magnitude of amplitude that is due to different sources of strain(i.e., the strain of the experiment comes from the voltage, the strain of the simulation comes from the actual displacement, and the strain of the theoretical result comes from the theoretical equations). Each response is divide by it's maximum amplitudes for normalization. Appendix C introduces the Matlab codes which are used in the data conversion and comparison.

Table 7: Formation of the Experimental data file

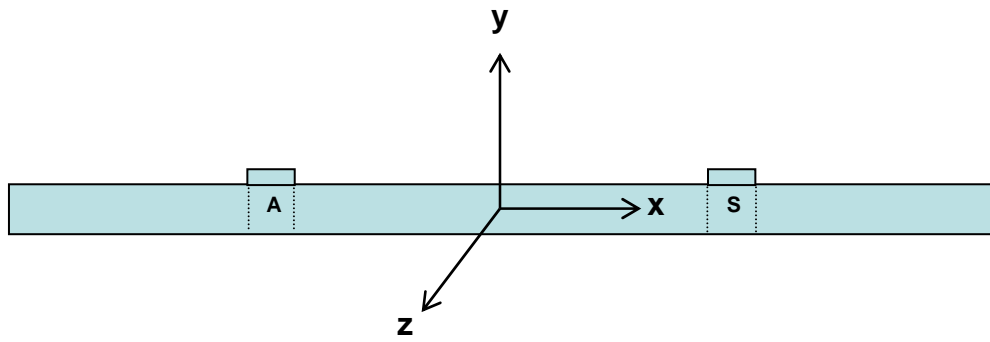
Time index(sec)	Excitation voltage	Response(Strain) voltage
0.0	##	##
4E-7	##	##
8E-7	##	##
1.2E-6	##	##
.	.	.
.	.	.

* Reference Appendix D for actual data file

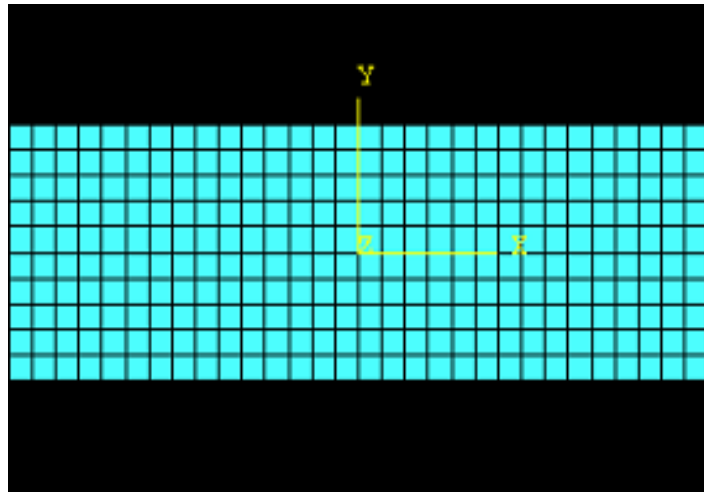
Table 8: Formation of the Simulated data file

Time index(sec)	Sensing points on the sensor		
	u_i	u_{i+1}	u_{i+2}
0.0	##	##	##
4E-7	##	##	##
8E-7	##	##	##
1.2E-6	##	##	##
.	.	.	.
.	.	.	.

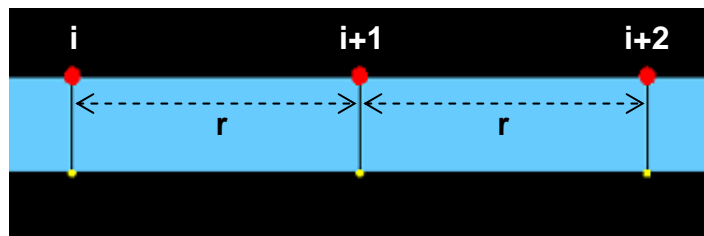
* Reference Appendix D for actual data file



(a)



(b)



(c)

Figure 23 : Modeling of the actuating and sensing transducers in ABAQUS CAE

3.7 Convergence Study

In this section, a convergence study is carried out to verify the modeling methods used in this thesis. For the convergence study, element edge length (L_e) of 0.05mm (i.e., a half of original element edge length) is used with a 300kHz excitation signal in the specimen I. Table 9 shows the element edge lengths, number of elements, and temperature of the plate that are used in this study for both of the established model and developed model.

Table 9: Data for convergence study

	Established model in this thesis	Developed model for convergence study
Element edge length (L_e)	0.1 mm	0.05 mm
Number of elements	47,500	190,000
Temperature	190°F	190°F

Figure 24 shows visual comparison of S_0 responses in both models. As shown in the figure, both S_0 responses are fairly similar. Different percentage between two peaks is calculated as 1.3 % and thus the model chosen for all of the analysis is based on established model indicated in Table 9.

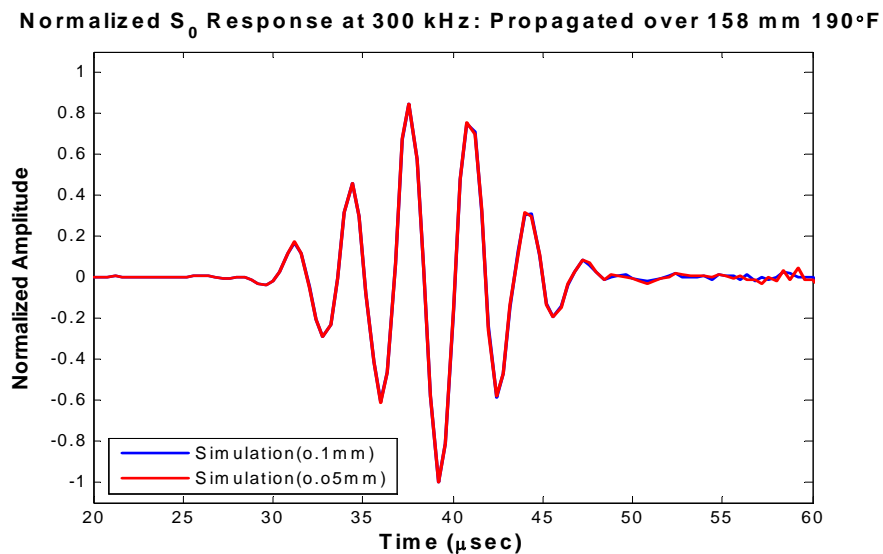


Figure 24: Comparison of S_0 response in convergence study

Chapter 4 Results and Discussion

Chapter 4 presents the results obtained from both the isothermal and thermal gradient simulations. The data obtained for the isothermal testing is based on the use of Specimen I and the data obtained for the thermal gradient testing is based on the use of Specimen III.

Specifically, Section 4.1 covers the isothermal testing to compare simulated wave propagation results with theoretical and experimental wave propagation results. Thermal gradient testing is covered in Section 4.2.

4.1 Isothermal Testing of the Specimen I

The isothermal condition is analyzed using specimen I. The analysis focuses on the delayed TOA(time of arrival) that is due to the elevated temperature and the TOA agreement between the simulated, theoretical, and experimental S_0 responses.

4.1.1 S_0 Response at 100 kHz

For this analysis, the 100 kHz excitation signal, that is shown in Section 3.5, is used to generate a response. The S_0 responses of the experiment in this low frequency is mixed with magnetic noise, so it is not possible to compare with other results. The magnetic noise is a waveform present at the same point in time the excitation signals are transmitted to the specimen. This anomaly is due to magnetic induction between the wires transmitting the signals. Magnetic induction occurs when the magnetic field generated from a current in one wire generates an electric current in an adjacent wire. Since the wires are in close proximity to each other during testing, the magnetic field around the wire carrying the excitation signal transmits the same signal over to the receiving wire(4). The existence of magnetic induction can be seen in the raw signal at 300kHz as shown in Figure 25.

Therefore, in this section, two types of S_0 responses are compared under the 0, 25, 50, 75, 100, 125, 150, 175 and 190°F isothermal conditions. The first type of S_0 response is the finite

element result of an ABAQUS simulation. In this thesis, ABAQUS provides displacements of the three sensing points, thus a conversion from displacement to strain is conducted using the Matlab code in Appendix C. The basic concept of the conversion is shown in Section 3.6. The second type of S_0 response is the theoretical response. The previous researcher, Andrews(4), and AFRL provided the Matlab codes which can generate a theoretical excitation signal and S_0 responses using Rayleigh-Lamb equations.

Figures 26 - 34 show a waveform comparison between two types of S_0 response on each step of the temperature condition. Table 10 shows the time of arrival(TOA) differences between two types of S_0 responses. The TOA is calculated by measuring the peak amplitude time of the S_0 response. However, visual modification is needed since not all of the peak appears in the middle of the waves. In the cases of the 100 and 125°F temperatures, the peak amplitudes do not appeared in the middle of the simulated responses, they are located at a distance forward from the middle as shown in Figure 30 and 31. In these cases, the mid-wave amplitude is the criteria for TOA calculation even though its amplitude is not the largest. In order to reduce the complexity when deciding the criteria of the waves, a reading technique from the back to the front in the wave is recommended.

Before we compare the waveform and the TOA, both S_0 responses are normalized with respect to its absolute maximum amplitude and the time delay between simulated and theoretical excitation signals is considered for plotting and TOA calculating.

In Table 10 and Figures 26 - 34, we can observe and conclude four things. First, the theoretical S_0 responses are a little faster than the simulated S_0 responses. Second, as the temperature increased the two types of S_0 responses are delayed by a small amount of time. The second phenomenon is related to the delayed TOA due to the elevated temperature. This concept is introduced and anticipated in Section 2.5.2. Third, some fluctuations in simulated responses

can be observed around 80 to 95 μ sec. These are explained by the differences between the simulated excitation signal and the theoretical excitation signal. As shown in Figures 19 – 22, each simulated excitation has some noise after its five and a half cycles have completed. This noise can possibly affect the response. Fourth, most important reason that causes the differences is different types of analysis between ABAQUS and Matlab. ABAQUS conducts actual wave traveling, thus the waves in the simulated responses are the wave packet that is generated by interaction between component waves during propagation. However, Matlab does not carry out actual wave traveling. It just shows same waveform as the excitation signal at the response. That is the reason there is no fluctuation in the theoretical responses.

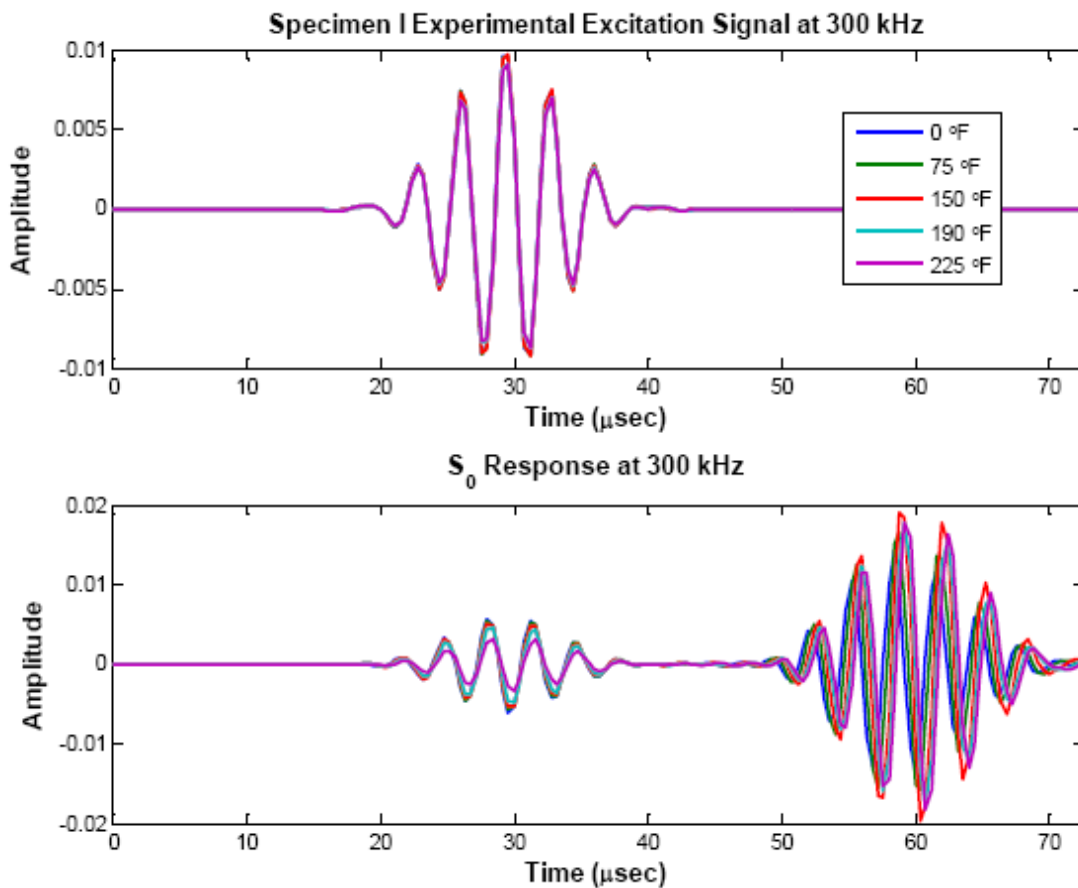


Figure 25 : The existence of the magnetic noise(4)

Table 10: Specimen I TOA of S_0 response at 100kHz

Temperature (°F)	Time of Arrival (TOA)		TOA difference
	Simulation TOA (μ sec)	Theoretical TOA (μ sec)	SIM – THEO (μ sec)
0	59.2	57.2	2.0
25	59.2	57.2	2.0
50	60.8	57.2	3.6
75	60.8	57.2	3.6
100	60.8	57.6	3.2
125	61.2	57.6	3.6
150	61.2	57.6	3.6
175	61.6	58.0	3.6
190	60.8	58.0	2.8

Normalized S_0 Response at 100 kHz: Propagated over 158 mm 0°F

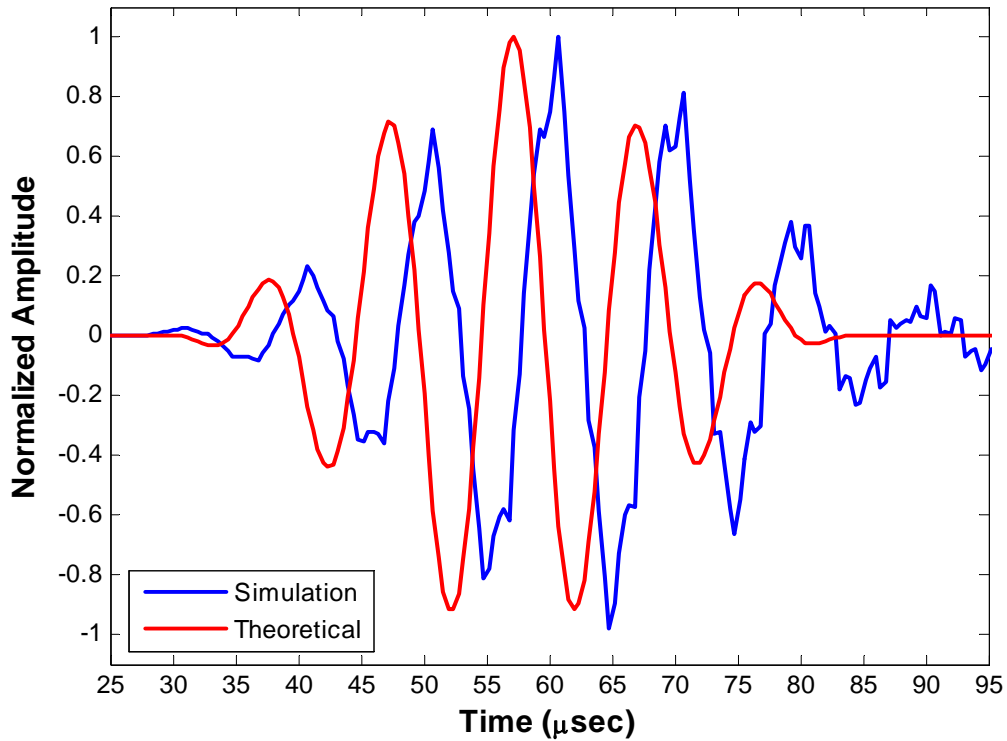


Figure 26: Specimen I S_0 response at 100kHz (0°F)

Normalized S_0 Response at 100 kHz: Propagated over 158 mm 25°F

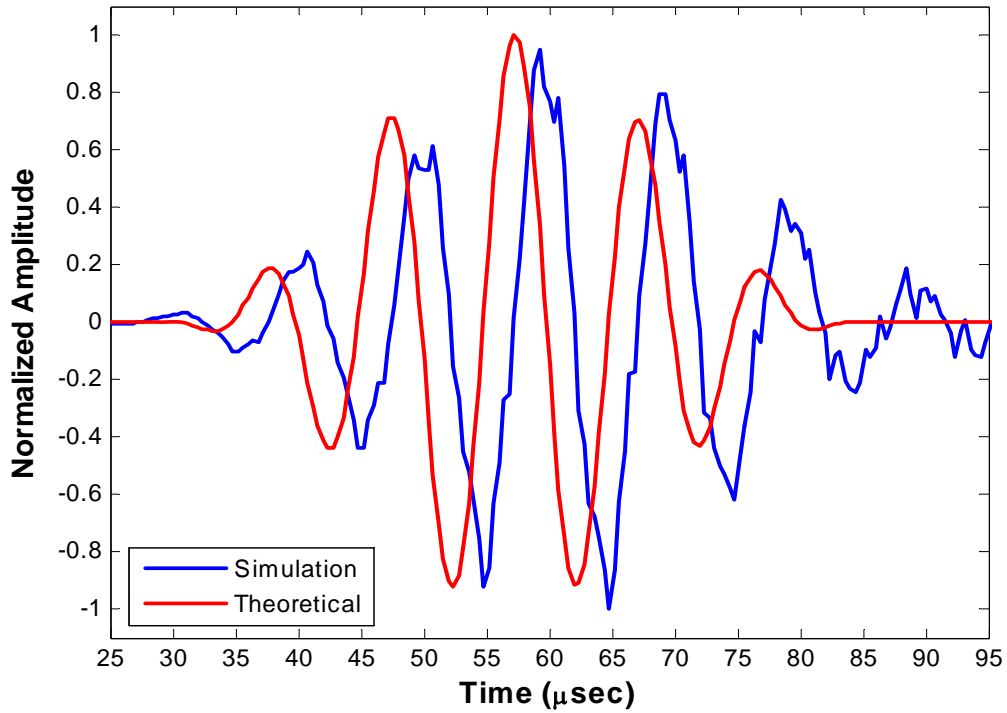


Figure 27: Specimen I S_0 response at 100kHz (25°F)

Normalized S_0 Response at 100 kHz: Propagated over 158 mm 50°F

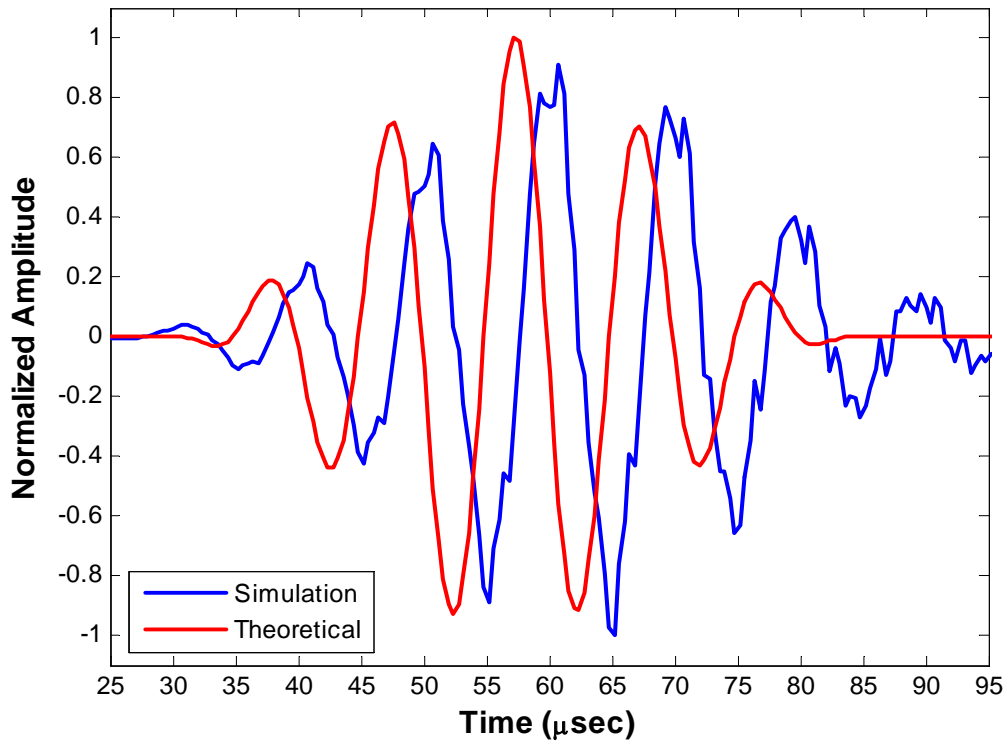


Figure 28: Specimen I S_0 response at 100kHz (50°F)

Normalized S_0 Response at 100 kHz: Propagated over 158 mm 75°F

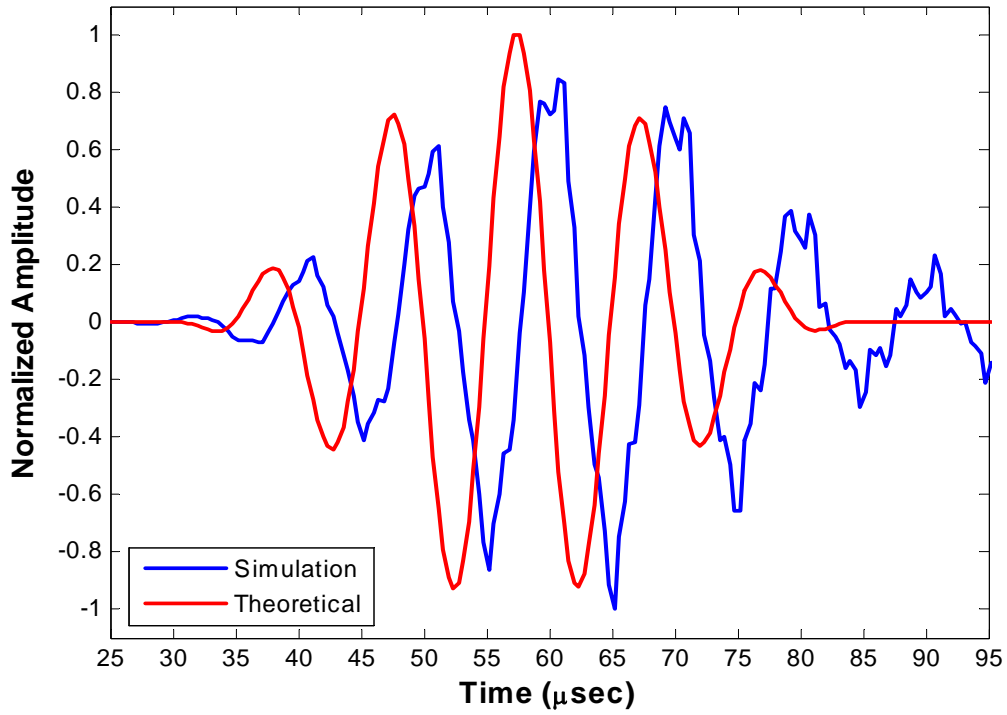


Figure 29: Specimen I S_0 response at 100kHz (75°F)

Normalized S_0 Response at 100 kHz: Propagated over 158 mm 100°F

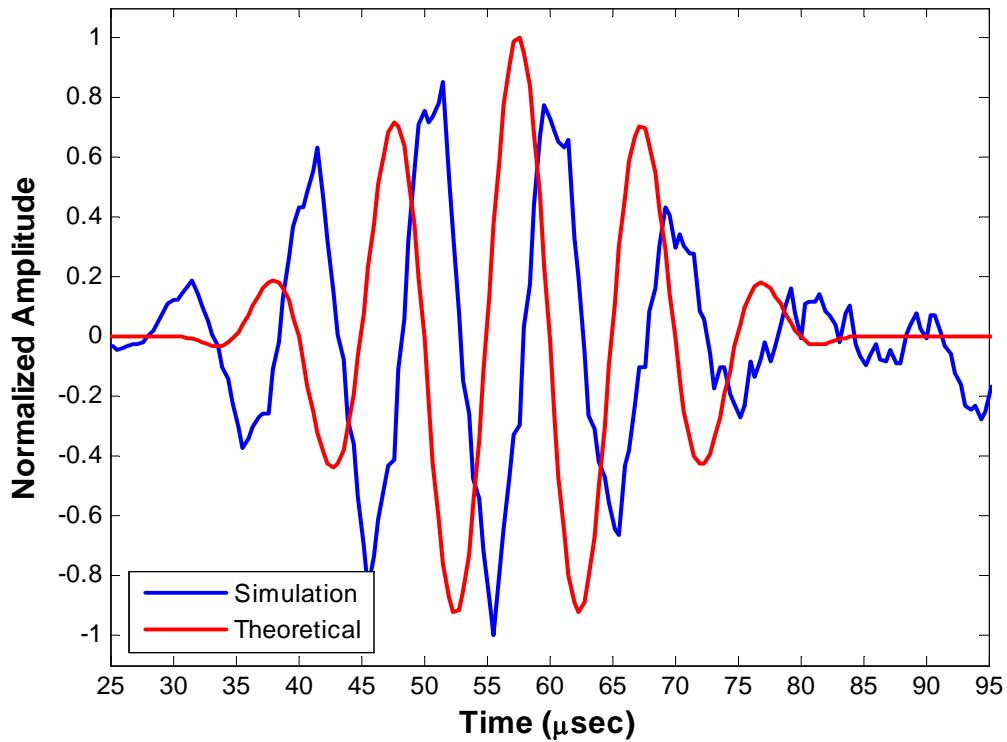


Figure 30: Specimen I S_0 response at 100kHz (100°F)

Normalized S_0 Response at 100 kHz: Propagated over 158 mm 125°F

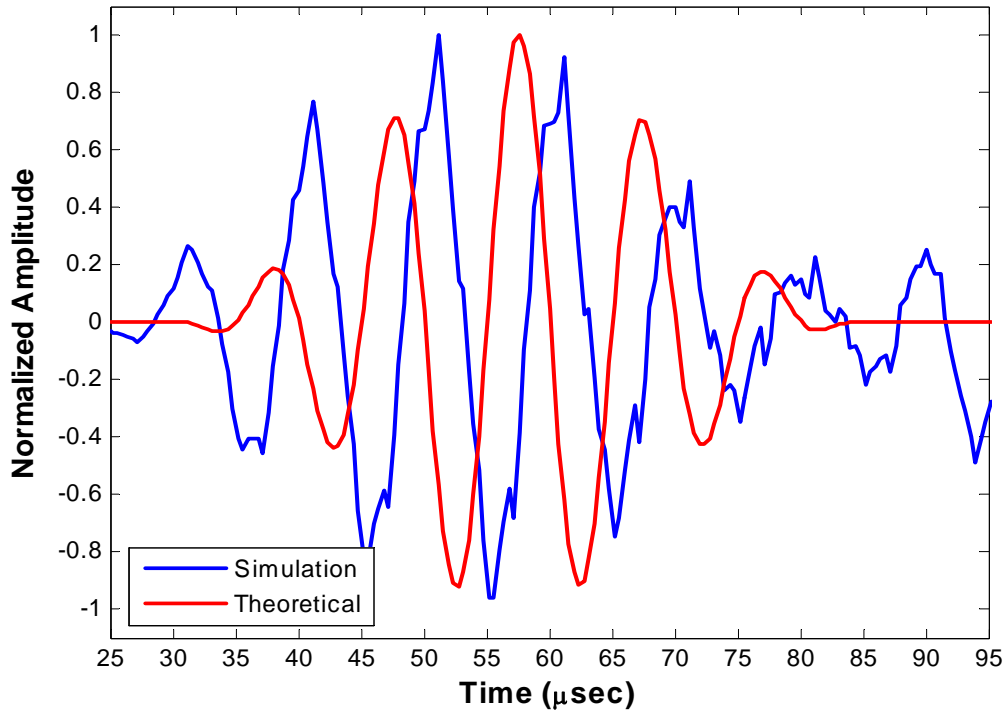


Figure 31: Specimen I S_0 response at 100kHz (125°F)

Normalized S_0 Response at 100 kHz: Propagated over 158 mm 150°F

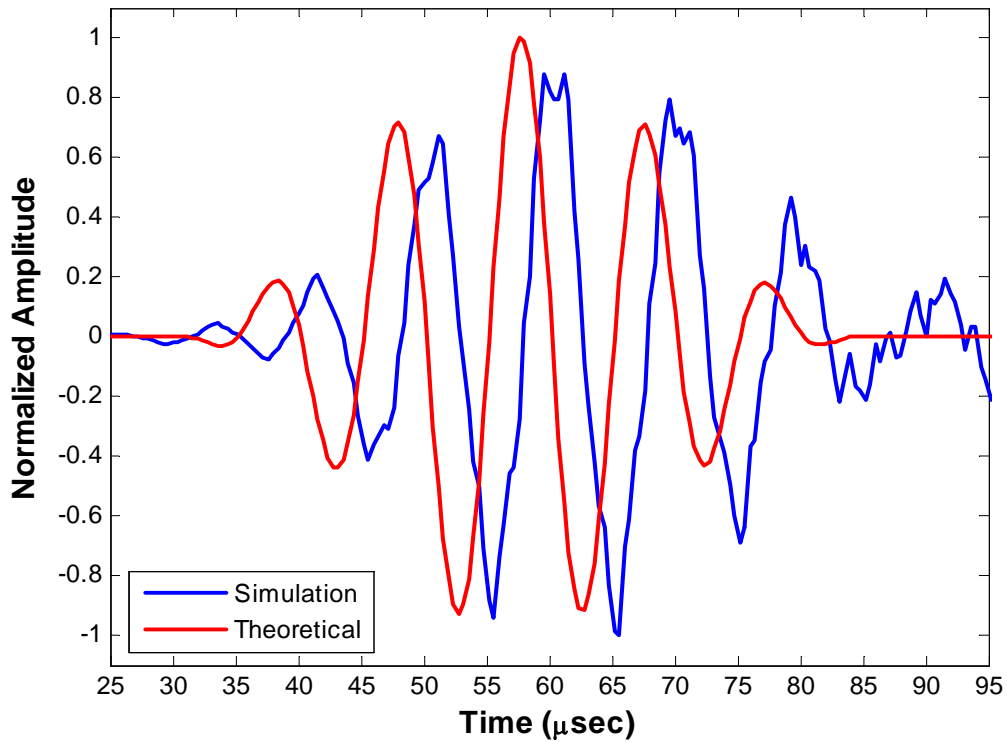


Figure 32: Specimen I S_0 response at 100kHz (150°F)

Normalized S_0 Response at 100 kHz: Propagated over 158 mm 175°F

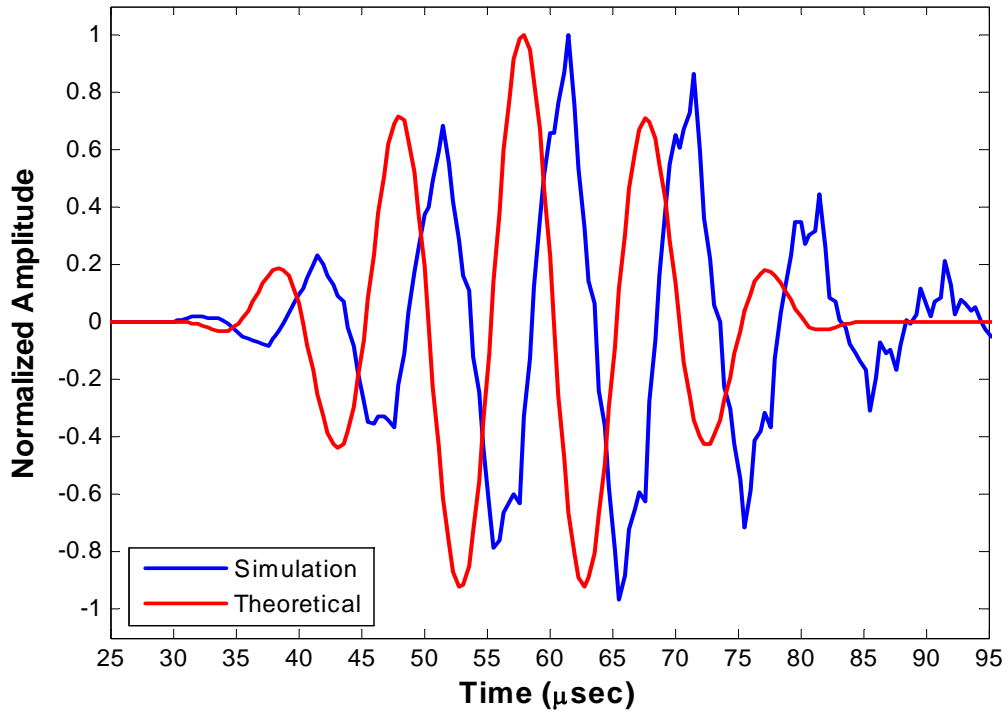


Figure 33: Specimen I S_0 response at 100kHz (175°F)

Normalized S_0 Response at 100 kHz: Propagated over 158 mm 190°F

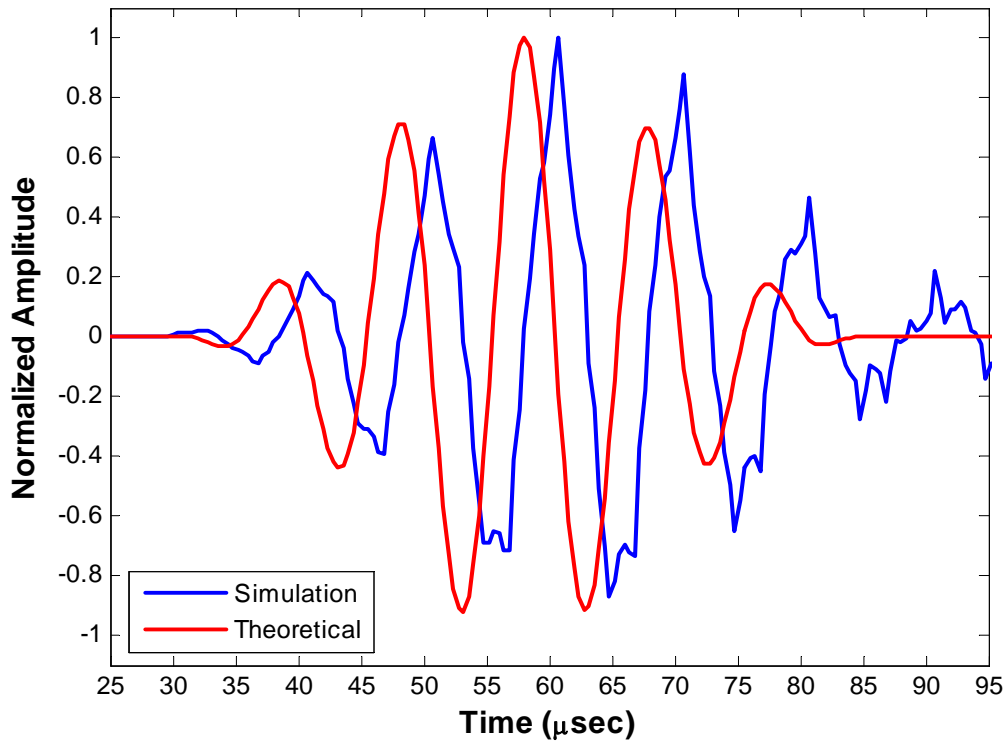


Figure 34: Specimen I S_0 response at 100kHz (190°F)

4.1.2 S_0 response at 300kHz

In this section, the experimentation carried out in reference(4) is included with respect to the S_0 responses and compared under the 0, 50, 100, 125, 150, 175 and 190°F isothermal conditions using the 300 kHz excitation signal, that is discussed in Section 3.5.

Figures 35 - 41 show the visual waveform comparison between the three types of S_0 response on each step of the temperature condition. Table 11 shows time of arrival(TOA) differences between the three types of S_0 responses. Before comparison of the waveform and the TOA, the three types of S_0 responses are normalized with respect to its own absolute maximum amplitude and the time delay between simulated, theoretical, and experimental excitation signals are considered for plotting and TOA calculation.

Like the previous conclusion in Section 4.1.1, the theoretical S_0 responses are a little bit faster than the experimental S_0 responses and the experimental S_0 responses are little bit faster than the simulated S_0 responses. Also, as anticipated in Section 2.5.2, the three types of S_0 responses are delayed by a small amount of time as the temperature is increased.

In addition, some small and large fluctuations in experimental responses are observed before and after the S_0 responses. These can be explained by two factors. First, the difference between simulated/experimental(they use the same excitation) excitation signal and the theoretical excitation signal. As discussed before in Section 4.1.1, this noise could possibly affect the response. However, the first factor is not sufficient to explain the existence of the small fluctuations before the S_0 responses and the large fluctuations after the S_0 responses, it just explains small fluctuations after the S_0 responses. Secondly, the magnetic noise, that is introduced in Section 4.1.1, needs to be considered to explain the fluctuations in this analysis. As mentioned before, the magnetic noise is a weakened excitation signal which is generated at the

sensor. After the magnetic noise is generated, it is propagated to the circumference of the sensor. The small fluctuations before the S_0 responses are explained by the residual effect after the magnetic noise is propagated since the noise does not sufficiently damp out.

The large fluctuations after the S_0 responses can be explained by the interaction between two reflected waves of the magnetic noise. As shown in the figures, the wave propagates 158mm(length of the wave path) for 30 μ sec. Since the magnetic noise, which propagates into the x and z-direction of the sensor(see Figure 14 for directions), is reflected by the boundary condition of the specimen I, it returns to the sensor. The reflected magnetic noise is captured by the sensor around 54 and 42 μ sec because it travels about 320 and 248mm, respectively. Interaction of these two reflected noise appears as various noises. Arrival time calculation can be easily verified using equation 2.1.3.

Table 11: Specimen I TOA of S_0 response at 300kHz

Temperature (°F)	Time of Arrival (TOA)			TOA difference	
	Simulation TOA(μ sec)	Experimental TOA(μ sec)	Theoretical TOA(μ sec)	Sim – Exp (μ sec)	Sim – Theo (μ sec)
0	40.4	39.6	38.8	0.8	1.6
50	40.4	39.6	38.8	0.8	1.6
100	40.4	40.4	39.2	0.0	1.2
125	40.8	40.4	39.2	0.4	1.6
150	40.8	40.8	39.6	0.0	1.2
175	41.2	40.8	39.6	0.4	1.6
190	41.2	40.8	39.6	0.4	1.6

Normalized S_0 Response at 300 kHz: Propagated over 158 mm 0°F

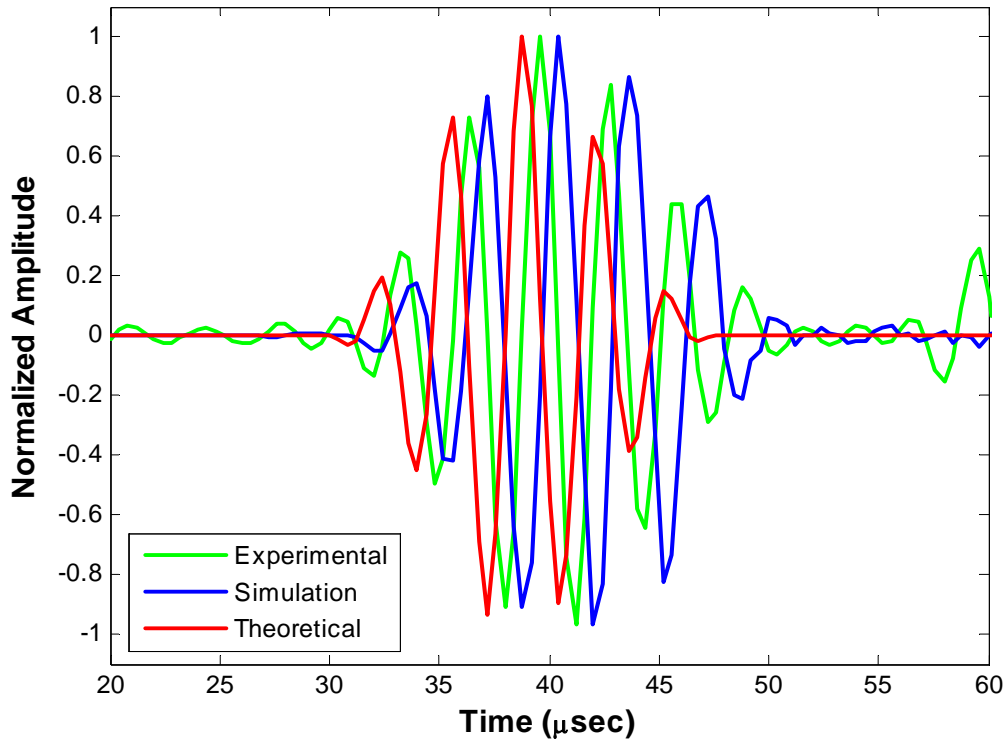


Figure 35: Specimen I S_0 response at 300kHz (0°F)

Normalized S_0 Response at 300 kHz: Propagated over 158 mm 50°F

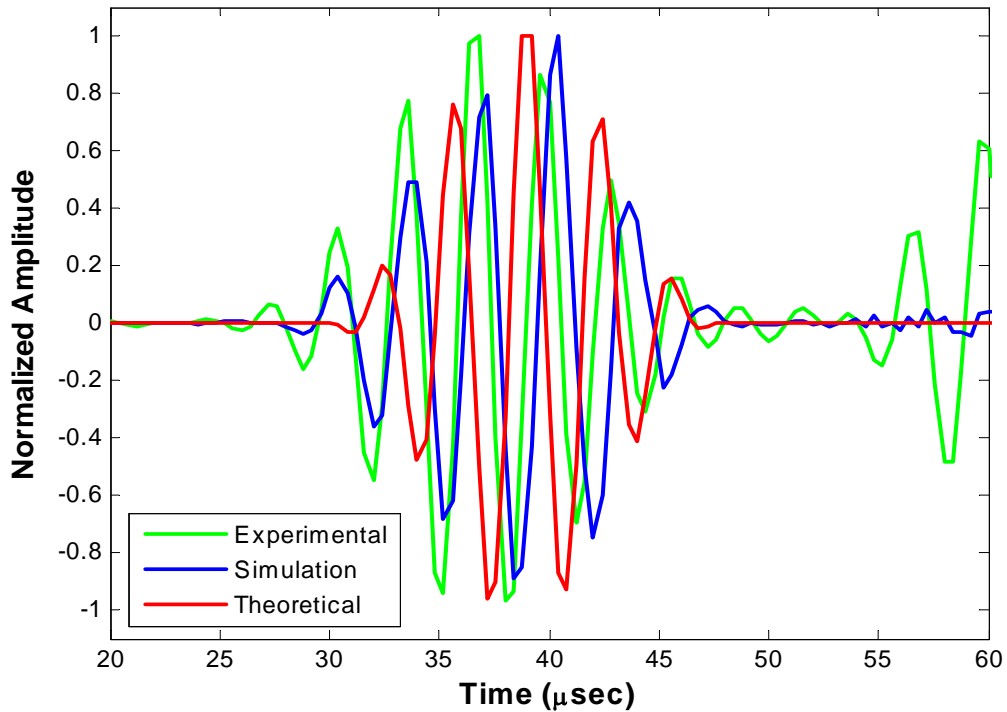


Figure 36: Specimen I S_0 response at 300kHz (50°F)

Normalized S_0 Response at 300 kHz: Propagated over 158 mm 100°F

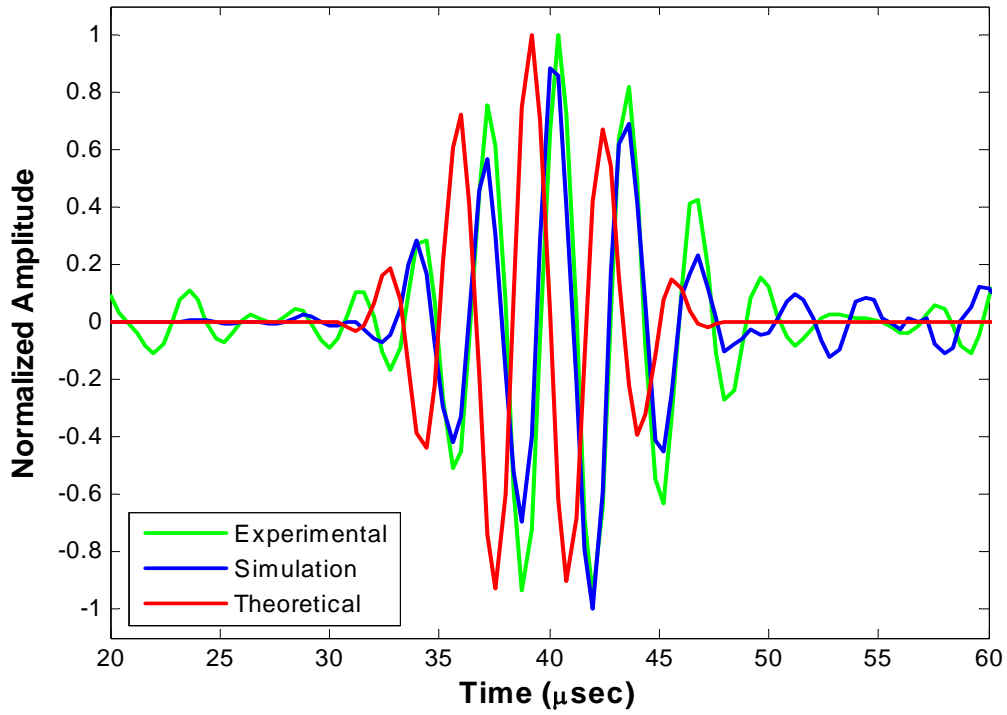


Figure 37: Specimen I S_0 response at 300kHz (100°F)

Normalized S_0 Response at 300 kHz: Propagated over 158 mm 125°F

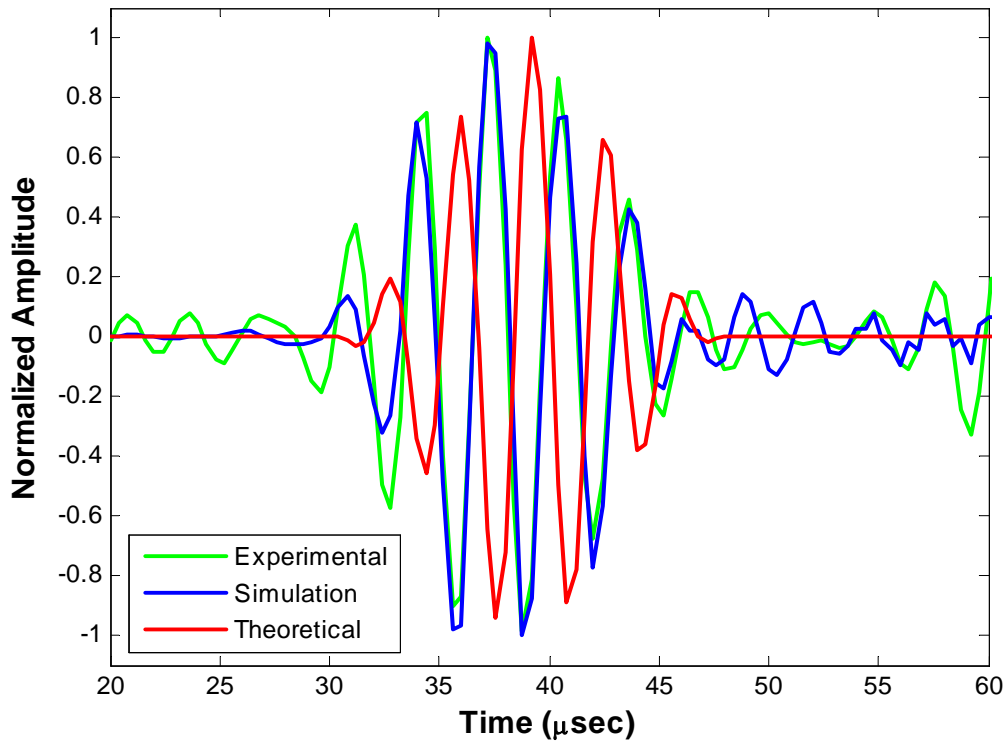


Figure 38: Specimen I S_0 response at 300kHz (125°F)

Normalized S_0 Response at 300 kHz: Propagated over 158 mm 150°F

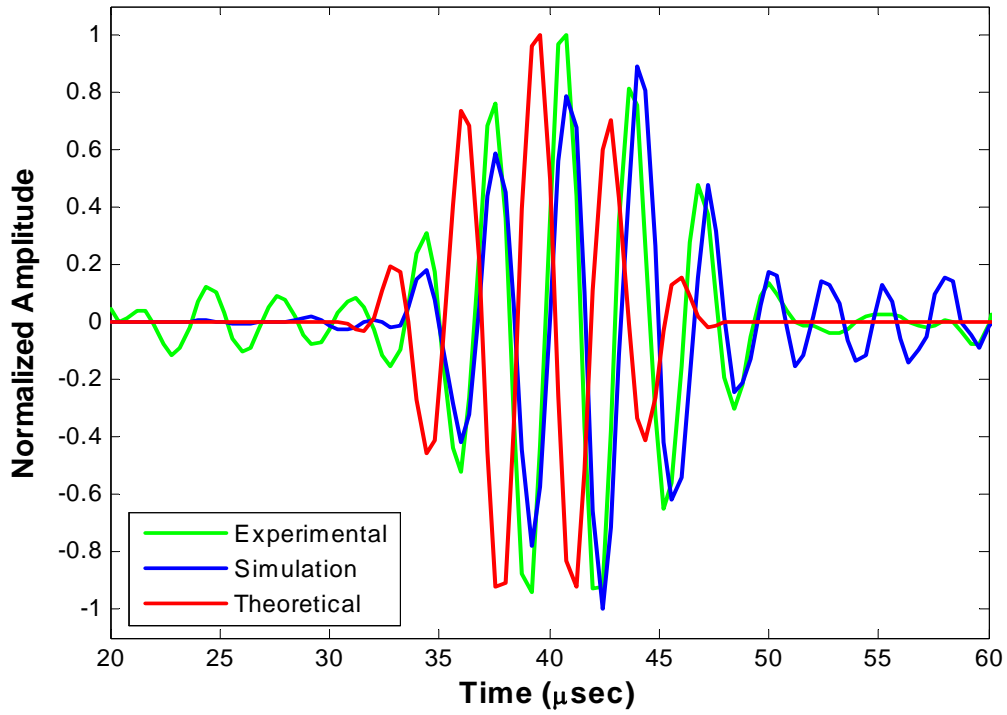


Figure 39: Specimen I S_0 response at 300kHz (150°F)

Normalized S_0 Response at 300 kHz: Propagated over 158 mm 175°F

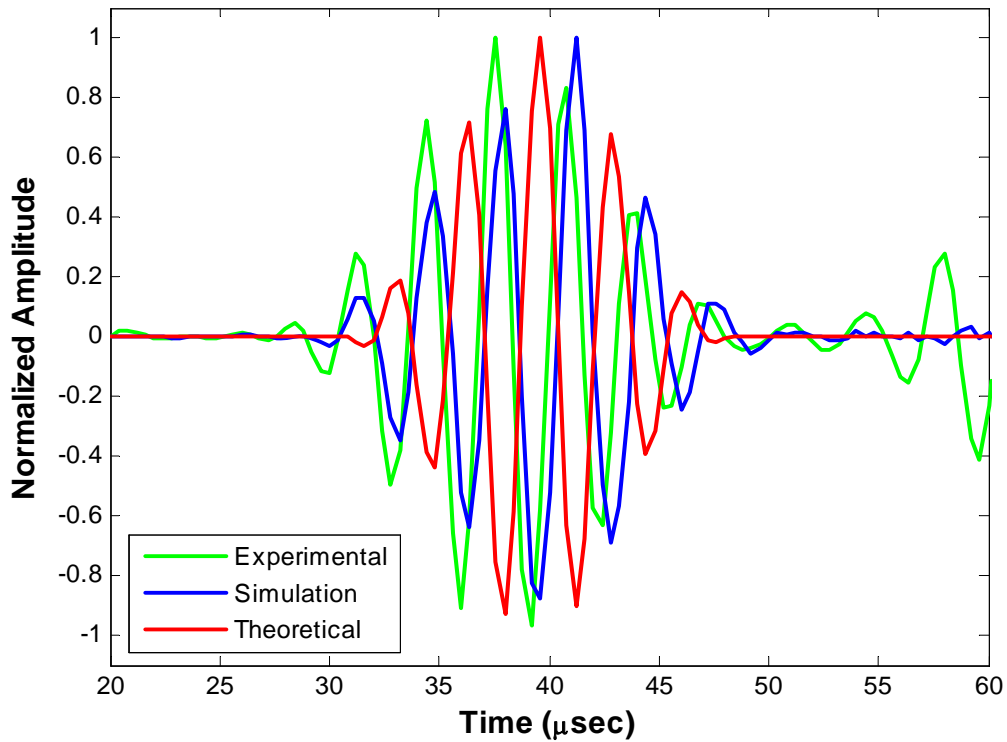


Figure 40: Specimen I S_0 response at 300kHz (175°F)

Normalized S_0 Response at 300 kHz: Propagated over 158 mm 190°F

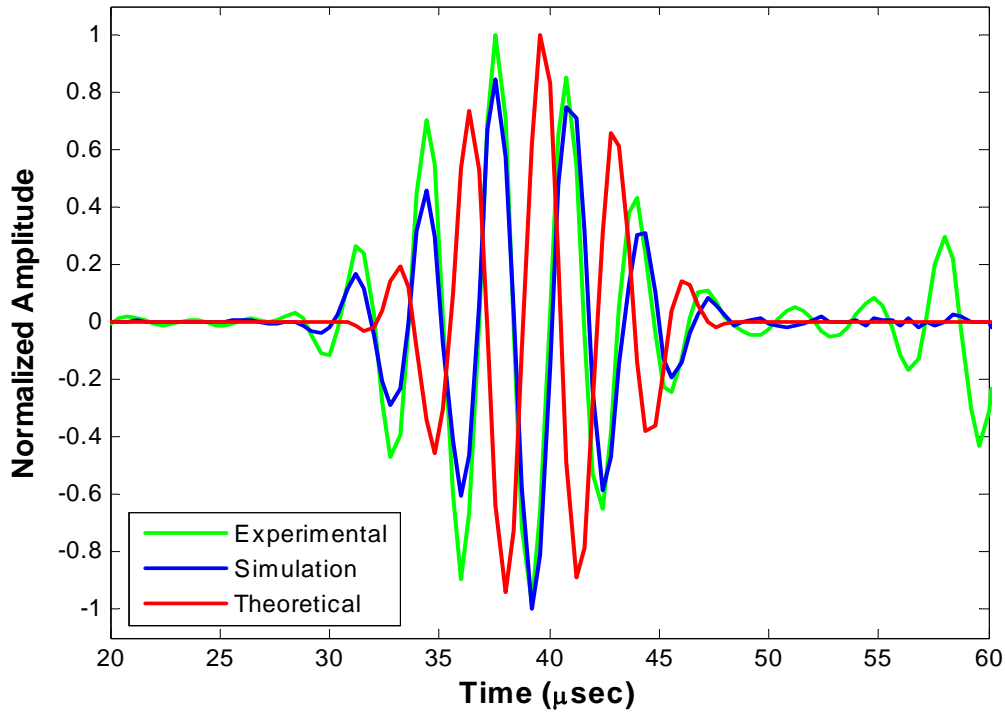


Figure 41: Specimen I S_0 response at 300kHz (190°F)

4.2 Thermal Gradient Testing of the Specimen III

The thermal gradient condition that is introduced in Section 3.1.2 is analyzed using specimen III. The analysis focuses on the delayed TOA that is due to the elevated temperature region between the actuator and the sensor. The thermal stress effects on the TOA and the waveform are also considered.

4.2.1 S_0 Response Comparison

In this section, the three types of S_0 responses are compared under the three thermal gradient conditions (i.e., TG 1, TG 2, TG 3) and room temperature (RM). For this analysis, the 200, 300 and 500 kHz excitation signals, that are shown in Section 3.5, are used to generate the responses. The first, second, and third types of S_0 responses are the simulated response, the theoretical response, and the experimental response, respectively, as introduced in Section 4.1.1 and 4.1.2.

Figures 42 to 50 show the visual waveform comparison between the three types of S_0 responses for each step of thermal gradient condition. Table 12 shows the time of arrival(TOA) differences between the three types of S_0 responses. Before comparison of the waveform and the TOA, three types of S_0 responses are normalized with respect to its own absolute maximum amplitude and the time delay between simulated, theoretical, and experimental excitation signals is considered for plotting and TOA calculation.

Unlike the previous results in Section 4.1, the theoretical S_0 responses are little bit slower than experimental and simulated S_0 responses. However, when comparison of the simulated S_0 responses and theoretical S_0 responses are performed, they still show the close TOA. The small TOA differences are due to the different analyzing abilities between ABAQUS and Matlab. Also, the simulated and experimental S_0 responses are delayed by a small amount of time as the temperature of the thermal gradient region increases. This phenomenon is similar to the isothermal condition. However, when we consider the specific condition of the thermal gradient(i.e., thermal stress exists along the wave path), the particular changes of the waveform and the large amount of TOA difference are not observed. We can conclude the effect of the thermal stress doesn't significantly change the wave propagation analysis. More detailed analysis of the thermal stress is discussed in next section.

In addition, like previous responses, various noises and differences are observed between the results. Most of the differences can be explained by using the same reasons which are discussed in the previous section. However, existence of the different experimental waveforms in Figures 42 – 44(at 200 kHz) can not properly be explained. In these figures, the experimental S_0 responses appear a lot faster than other S_0 responses. In order to find out the reason of this phenomenon, the raw experimental signal is analyzed. In the raw experimental response signal,

another large noise is observed between the magnetic noise and the S_0 responses. This noise could possibly change the waveform of the experimental response. However, the reason which generates the noise is not revealed.

Table 12: Specimen III TOA of S_0 response

		Time of Arrival (TOA)			TOA difference	
		Simulation TOA(μ sec)	Experimental TOA(μ sec)	Theoretical TOA(μ sec)	Sim – Exp (μ sec)	Sim – Theo (μ sec)
200kHz	RM	109.2	106.4	110.8	2.8	-1.6
	TG 1	110.0	107.2	•	2.8	•
	TG 2	110.0	106.8	•	3.2	•
	TG 3	109.6	106.8	•	2.8	•
300kHz	RM	105.6	105.6	106.0	0.0	-0.4
	TG 1	106.0	106.0	•	0.0	•
	TG 2	106.0	106.0	•	0.0	•
	TG 3	106.0	106.0	•	0.0	•
500kHz	RM	101.2	100.8	102.4	0.4	-1.2
	TG 1	102.0	101.2	•	0.8	•
	TG 2	102.0	101.2	•	0.8	•
	TG 3	101.6	101.2	•	0.4	•

Normalized S_0 Response at 200 kHz: Propagated over 512 mm

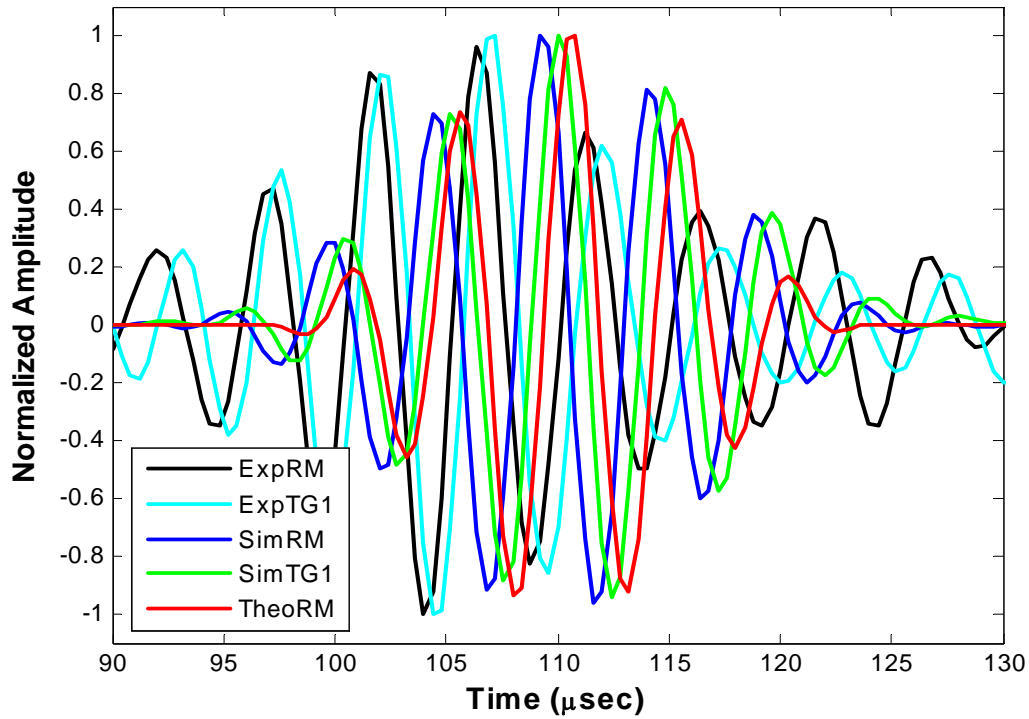


Figure 42: Specimen III S_0 response comparison(RM vs TG 1) at 200kHz

Normalized S_0 Response at 200 kHz: Propagated over 512 mm

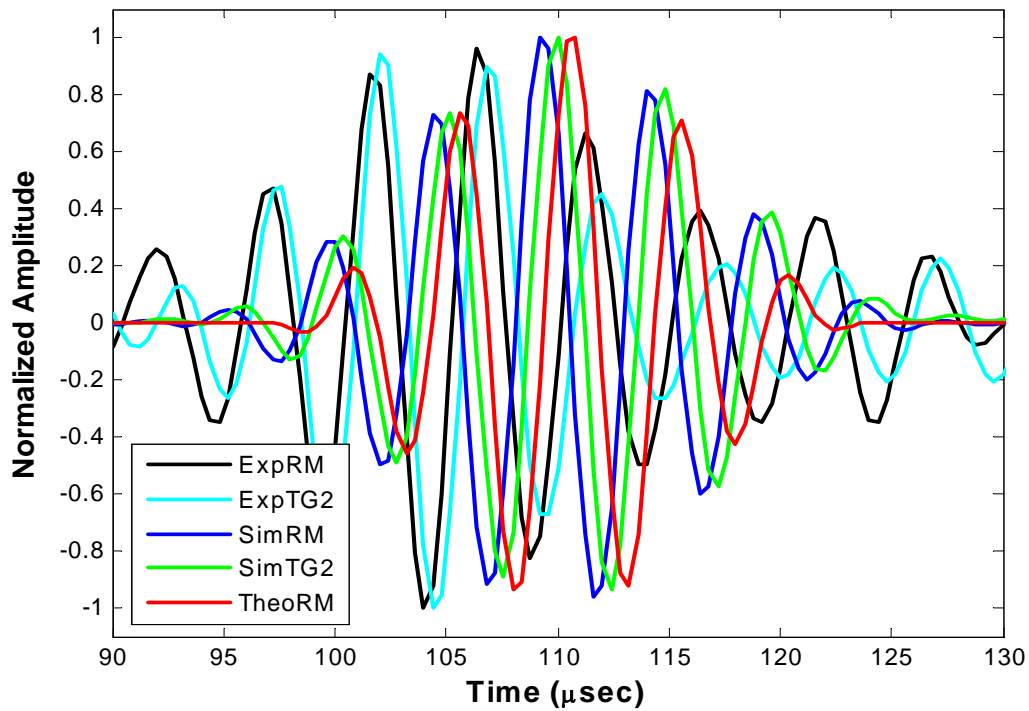


Figure 43: Specimen III S_0 response comparison(RM vs TG 2) at 200kHz

Normalized S_0 Response at 200 kHz: Propagated over 512 mm

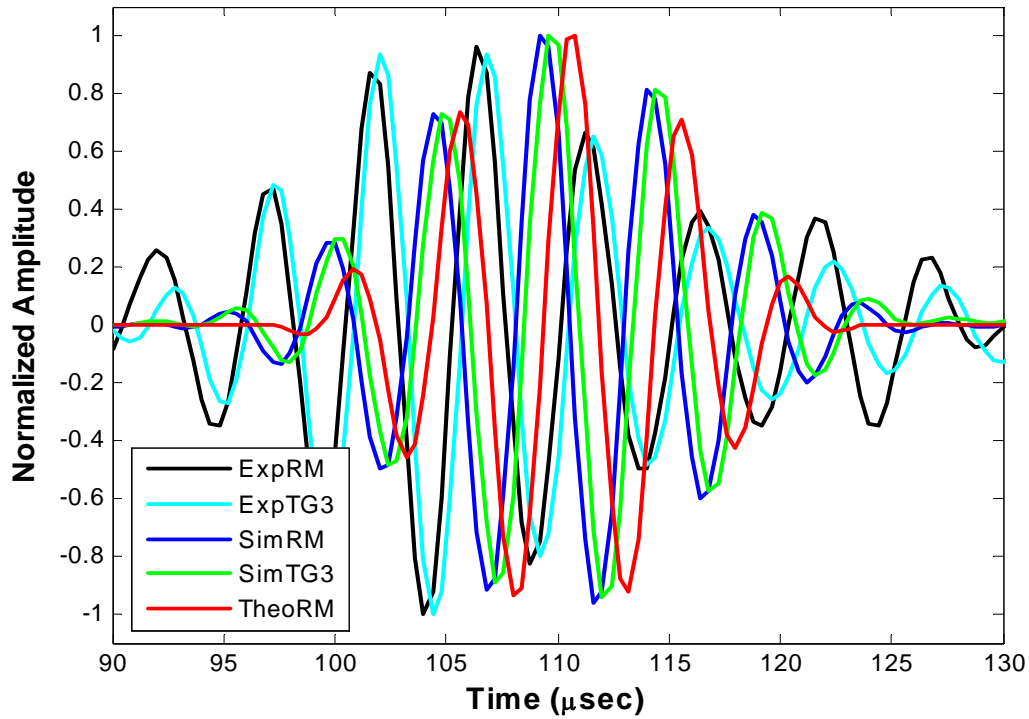


Figure 44: Specimen III S_0 response comparison(RM vs TG 3) at 200kHz

Normalized S_0 Response at 300 kHz: Propagated over 512 mm

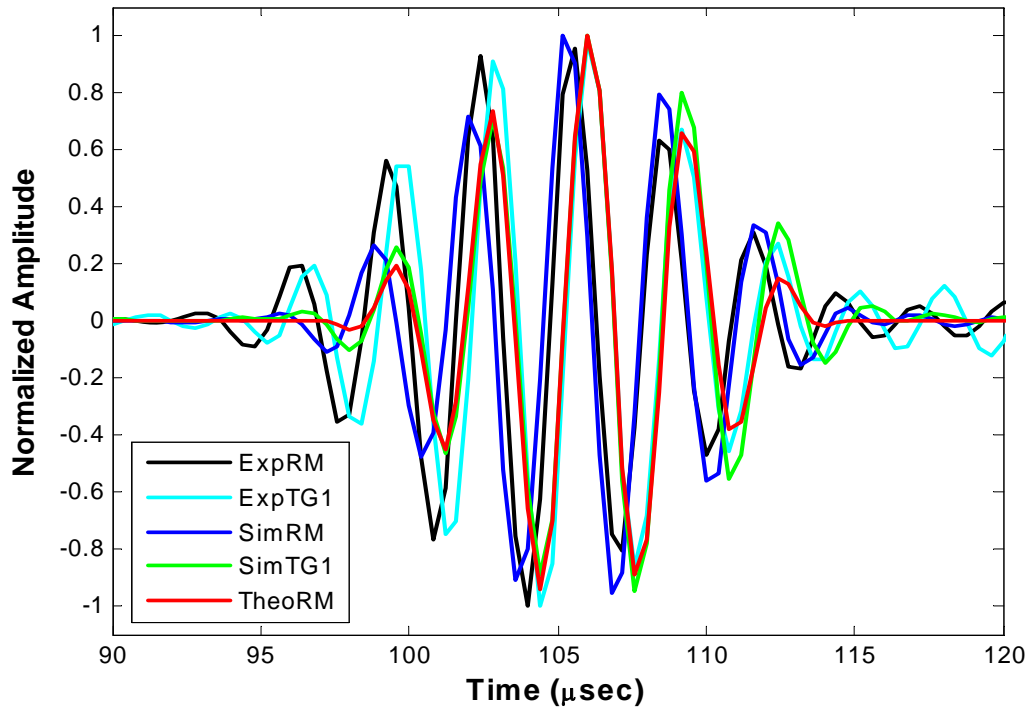


Figure 45: Specimen III S_0 response comparison(RM vs TG 1) at 300kHz

Normalized S_0 Response at 300 kHz: Propagated over 512 mm

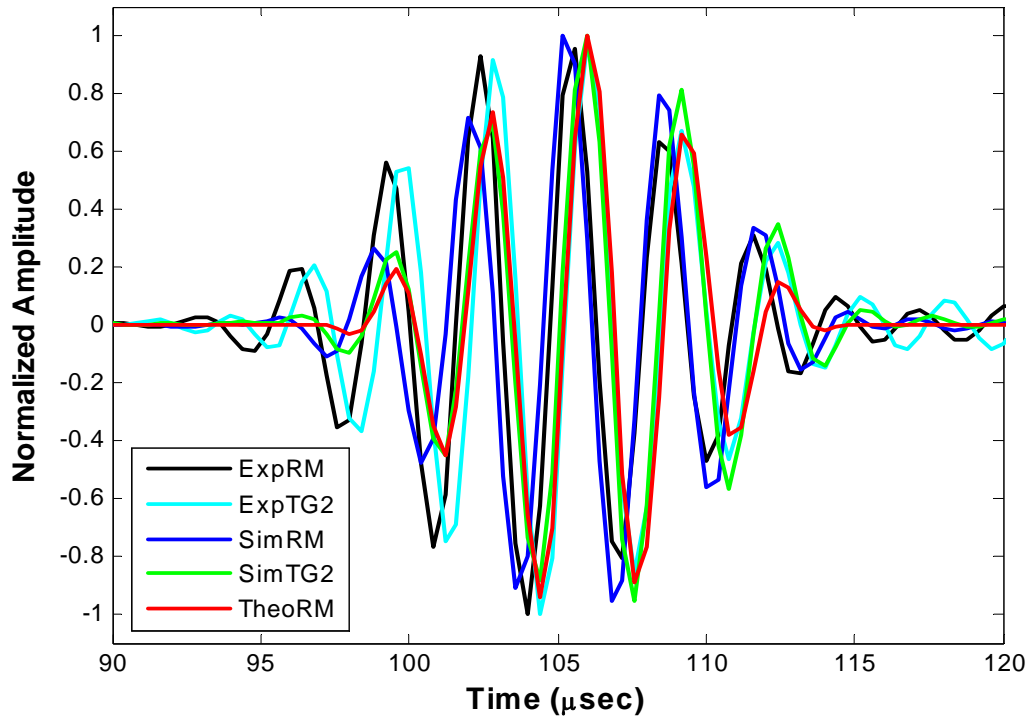


Figure 46: Specimen III S_0 response comparison(RM vs TG 2) at 300kHz

Normalized S_0 Response at 300 kHz: Propagated over 512 mm

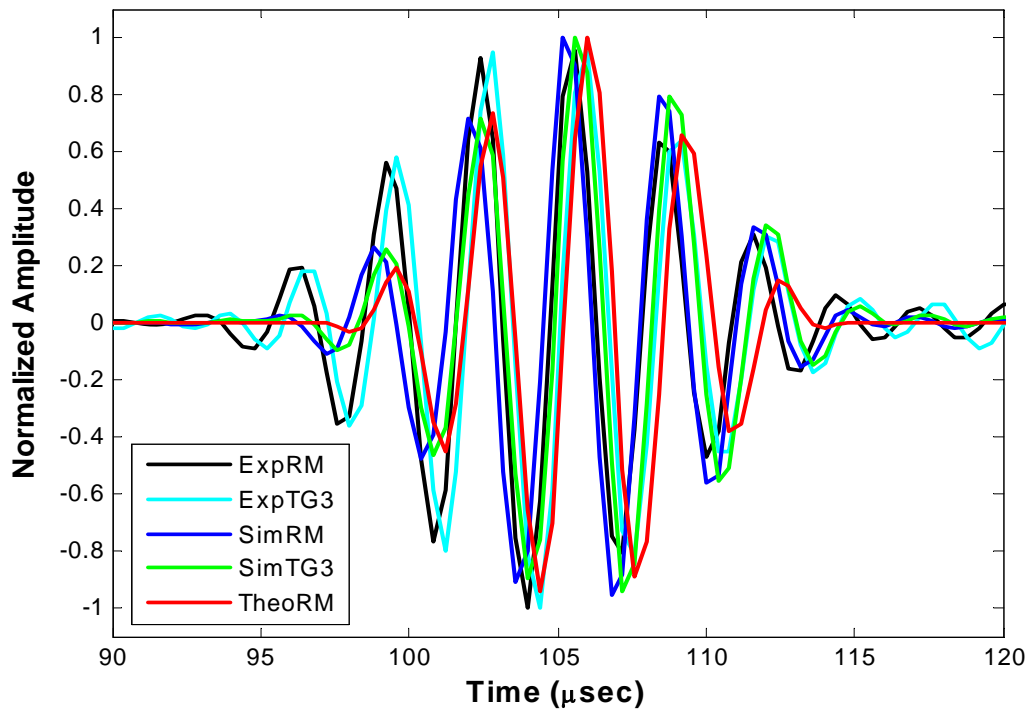


Figure 47: Specimen III S_0 response comparison(RM vs TG 3) at 300kHz

Normalized S_0 Response at 500 kHz: Propagated over 512 mm

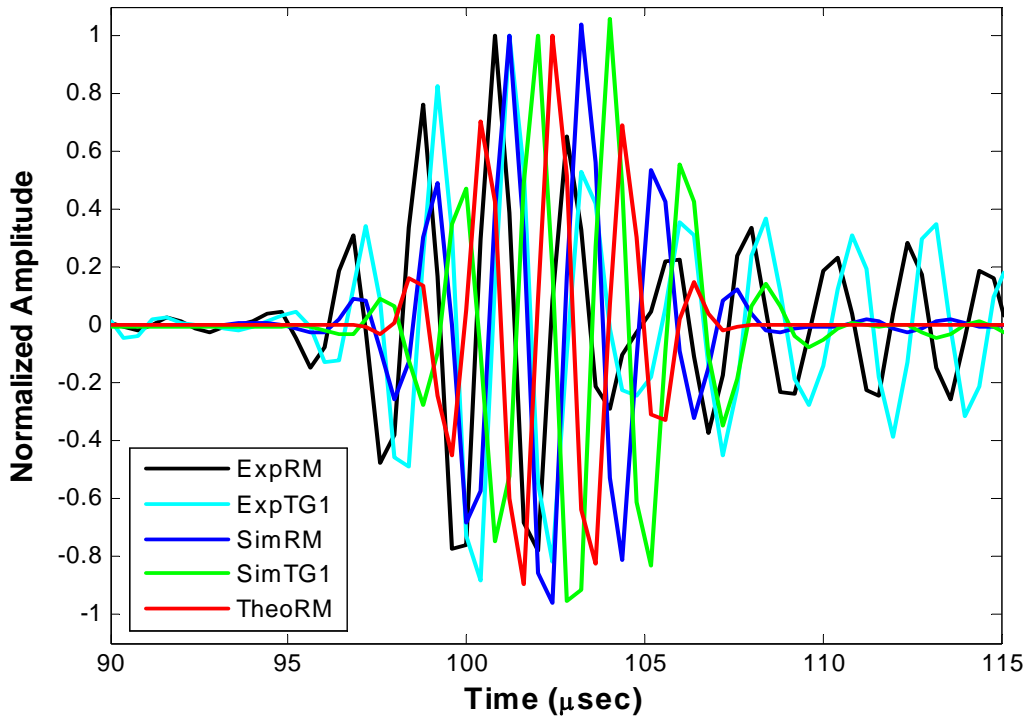


Figure 48: Specimen III S_0 response comparison(RM vs TG 1) at 500kHz

Normalized S_0 Response at 500 kHz: Propagated over 512 mm

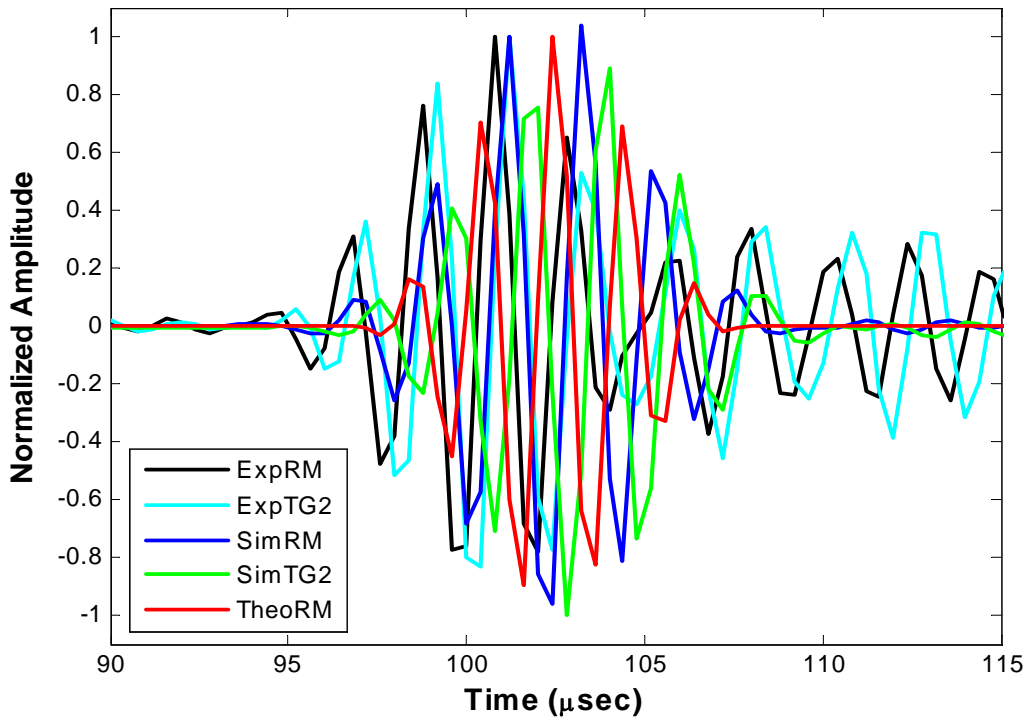


Figure 49: Specimen III S_0 response comparison(RM vs TG 2) at 500kHz

Normalized S_0 Response at 500 kHz: Propagated over 512 mm

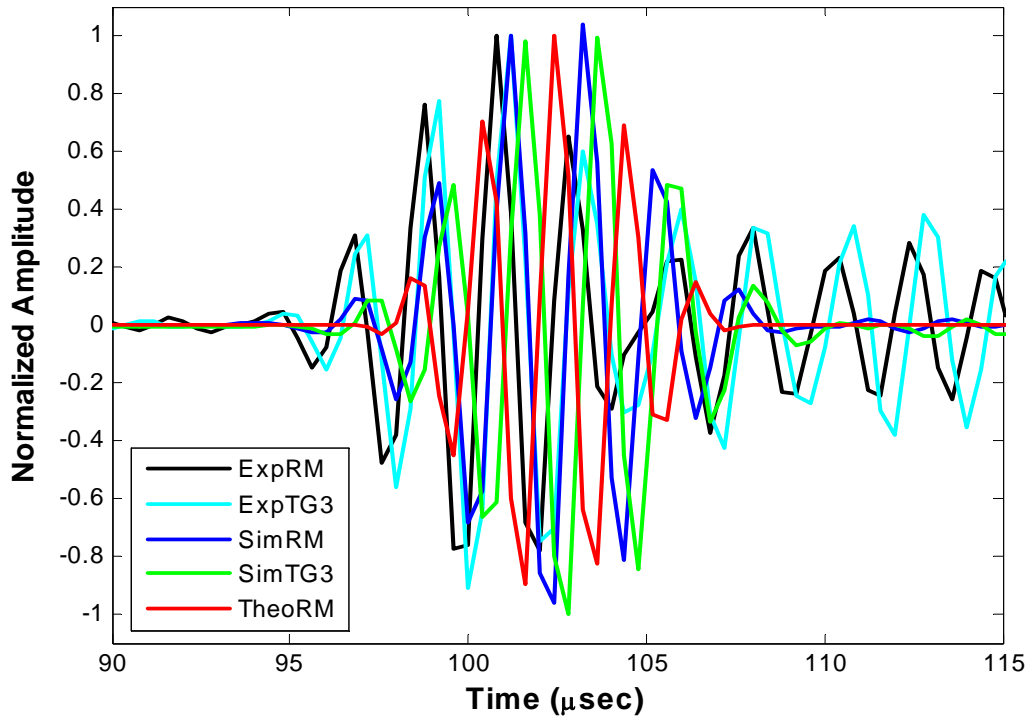


Figure 50: Specimen III S_0 response comparison(RM vs TG 3) at 500kHz

4.2.2 Thermal Stress and Bowing Phenomenon

In this thesis, the thermal gradient field is imposed onto the wave propagation analysis by importing the result of ABAQUS Standard to the ABAQUS Explicit. Since the quasi-static state is difficult to obtain when ABAQUS Explicit is dealing with the heat transfer problem, ABAQUS Standard is used to get the quasi-static thermal gradient state.

The thermal gradient has two types of fields. The one is the temperature variation along with the wave path. The other is the thermal stress field that is generated by thermal expansion of the model. The simple theory of thermal stress is introduced in Section 2.5.1.

The first object of the thermal gradient test is to verify the effect of the thermal stress on the wave propagation. However, since the wave propagation analysis is conducted when the thermal gradient reaches the steady state condition, the effect does not look significant. After the

specimen reaches the steady state condition, the thermal stress field almost becomes uniform since strong stresses are dispersed to the circumference through time. Stresses of only -0.176 N/mm^2 are observed in the steady state.

In this section, the bowing phenomenon is explained using the thermal stress simulation. The thermal stress field, that is generated in the specimen III, does not look like the thermal stress field that is generated in the simple Timoshenko(25) model introduced in Section 2.5.1, even though the temperature field in the steady state is uniform through the thickness. The reason why they are different is in the temperature function. In Timoshenko(25) model, the temperature function depends only on the x-variable. However, in this model, the temperature function does not only depend on the x-variable, the y and time variables are also included in the temperature function.

Since the temperatures of the thermal gradient are measured at the 10 thermocouples(TCs), each node point which is located at the same location with the TCs is designed in the model as a heat source as shown in Figure 51. T1 and T2 indicate different temperatures of the thermal gradient that are applied to the nodes. These node points are called heating points in this thesis. The heat is transferred to the plate radially from each heating point as the temperature of the heating point is increased. This heat transfer phenomenon generates a more complex thermal stress field through the whole specimen, since the stresses that are generated due to the restriction of expansion in x and y-direction, are generated from the heating points to the circumference as the temperature field propagates.

The temperature function, which is applied to the heating points, is shown in Figure 52. The temperatures of the source node points are increased to the specific temperatures(i.e., the temperatures are measured at the TCs) smoothly for ten seconds. Then, the node points keep the same temperatures until the specimen reaches steady state. One thousand seconds is used in the simulation. Figure 53 shows the heat transfer from one heating point through time. As time

increases the non-uniform temperature through the thickness become uniform just as the Timoshenko model.

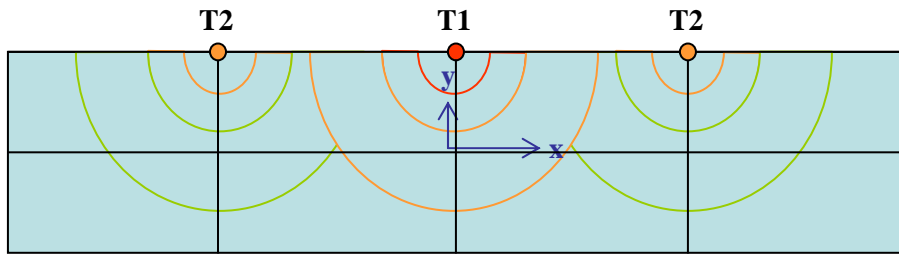


Figure 51: Heat transfer from the heating points

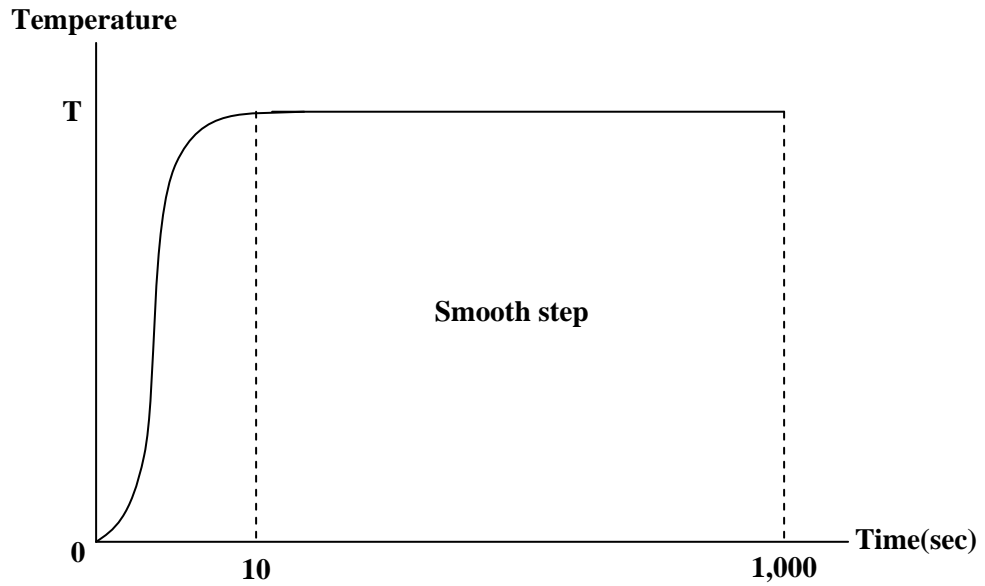


Figure 52: Temperature function at the heating points

The maximum thermal stress, the important factor of the bowing phenomenon, is generated at the beginning of the heat transfer, as anticipated, since the temperature differences between neighbor elements that cause the thermal stress are largest at the beginning. At the beginning, the high temperature at the heating point transfers to the room temperature, therefore, the temperature difference is large. However, as the temperature transfers, the circumferential temperature is increased and the temperature difference becomes small. Figure 54 (a) shows the maximum σ_x stress field through the thickness and the stress field is plotted in Figure 55. Figure 54 (b) shows the maximum σ_y stress field through the thickness and the stress field is plotted in Figure 56.

As mentioned previously, the different thermal stress field(i.e., asymmetric thermal stress field) through the thickness is observed in this simulation unlike the symmetric thermal stress field in the Timoshenko model. The through the thickness asymmetric thermal stress field can explain the bowing phenomenon of specimen III because the different stress on the top and bottom surface of the specimen III can cause a bending moment.

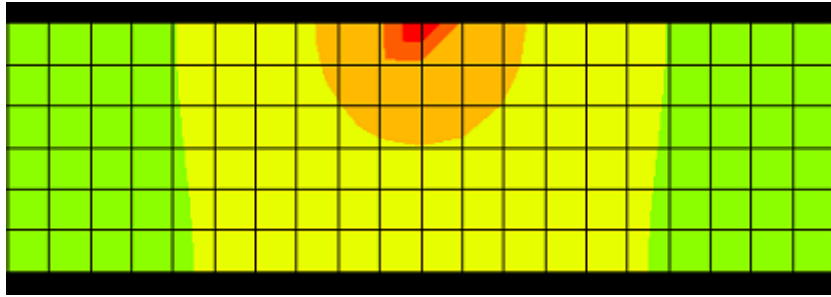
The bowing phenomenon is not occurring in the simulation since geometric instability is not considered but the maximum stress is -220 psi($-1.52 \text{ N} / \text{mm}^2$) as shown in Figure 54.

Additional real experimental conditions seem to contribute to increased thermal stresses. Since the thermal stress field is asymmetric, the increased thermal stress generates a stronger bending moment and causes the bowing of the plate.

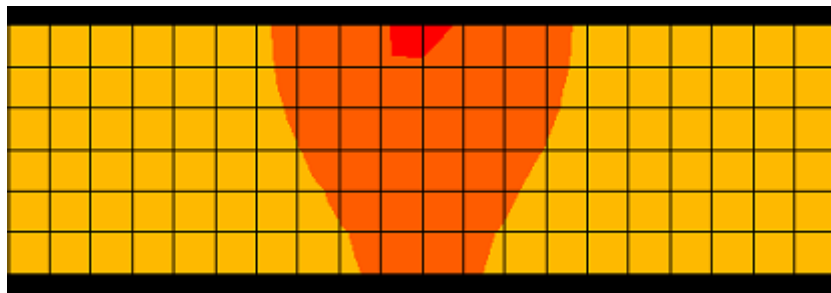
The additional factors which increase the thermal stress are as follows. First, friction between the support(felt) and the specimen increases the thermal stress because it restricts the expansion of the element. Second, effect of the gravity needs to be included since the gravity increases the friction between the support and the specimen. Third, as shown in Figure 16, the thermal gradient is not uniform through the width unlike experimental purposes. The uniform

thermal gradient is important because it generates the consistent thermal stress fields that is similar to the thermal stress field in the 2-D plane strain model. The non-uniform thermal gradient through the width generates more restrictions on the expansion and creates a complex thermal stress field.

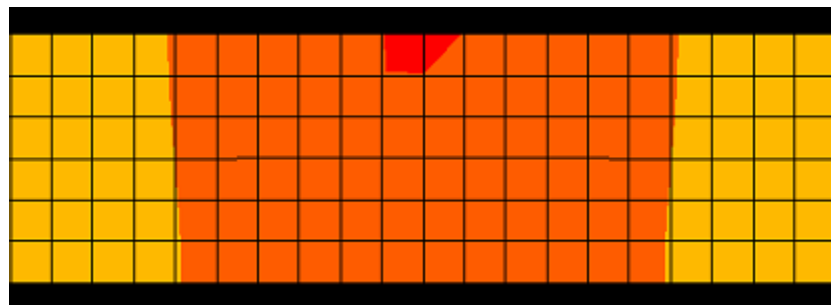
In addition, in the ABAQUS simulation, the thermal boundary condition(i.e., zero heat flux through the bottom surface) is used to alternate with the felt in the experiment. Since the felt insulates the heat transfer from the bottom surface of the specimen to an ambient material(like a lab table), making a zero heat flux at the bottom surface of the model in the simulation can show similar heat transfer phenomenon and thermal stress fields. Recall that the thermal stress field is related to the heat transfer phenomena.



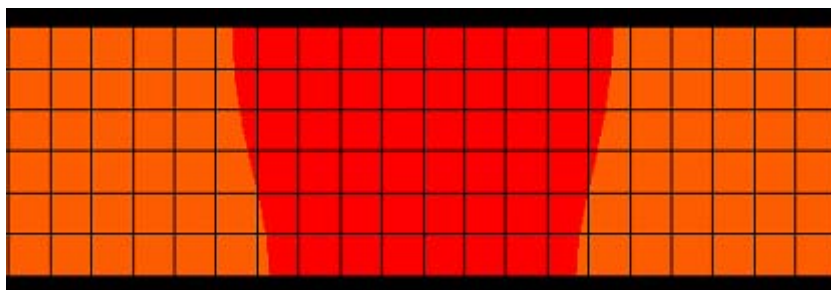
After one second



After three seconds

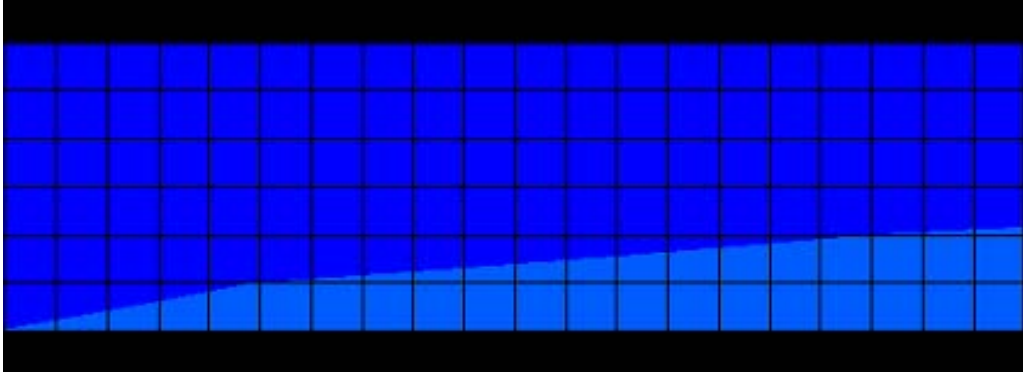


After four seconds

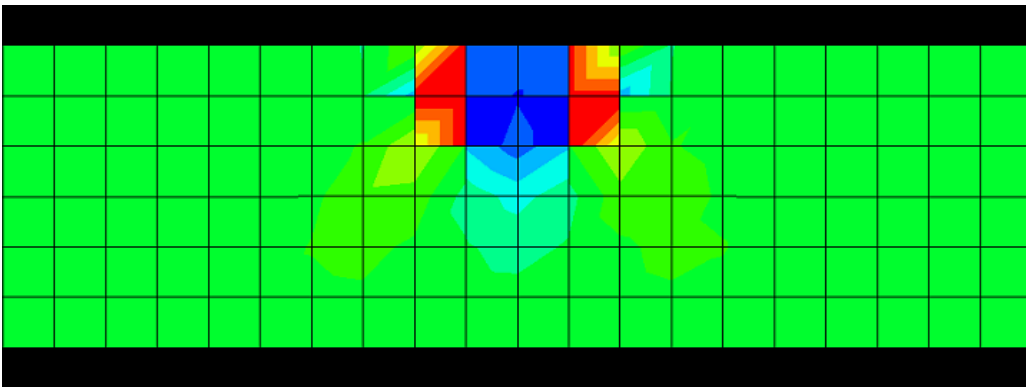


After seven seconds

Figure 53: Heat transfer from the one heating point through the time



(a)



(b)

Figure 54: Thermal stress field, (a) : σ_x , (b) : σ_y through the thickness

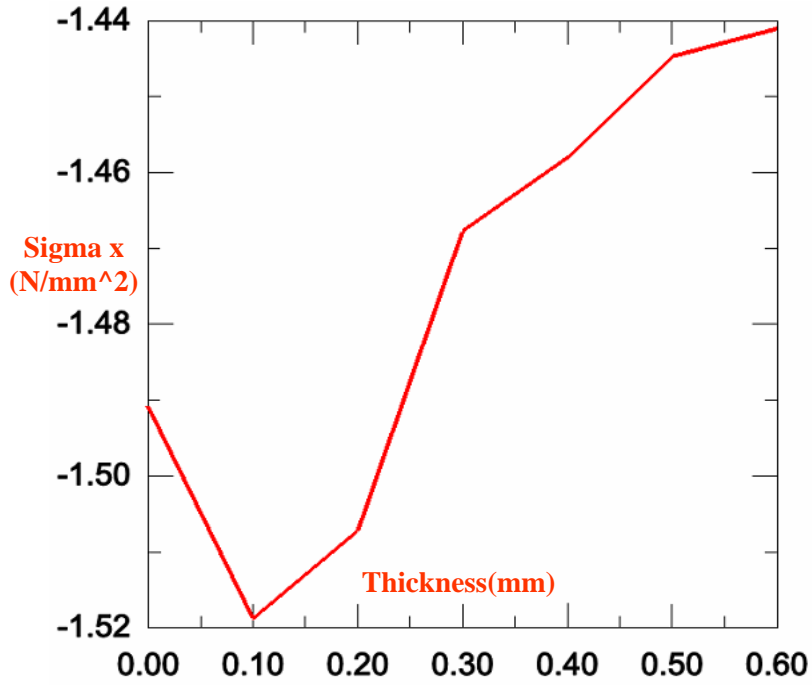


Figure 55: Plot of σ_x through the thickness

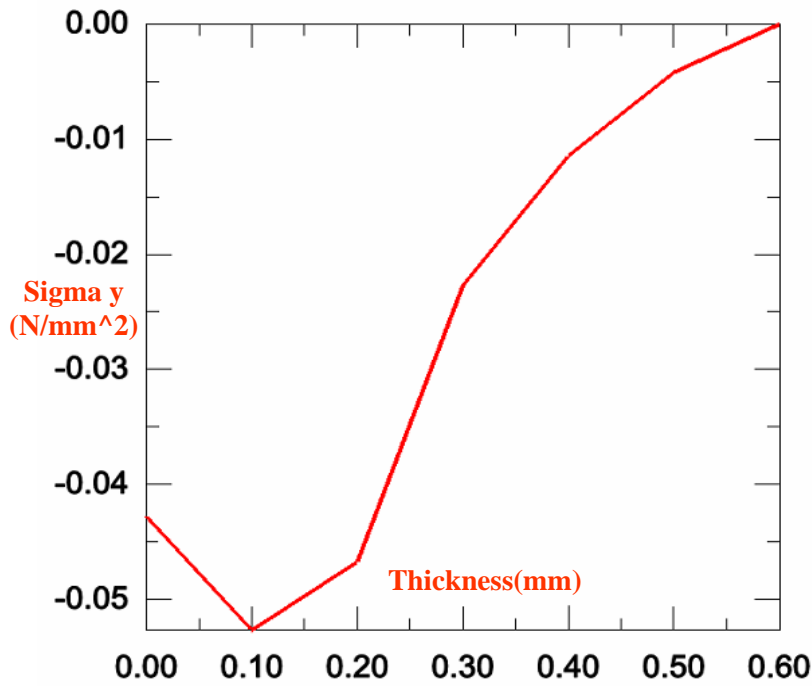


Figure 56: Plot of σ_y through the thickness

Chapter 5 Summary & Conclusions

The objective of this thesis is to evaluate Lamb wave propagation through an aluminum plate considering various signal pulse rates incorporating the finite element code ABAQUS CAE. These simulated results are compared to the theoretical predictions and experimental results under isothermal and thermal gradient conditions. To assess the sensitivity of the S_0 responses, the waveform and the time of arrival(TOA) are determined.

In order to accomplish the objectives, the isothermal ABAQUS simulation is conducted under 9 temperature(0, 25, 50, 75, 100, 125, 150, 175 and 190°F) and 2 frequency(100 and 300kHz) conditions. The thermal gradient ABAQUS simulation is conducted under three thermal gradient and three frequency conditions.

In all wave propagation analysis, it is apparent that the wave speeds are reduced by the increased temperature. As mentioned previously, these phenomena can be explained by the relations between elastic modulus and the temperature.

As shown in the results analysis of Chapter 4, similar waveforms and close TOA between the simulated results and the other two types of results are enough to explain the possibility of the ABAQUS simulation in Lamb wave analysis. However, some differences between these results are also observed. These differences are assumed to be affected by the noise that is brought by the experimental setting. The experimental results include not only the responses that we want to observe but also noise that is generated by a real experimental setting. For precise analysis, this unexpected noise needs to be distinguished and explained. In this meaning, ABAQUS can provide important criteria for distinguishing this noise from the pure results because the ABAQUS results include everything(i.e., combination of the various Lamb wave modes and reflected Lamb waves) that occur during the analysis except the noise that is related with the experimental setting. Thus, most close(wrt experiment) and ideal results are provide by ABAQUS. However, ABAQUS can not distinguish separately the Lamb wave modes and

reflected waves since everything is in one result. The Matlab program is useful since it provides every single Lamb wave mode for a specific time. Consequently, the simulation has an important meaning since it can verify the accuracy of the experimental setting and results. Also, the experiment verifies the theoretical appropriateness through the simulation.

Small fluctuations, which are observed after the simulated S_0 responses, are explained by the differences between simulated/experimental excitation signal and theoretical excitation signal. Each simulated/experimental excitation has some noise after its five and a half cycle pulse. This noise can affect the responses. Note, it can explain small fluctuations after the S_0 responses in the simulated and the experimental results.

In addition, some small and large fluctuations are observed before and after the experimental S_0 responses. These can be explained by the magnetic noise. As mentioned previously, the magnetic noise is a weakened excitation signal which is generated at the sensor at the same time the excitation signal is excited. After the magnetic noise is generated, it is propagating to the circumference of the sensor. The small fluctuations before the S_0 responses are explained by the residual effect after the magnetic noise propagates since it does not sufficiently damp out. The large fluctuations after the S_0 responses are explained by the interaction between two reflected waves of the magnetic noise. Note, it can explain small and large fluctuations before and after the experimental S_0 responses.

Existence of the different experimental waveforms in Figures 42 – 44(at 200 kHz) is not explained properly. In these figures, the experimental S_0 responses appear a lot faster than other S_0 responses. In order to find out the reason for this phenomenon, a raw experimental signal is analyzed. In the raw experimental response signal, another large noise is observed between the magnetic noise and S_0 responses. This noise can change the waveform of the experimental response, however proper reason which generates the noise is not revealed.

To generate more ideal responses, wave absorability that occurs through the supports and air boundary conditions in the experiment needs to be built in the simulation and additional efforts to reduce the noise in the experimental responses are needed.

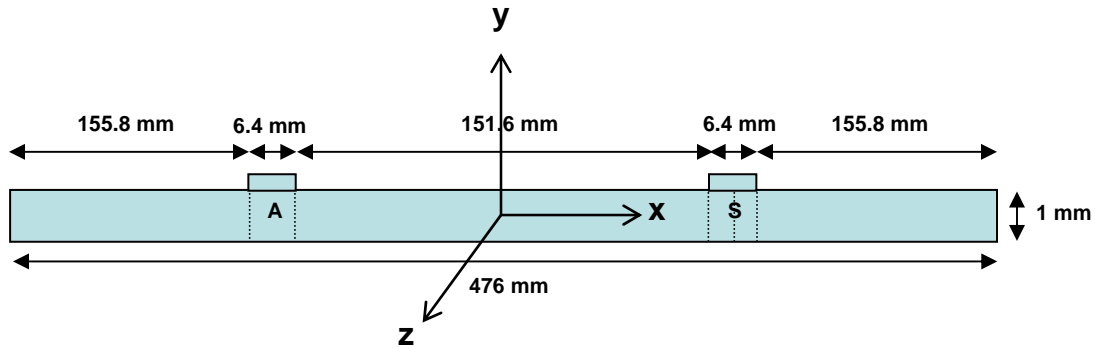
The wave propagation analysis is conducted after the thermal gradients reach steady state. The thermal stress field is evaluated for the wave propagation analysis. However, any significant changes, due to the effect of the thermal stress, in the waveform and TOA of the response are not observed. This is because of the low stress value (-0.176 N / mm^2) of the steady state thermal stress field. Since we can only use the steady state thermal stress field because of the sensitivity of the wave, it seems to be difficult to observe the effect of the thermal stress on the wave propagation. Obviously, if high stress is used for the wave analysis, it will cause deformation and displacement on the specimen and it will disturb the wave analysis.

In the thermal gradient experiment, a plate bow occurs. Since the low thermal stress in the steady state is not enough to explain the bowing phenomenon in the experiment, the high thermal stress field at the beginning of the simulation is considered and compared with Timoshenko's(25) basic thermal stress theory. Timoshenko's(25) model generates a symmetric thermal stress field through the thickness, therefore it can not explain the bowing phenomenon. However, the simulation, which is designed for the purpose of generating the same thermal stress field as the experiment, shows the asymmetric thermal stress field through the thickness. The bowing phenomenon is explained by the asymmetric thermal stress characteristic since the differences between the thermal stress at the top and bottom surfaces generate a bending moment with respect to the mid-plane of the specimen.

APPENDIX A: ISOTHERMAL SIMULATION WITHIN ABAQUS CAE

A. Mission

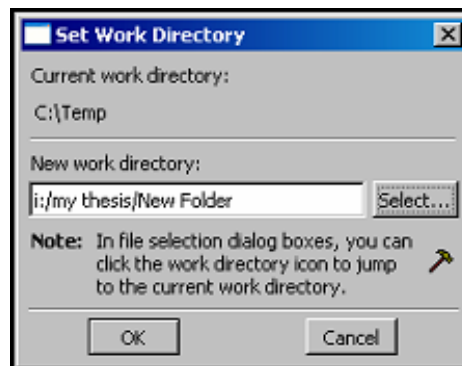
1. The dimension of the SPECIMEN I is shown below:



2. The material properties of the SPECIMEN I is shown in Table 4 & 5.
3. Use the total time of $400 \mu \text{ sec}$, the time increments of 5 nsec, the element length of 0.1mm.
4. To match with the experimental data, the output data of this simulation should be collected every $0.4 \mu \text{ sec}$.
5. The objective of this simulation is getting the U displacements at the three sensing points. (i.e., i, i+1, i+2 in Figure 23)

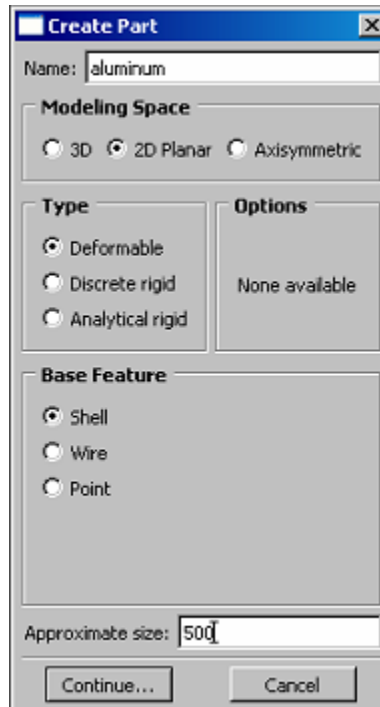
B. Preliminaries


1. File > Set Work Directory : All files which are generated will be saved in this directory.




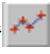
C. Module : Part

1. To create a part, go to the menu bar at the top of the screen and click on “Part > Create” and do the following:
 - a) Choose the setting in the pop-up window as shown below.



- b) Click “Continue”.
- c) Next click “ Create Lines : Rectangle (4 Lines)” icon in the toolbox window on the left of the screen.
- d) Move the cursor to the sketch pad window and click on a point that locates the upper left corner of the model, next drag the cursor and click on a point that locates the lower right corner of the model.
- e) Click the “Create Lines : Rectangle (4 Lines)” icon once again.
- f) Click “done”

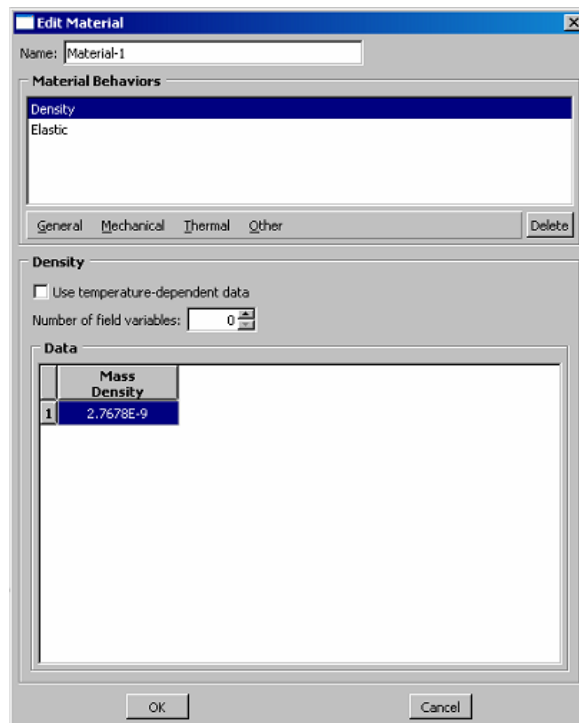
2. To split the beam into six sections, do the following:

- a) Click on the icon  “Partition Face : Sketch”.
 - b) Click on the icon  “Create Lines : Connected”.
 - c) Move the cursor to the specific points(i.e. edge of the actuator and edge & mid point of the sensor) of the model on the top surface and click. Next move the cursor downward and click on the points of the model on the bottom surface.
 - d) Click on the icon “Create Lines : Connected” once again.
 - e) Click “done”.
- ✳ The beam is now split into six sections.

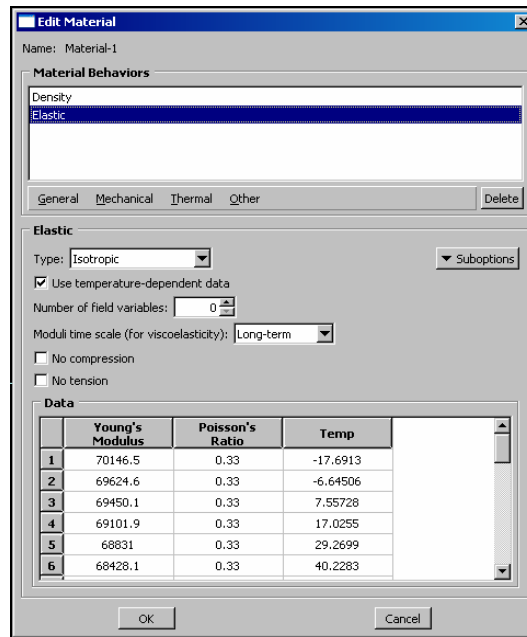
D. Module : Property

1. To create the material definition, do the following:

- a) Click on Material > Create and enter a material name and click General > Density and input the value as shown below.

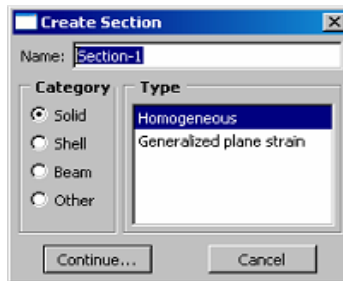


- b) Click Mechanical >Elasticity > Elastic and input values for elasticity and Poisson’s ratio, click “OK” as shown below.

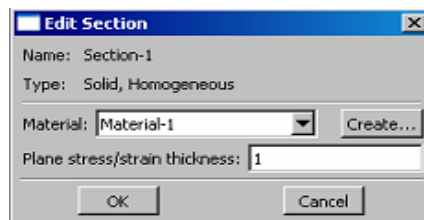


2. To define the section properties, do the following:

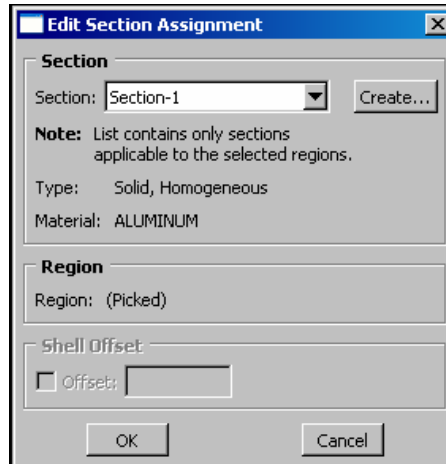
- a) Choose Section > Create from the toolbar.
 b) Give the section a name and click the radio buttons Category : Solid, Type : Homogeneous. Click “Continue” as shown below.



- c) Choose defaults. Click “OK” as shown below.



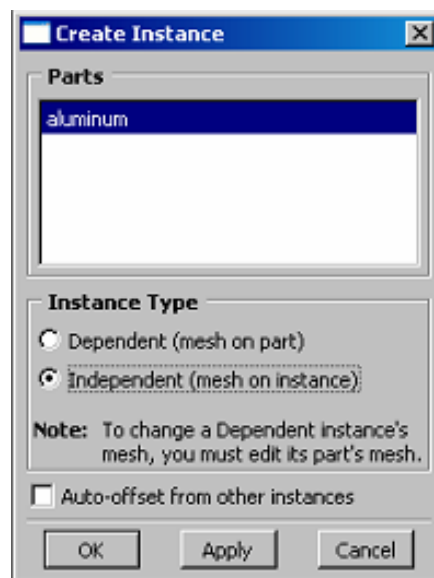
3. To assign the section properties to the section of the model, do the following:
 - a) Choose Assign > Section from the toolbar.
 - b) Click entire model. Click “Done”.
 - c) The Edit Section Assignment window pops up, click “OK” as shown below.



- d) Click “Done”.

E. Module : Assembly

1. To assemble the model, do the following:
 - a) Choose Instance > Create.
 - b) Choose Instance Type : Independent (mesh on instance), click “OK” as shown below.

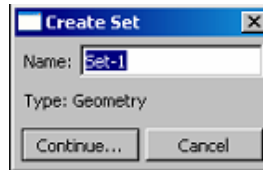


F. Module : Step

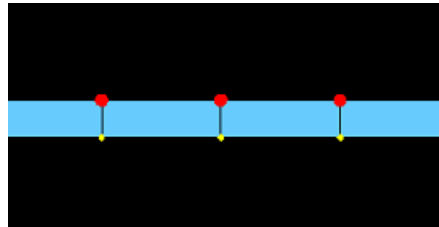
1. To create the node set do the following:

a) Choose Tools > Set > Create.

b) Create Set window pops up, Give a name for the set, click “Continue” as shown below.



c) Click on the edges and the mid-point location of the sensor as shown below.



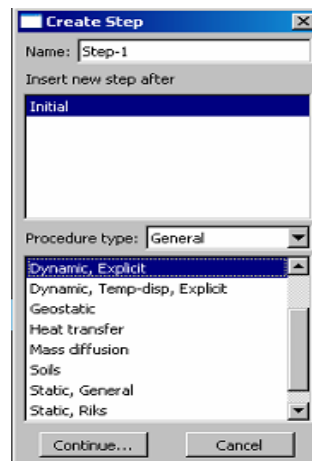
d) Click “Done”.

✳ The sensing points(i, i+1, i+2) are generated using node set(Set-1).

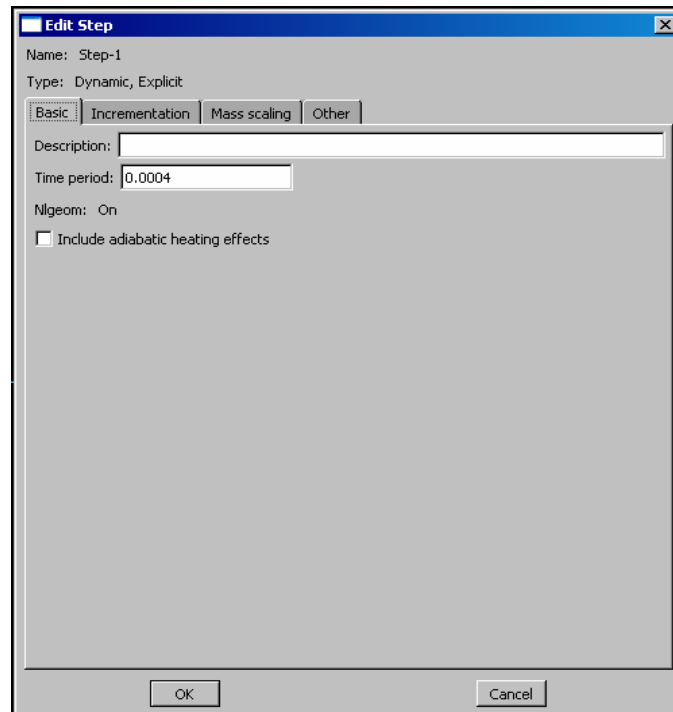
2. To configure the analysis, do the following:

a) Choose Step > Create.

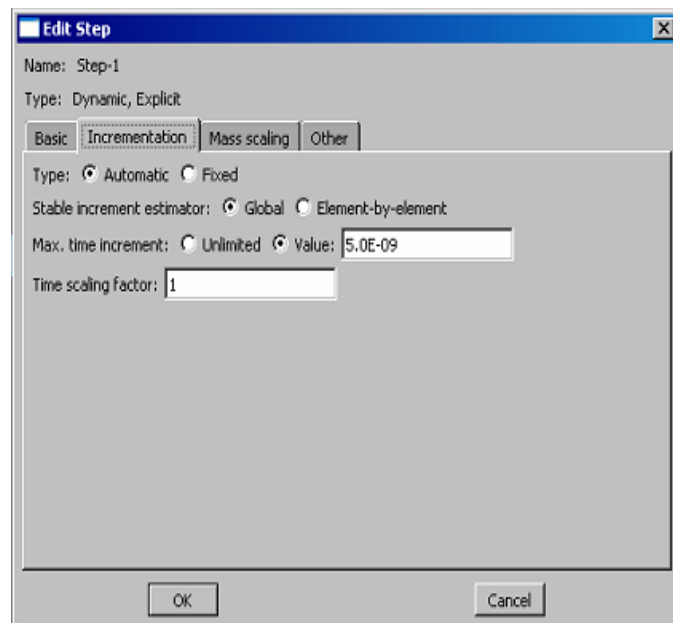
b) Give a name for the step, click “Dynamic, Explicit” and click “Continue” as shown below.



c) Under the Basic tab, input the total time in the Time period as shown below.

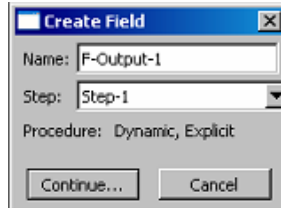


d) Under the Incrementation tab, input the time increment in the Max. time increment and click “OK” as shown below.

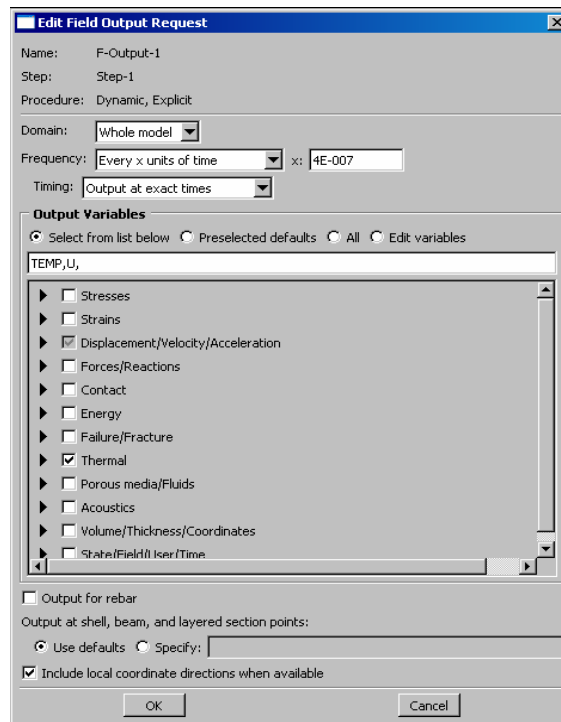


3. To control the output database(ODB), do the following:

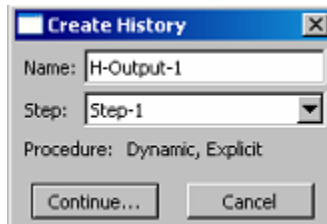
- a) Choose Output > Field Output Requests > Create, give a name for the field output and click “Continue” as shown below.



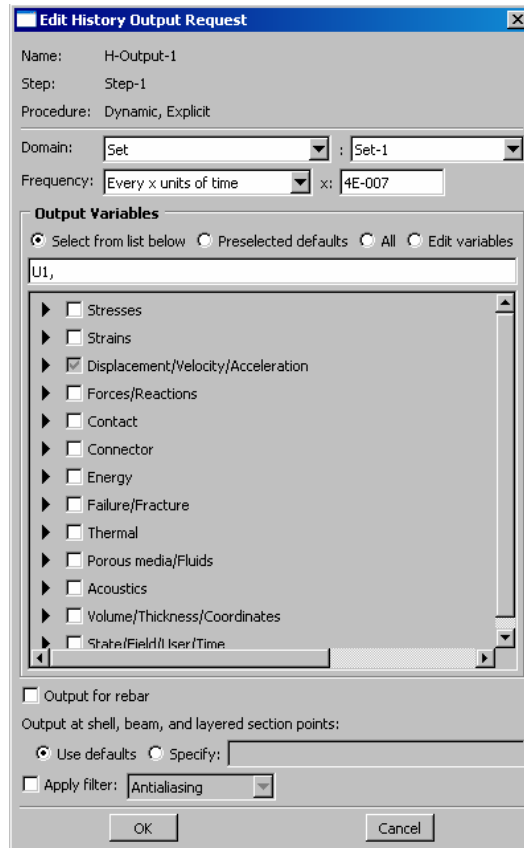
- b) Set as shown below and click “OK”.



- c) Choose Output > History Output Requests > Create, give a name for the history output and click “Continue” as shown below.



d) Set as shown below and click “OK”.



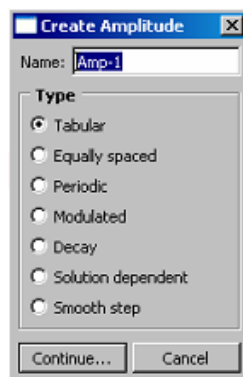
✳ Through this procedure the output data of this simulation will be collected every 0.4μ sec.

G. Module : Load

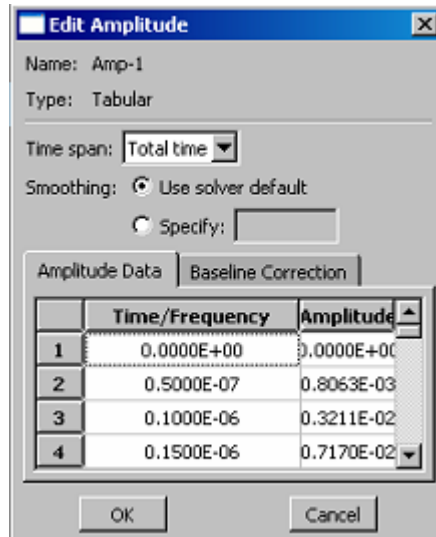
1. To product the excitation signal at the edges of the actuator, do the following:

a) Choose Tools > Amplitude > Create.

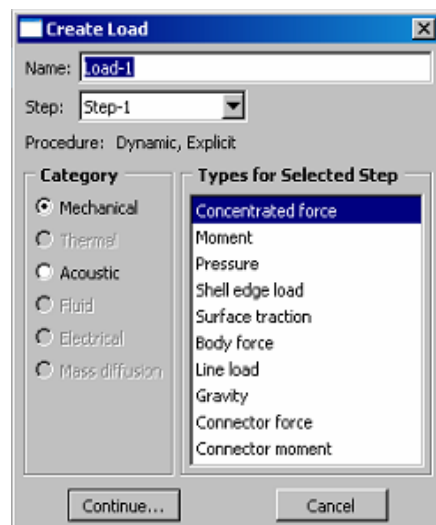
b) Give a name, choose “Tabular” radio button and click “Continue” as shown below.



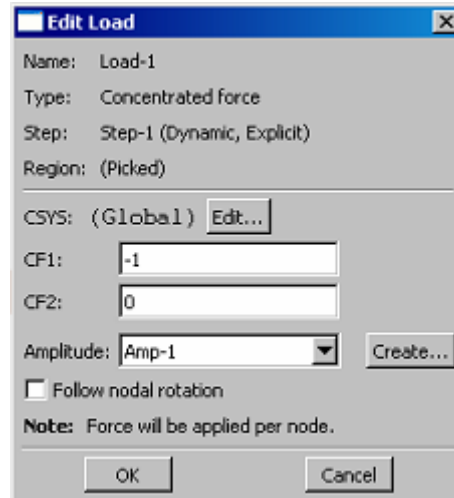
- c) Choose “Total time” in Time span and the amplitude data can be read from the experimental data files(first & second rows in Appendix D).



- d) Click “OK”.
- e) Choose Load > Create
- f) Give a name for load, choose “Mechanical” radio button in Category & “Concentrated force” in Types for Selected Step and click “Continue” as shown below.



g) Choose the CF1 value to be non-zero(left edge of the actuator : -1, right edge of the actuator : +1), CF2 value to be zero. And apply the same amplitude which we made on both of the Loads and click “OK” as shown below.

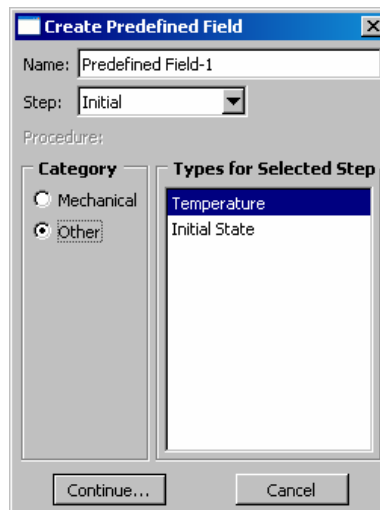


※ Apply two opposite loads at the edges of the actuator.

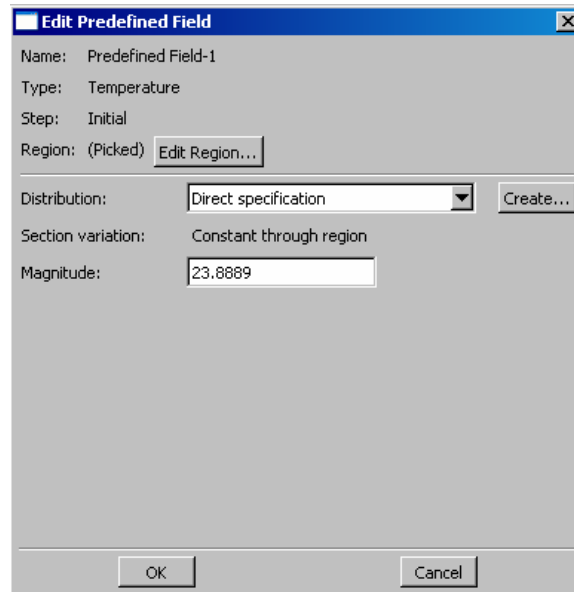
2. To decide initial temperature of the model, do the following:

a) Choose Predefined Field > Create.

b) Give a name, choose “Other” radio button in Category, Click “Temperature” in Types for Selected Step and click “Continue” as shown below.

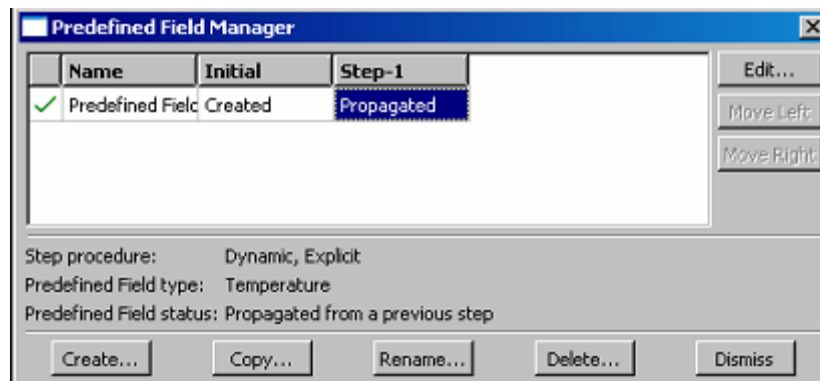


c) Input the temperature value in Magnitude and click “OK” as shown below.



✳ In this simulation, °C is used. All units in this simulation must be consistent.


✳ Initial temperature will be propagated as shown below, so during the analysis the model will keep the same temperature.



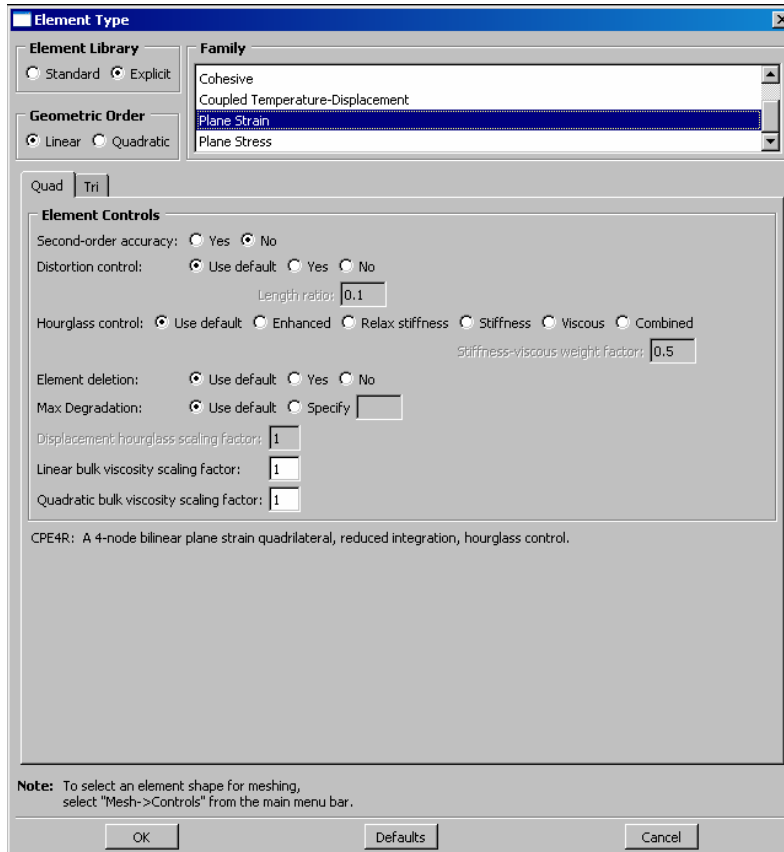
✳ Temperature of the model can be decided in this procedure. ABAQUS will use proper temperature-dependent material property during the analysis.

H. Module : Mesh

1. To decide the element type of the model, do the following:

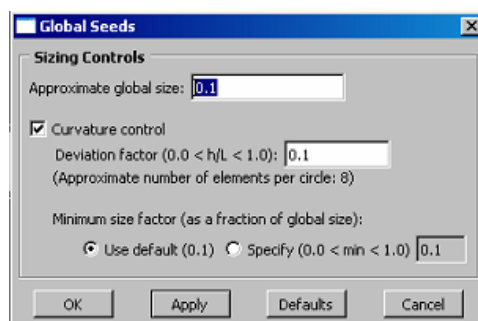
a) Choose Mesh > Element type or click on the icon “ Assign Element Type”.

- b) Click whole model by using “Shift Key” then click “Done”.
- c) Choose “Explicit” in Element Library , choose “Plane Strain” in Family and click “OK” as shown below.

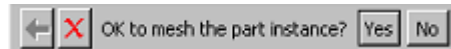


2. To mesh the model, do the following:

- a) Choose Seed > Instance, when the Global Seeds window pops up, put in the element length in Approximate global size. Click “Apply” to see how the mesh is seeded, if the mesh is seeded properly then click “OK” as shown below.



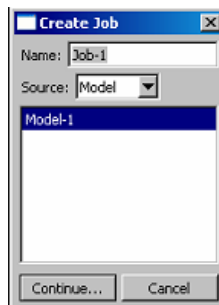
b) Choose Mesh > Instance and click “Yes” as shown below.



I. Module : Job

1. To create and submit Job, do the following:

a) Choose Job > Create, give a name to the Job(This will also become the name of the ODB file.) and click “Continue” as shown below.

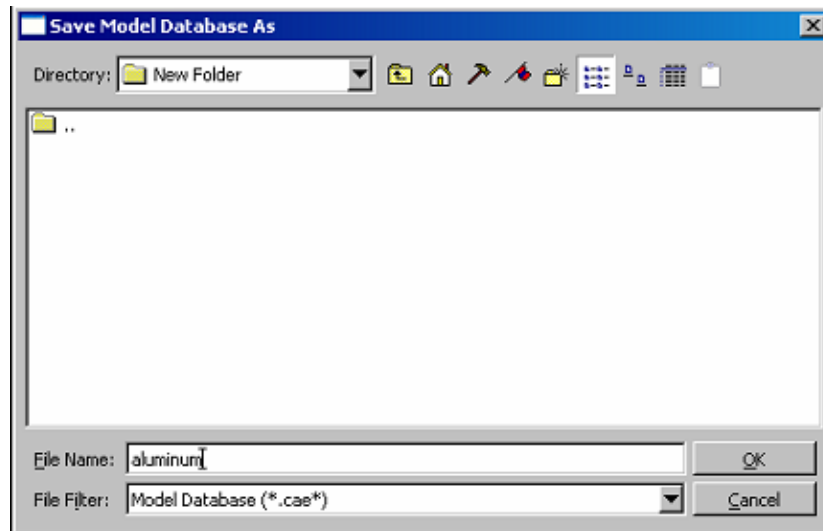


b) When the Edit Job window pops up, set “Double” in ABAQUS/Explicit precision and “Full” in Nodal output precision under Precision tab and click “OK” as shown below.



c) Choose Job > Manager, click “Submit”, then click “Monitor” to view the program execution. When Job is completed click “Dismiss” on the monitor window and click “Results” on the Job Manager window and view result.

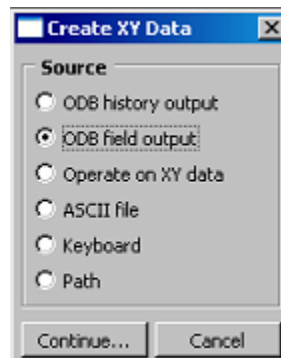
d) Save CAE file by clicking File > Save As and giving a file name.



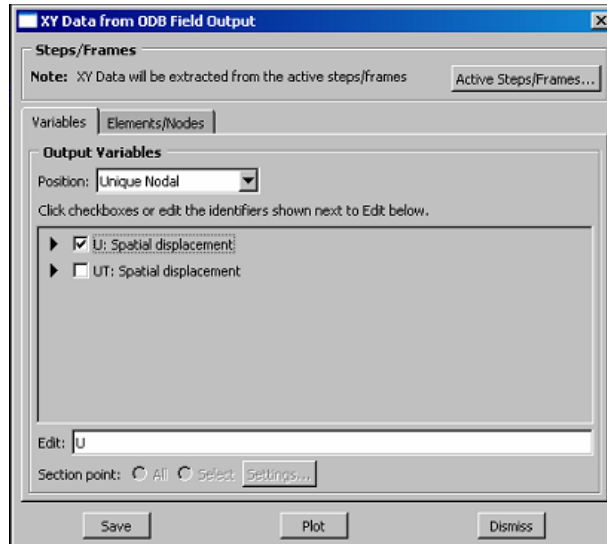
J. Module : Visualization

1. To product the rpt(report) file that contains the U displacements of the node set, do the following:

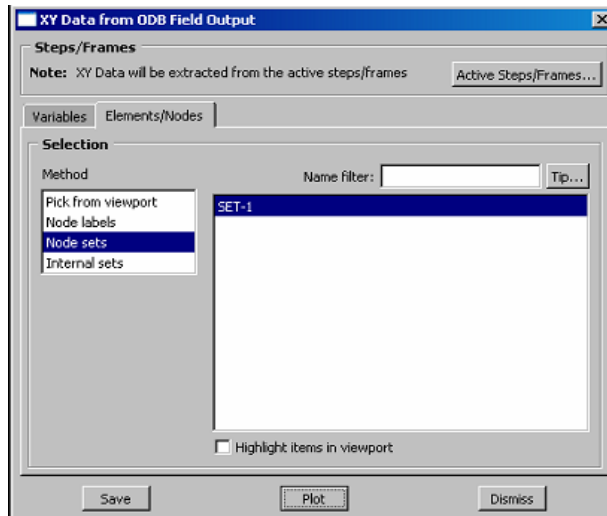
- a) Choose Tools > XY Data > Create.
- b) Choose ODB field output and click “Continue” as shown below.



c) Under Variables tab, choose “Unique Nodal” and click “U : Spatial displacement” as shown below.

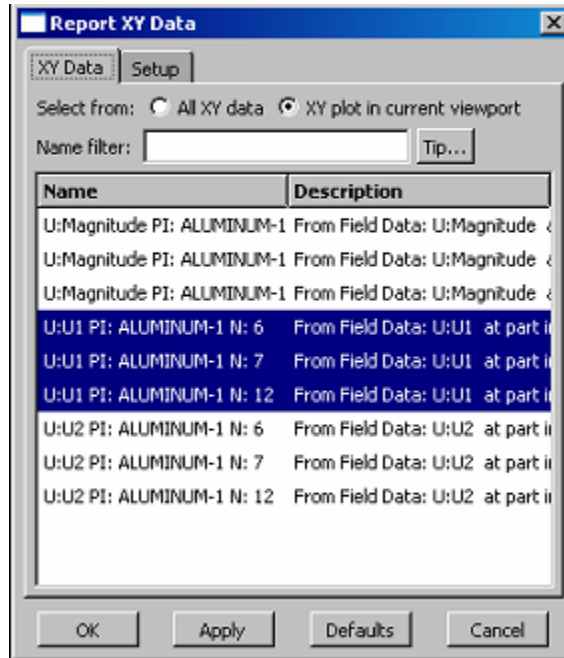


d) Under Elements/Nodes tab, choose “Node sets” in Method and click “Save” as shown below.

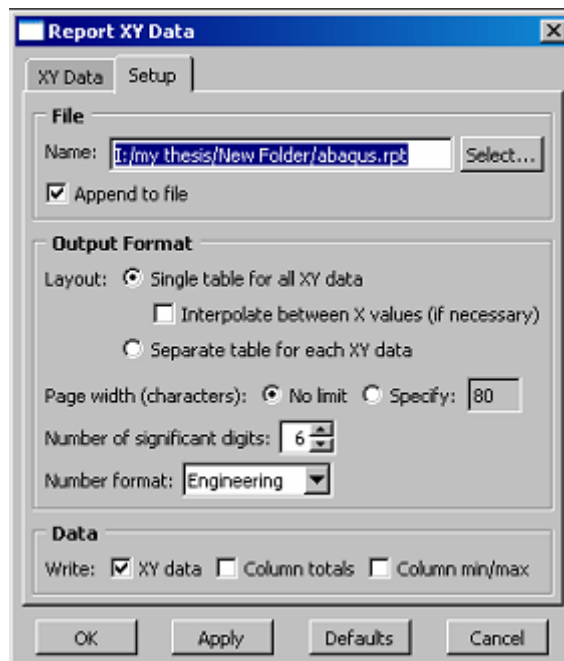


e) Choose Report > XY Data.

f) Under XY Data tab, choose “U:U1” as shown below.



g) Under Setup tab, decide “*.rpt” file name, directory and click “OK” as shown below.



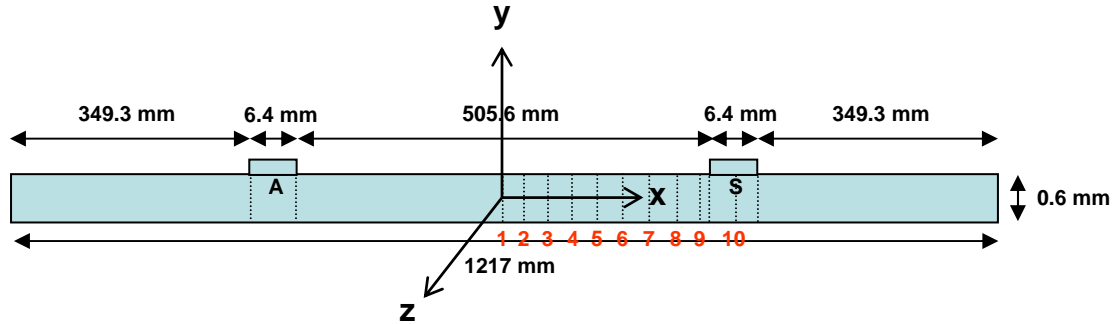
h) “*.rpt” file(i.e., Simulated S_0 response data file) is created in the Work directory.

✳ Reference Table 8 and Appendix D for the formation of the “*.rpt” file.

APPENDIX B: THERMAL GRADIENT SIMULATION WITHIN ABAQUS CAE

A. Mission

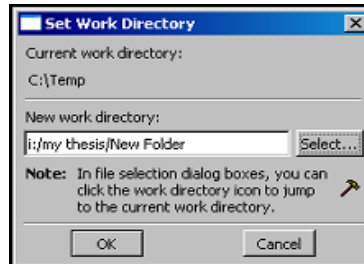
1. The dimension of the SPECIMEN III is shown below:



2. The ABAQUS Standard will be used in the thermal gradient analysis and the ABAQUS Explicit will be used in Lamb wave propagation analysis.
3. The material properties of the SPECIMEN III is shown in Table 4 & 5.
4. Three thermal gradients(i.e., TG 1, TG 2 and TG 3) of this simulation is shown in Table 3.
5. Use the total time of 1000 sec for the Standard, the total time of 400 μ sec for the Explicit, the time increments of 5 nsec and the element length of 0.1mm.
6. To match with the experimental data, the output data of this simulation should be collected every 0.4 μ sec.
7. The objective of this simulation is getting the U displacements at the sensing points.
(i.e., i, i+1, i+2 in Figure 23)

B. Preliminaries


1. File > Set Work Directory : All files which are generated will be saved in this directory.




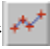
C. Module : Part

1. To create a part, go to the menu bar at the top of the screen and click on “Part > Create” and do the following:
 - a) Choose the setting in the pop-up window as shown below.



- b) Click “Continue”.
 - c) Next click “ Create Lines : Rectangle (4 Lines)” icon in the toolbox window on the left of the screen.
 - d) Move the cursor to the sketch pad window and click on a point that locates the upper left corner of the model, next drag the cursor and click on a point that locates the lower right corner of the model.
 - e) Click the “Create Lines : Rectangle (4 Lines)” icon once again.
 - f) Click “done”

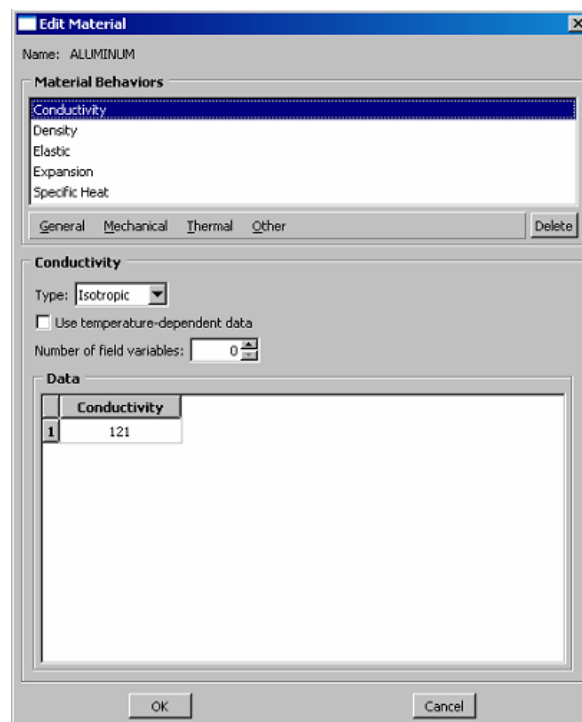
2. To split the beam into 24 sections, do the following:

- a) Click on the icon  “Partition Face : Sketch”.
 - b) Click on the icon  “Create Lines : Connected”.
 - c) Move the cursor to the specific points(i.e. edge of the actuator, edge & mid point of the sensor and location of the thermocouples) of the model on the top surface and click. Next move the cursor downward and click on the points of the model on the bottom surface.
 - d) Click on the icon “Create Lines : Connected” once again.
 - e) Click “done”.
- ※ The beam is now split into 24 sections.

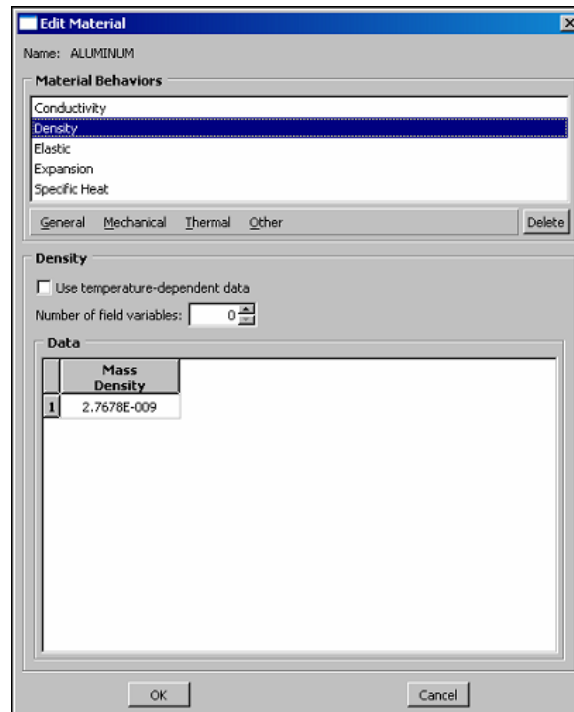
D. Module : Property

1. To create the material definition, do the following:

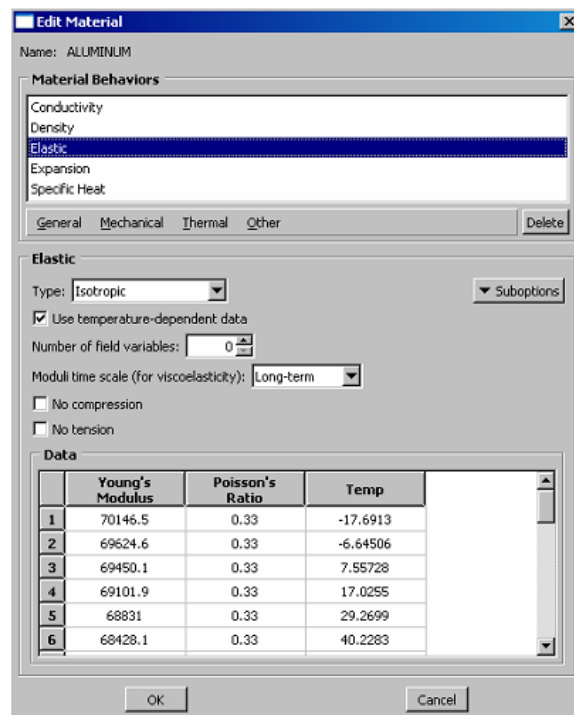
- a) Click on Material > Create and enter a material name and click Thermal > Conductivity and input the value as shown below.



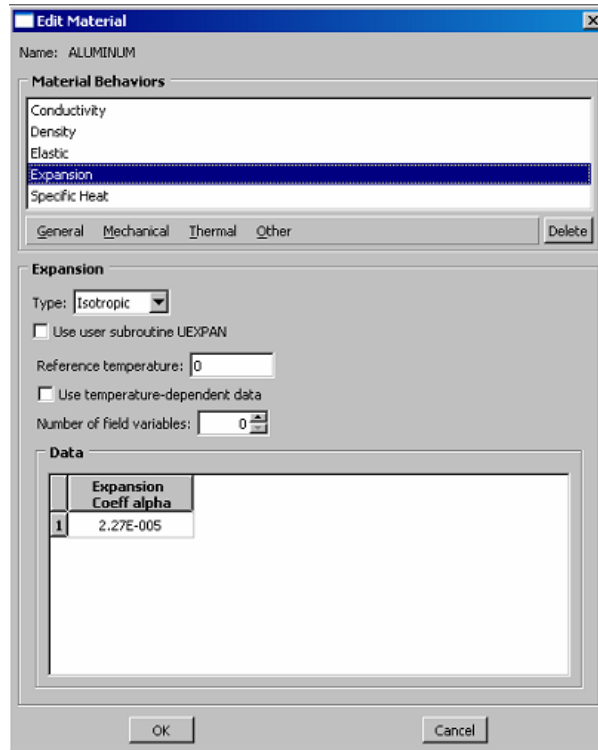
b) Click General > Density and input the value as shown below.



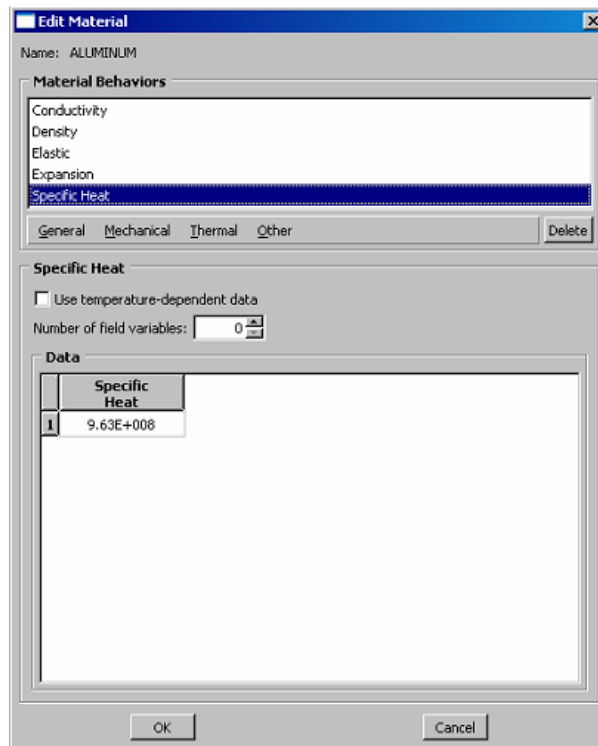
c) Click Mechanical > Elasticity > Elastic and input values for elasticity and Poisson's ratio, click "OK" as shown below.



d) Click Mechanical > Expansion and input the value as shown below.

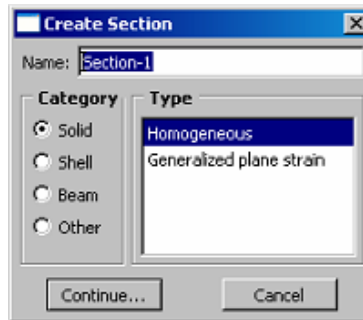


e) Click Thermal > Specific Heat and input the value as shown below.

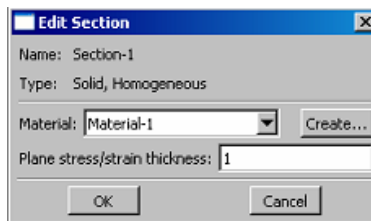


2. To define the section properties, do the following:

- a) Choose Section > Create from the toolbar.
- b) Give the section a name and click the radio buttons Category : Solid, Type : Homogeneous. Click “Continue” as shown below.

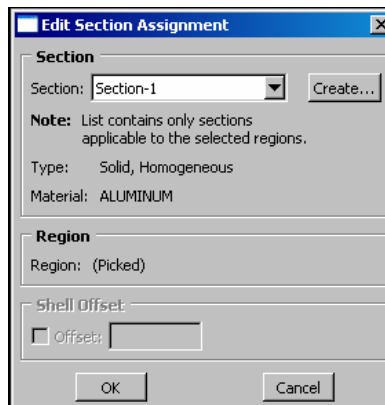


- c) Choose defaults. Click “OK” as shown below.



3. To assign the section properties to the section of the model, do the following:

- a) Choose Assign > Section from the toolbar.
- b) Click entire model. Click “Done”.
- c) The Edit Section Assignment window pops up, click “OK” as shown below.

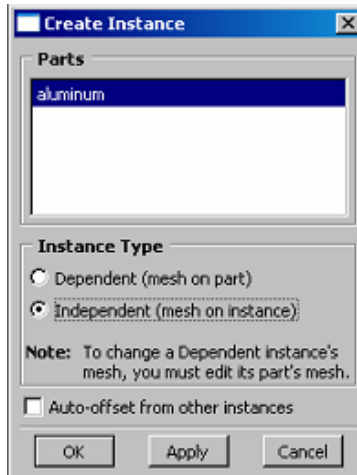


- d) Click “Done”.

E. Module : Assembly

1. To assemble the model, do the following:

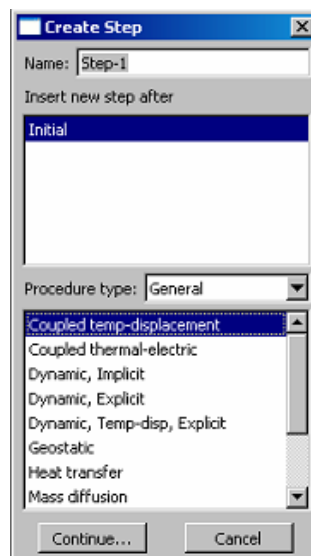
- a) Choose Instance > Create.
- b) Choose Instance Type : Independent (mesh on instance), click “OK” as shown below.



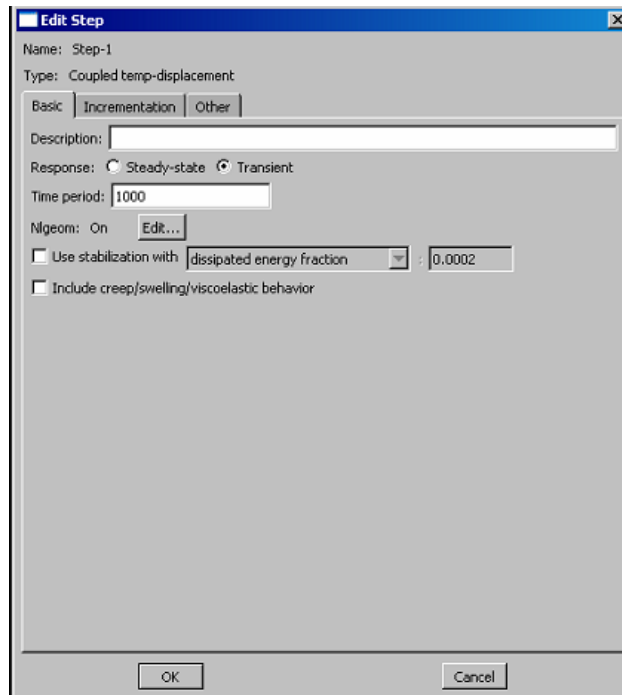
F. Module : Step

1. To configure the analysis, do the following:

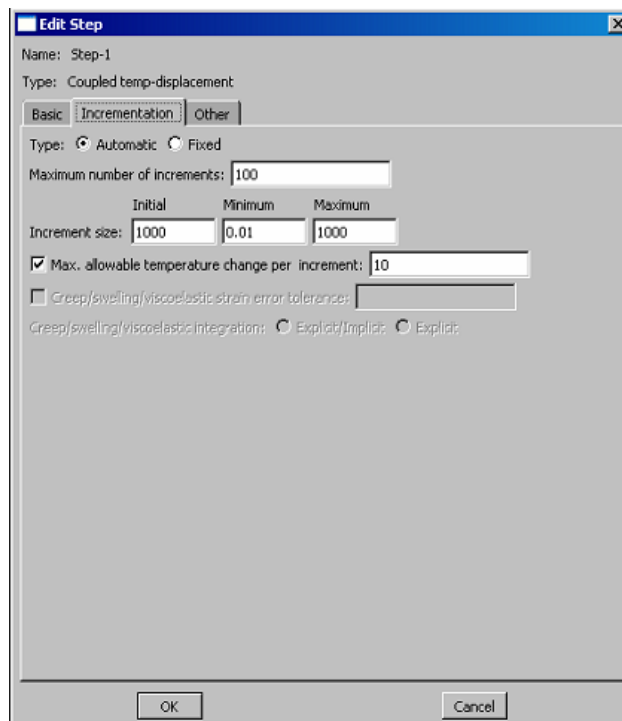
- a) Choose Step > Create.
- b) Give a name for the step, click “Coupled temp-displacement” and click “Continue” as shown below.



c) Under the Basic tab, input the total time in the Time period as shown below.

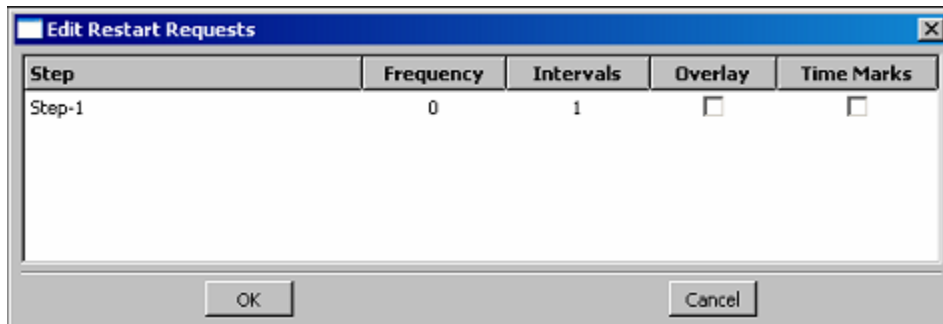


d) Under the Incrementation tab, input the value in Max. allowable temperature change per increment and click “OK” as shown below.



2. To request the restart data file, do the following:

a) Choose Output > Restart Requests and set as below.



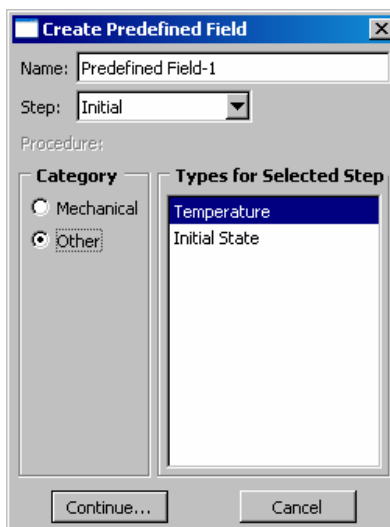
✳ Data files, which are needed when the Explicit imports the ODB of the Standard, can be produced through this procedure.

G. Module : Load

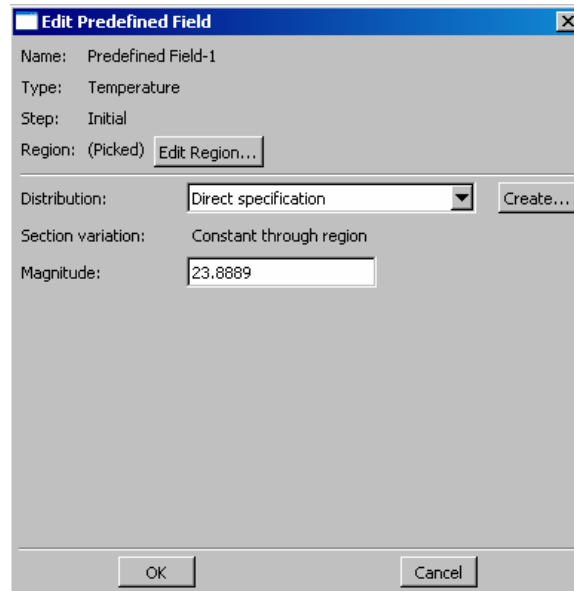
1. To decide initial temperature of the model, do the following:

a) Choose Predefined Field > Create.

b) Give a name, choose “Other” radio button in Category, Click “Temperature” in Types for Selected Step and click “Continue” as shown below.

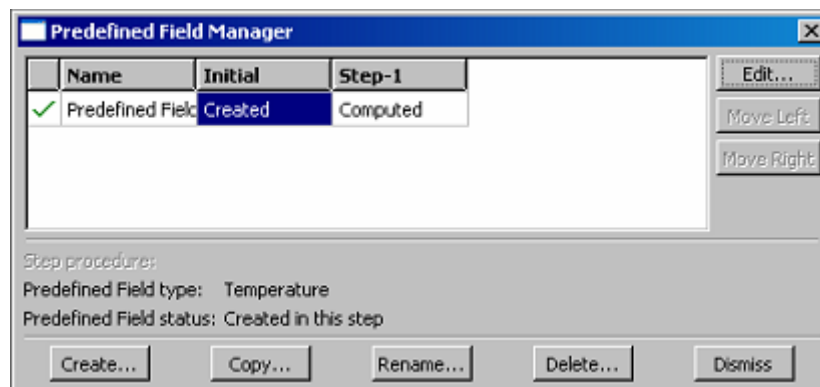


c) Input the temperature value in Magnitude and click “OK” as shown below.



✳ In this simulation, °C is used. All units in this simulation must be consistent.

✳ Initial temperature(room temperature) will be computed as shown below, so during the analysis the temperature of the model will be calculated.

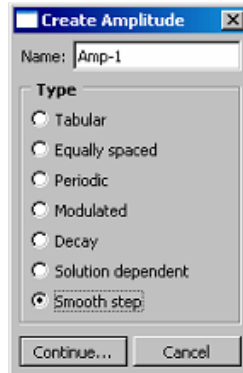


✳ Initial temperature of the model can be decided in this procedure.

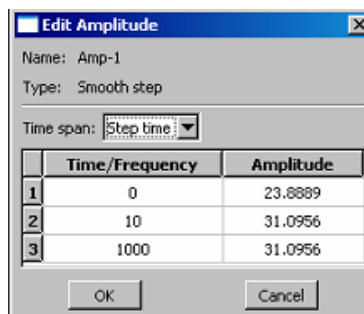
2. To create the thermal gradient, do the following:

a) Choose Tools > Amplitude > Create.

b) Give a name, choose “Smooth step” radio button and click “Continue” as shown below.

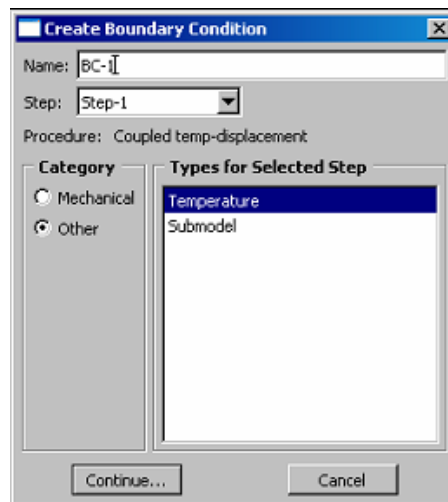


c) Choose “Step time” in Time span and the amplitude data can be read from Table 3.

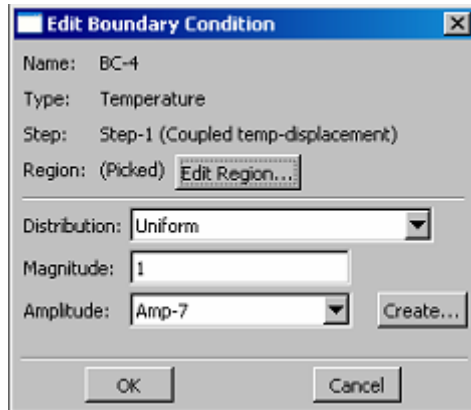


✳ Each thermocouple has its own amplitude, so make 10 amplitudes.

d) Choose BC > Create and the temperature can be decided using BC as shown below.



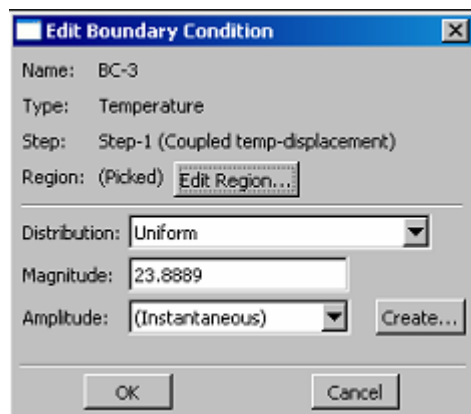
e) The thermal gradient can be produced by using amplitudes which we made at the locations of the thermocouples.



✳ Each of the thermocouple has its own BC. Since the thermal gradient is symmetric, only 10 BCs are needed.

✳ BC of the thermocouple will be applied only at the upper surface of the model like the experiment.

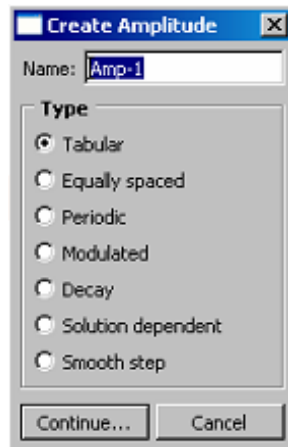
f) The rest of region(i.e., region except the thermal gradient) of the model will be set as the room temperature(same as initial temperature).



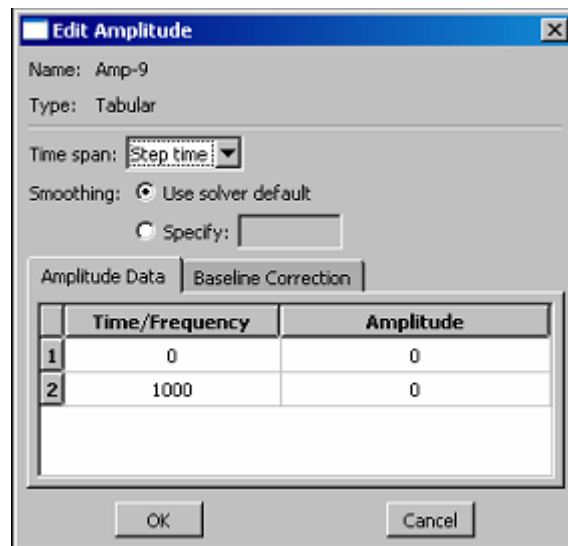
3. To create surface heat flux, do the following:

a) Choose Tools > Amplitude > Create.

b) Give a name, choose “Tabular” radio button and click “Continue” as shown below.

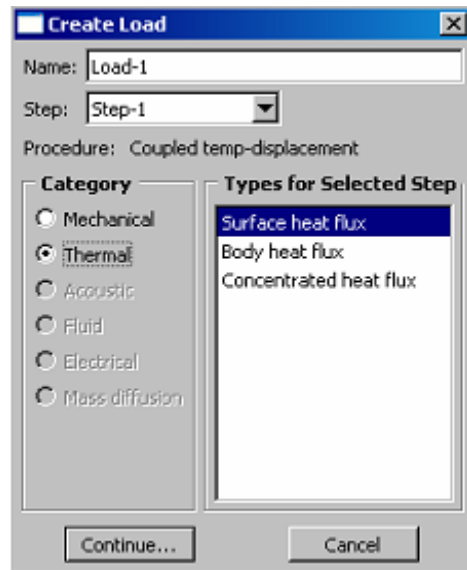


c) Choose “Step time” in Time span and set the amplitude data as shown below.

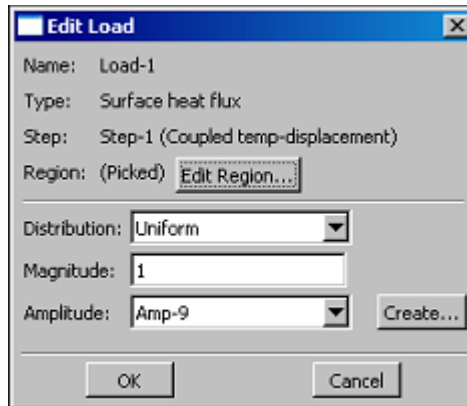


d) Choose Load > Create

- e) Give a name for load, choose “Thermal” radio button in Category & “Surface heat flux” in Types for Selected Step and click “Continue” as shown below.

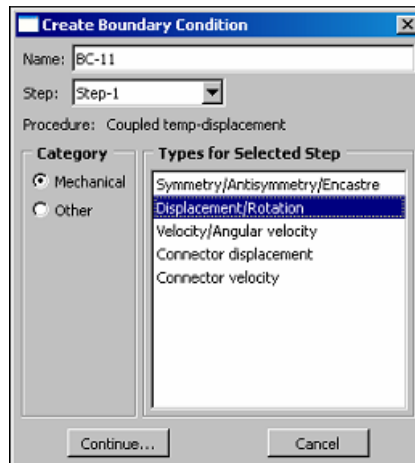


- f) Input a value in Magnitude, apply the amplitude which we made in previous procedure in Amplitude and click “OK” as shown below.

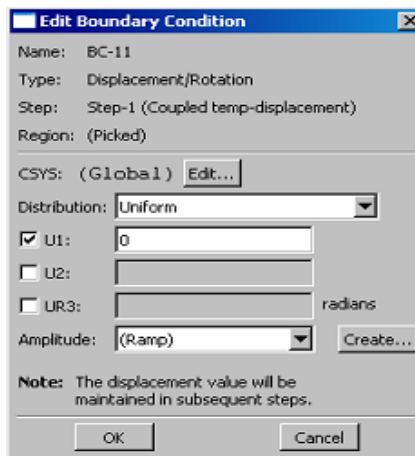


- ✳ Purpose of this procedure is making zero surface heat flux, however zero value can not be used in Magnitude. Therefore zero amplitude is used instead.
 - ✳ Zero surface heat flux allows uniform thermal gradient through the thickness at steady state.
4. Because of the instability of the simulation, physical boundary conditions are needed.

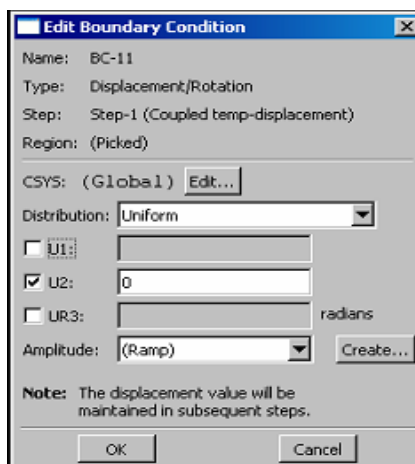
a) Choose BC > Create and the physical BC can be decided as shown below.



b) Restrict U-1 of the centerline of the sensor as shown below.




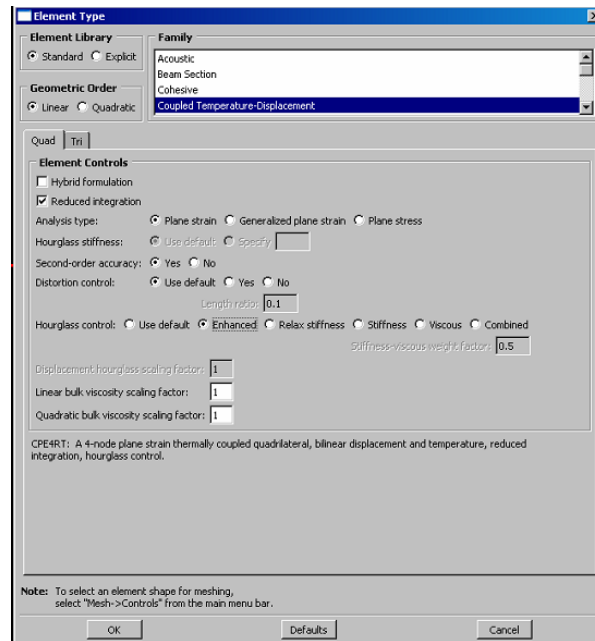
c) Restrict U-2 of the bottom surface of the model as shown below.



H. Module : Mesh

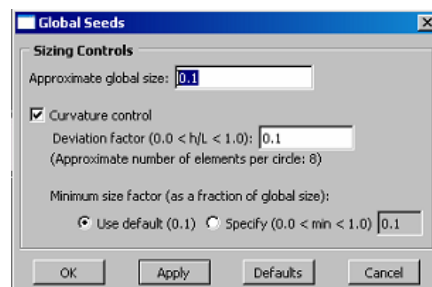
1. To decide the element type of the model, do the following:

- a) Choose Mesh > Element type or click on the icon  “Assign Element Type”.
- b) Click whole model by using “Shift Key” then click “Done”.
- c) Choose “Standard” in Element Library, choose “Coupled Temperature-Displacement” in Family, set as below and and click “OK”.

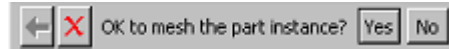


✳ Second-order accuracy and Enhanced Hourglass control are recommended.

- d) Choose Seed > Instance, when the Global Seeds window pops up, put in the element length in Approximate global size. Click “Apply” to see how the mesh is seeded, if the mesh is seeded properly then click “OK” as shown below.



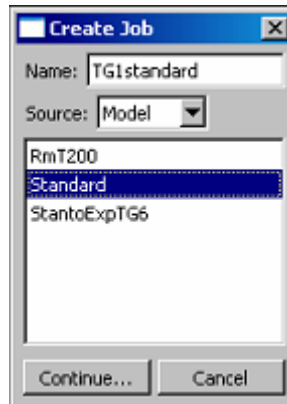
e) Choose Mesh > Instance and click “Yes” as shown below.



I. Module : Job

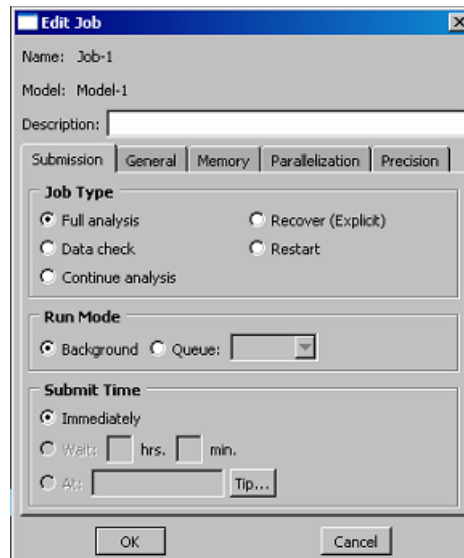
1. To create and submit Job, do the following:

a) Choose Job > Create, give a name to the Job(This will also become the name of the ODB file.) and click “Continue” as shown below.



✳ The name of this Job will be used in Explicit for importing the thermal gradient.

b) When the Edit Job window pops up use the defaults and click “OK” as shown below.



- c) Choose Job > Manager, click “Submit”, then click “Monitor” to view the program execution as shown below. When Job is completed click “Dismiss” on the monitor window and click “Results” on the Job Manager window and view result.

※ After checking the result of the Standard, Explicit will proceed subsequently.

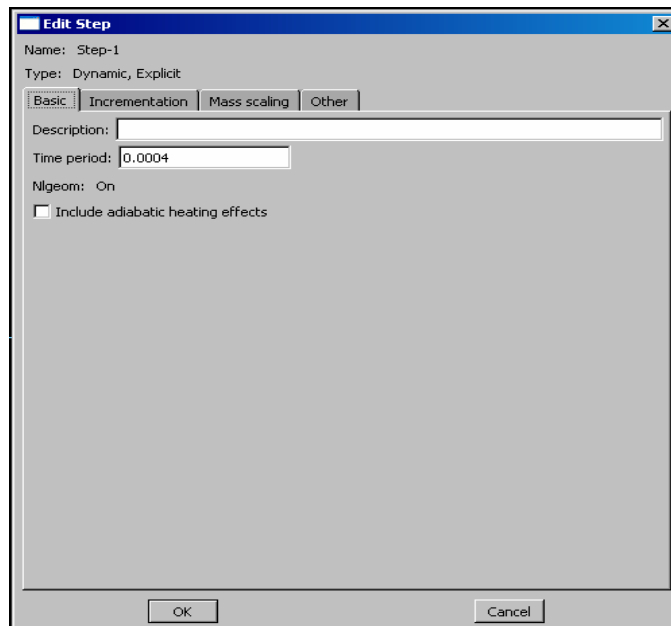
-----<EXPLICIT>-----

J. Preliminaries(From now on, a copied Standard model will be treated.)

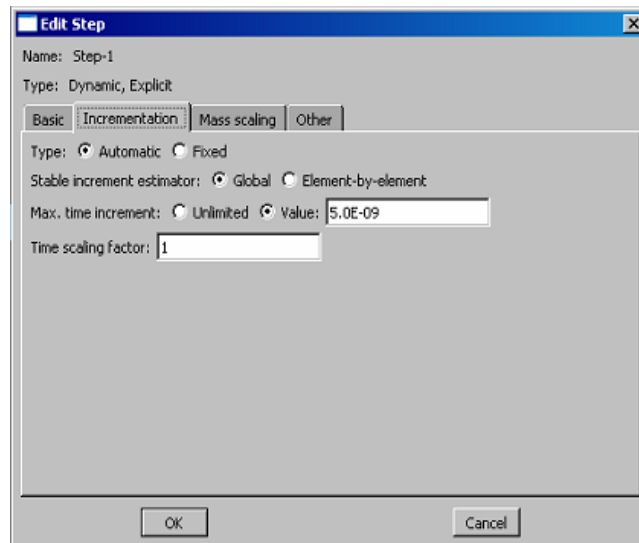
1. Make a copy of the Standard model by clicking right mouse button on the Standard model.
2. BC, Surface heat flux and Predefined field, which are made in Standard Load Module, are useless in Explicit. So they need to be erased before proceeding.

K. Module : Step

1. To replace the step, do the following
 - a) Choose Step > Replace.
 - b) Replace the “Coupled temp-displacement” step to “Dynamic, Explicit” and click “Continue”.
 - c) Under the Basic tab, input the total time in the Time period as shown below.

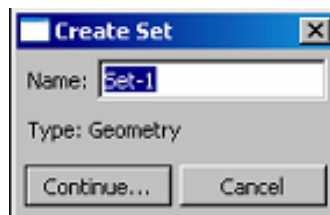


- d) Under the Incrementation tab, input the time increment in the Max. time increment and click “OK” as shown below.

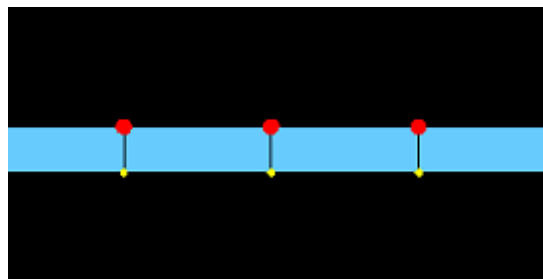


2. To create the node set do the following:

- a) Choose Tools > Set > Create.
b) Create Set window pops up, Give a name for the set, click “Continue” as shown below.



- c) Click on the edges and the mid-point location of the sensor as shown below.

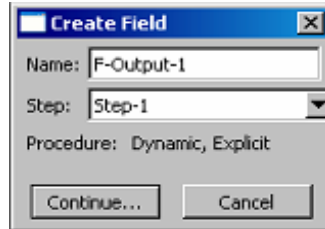


- d) Click “Done”.

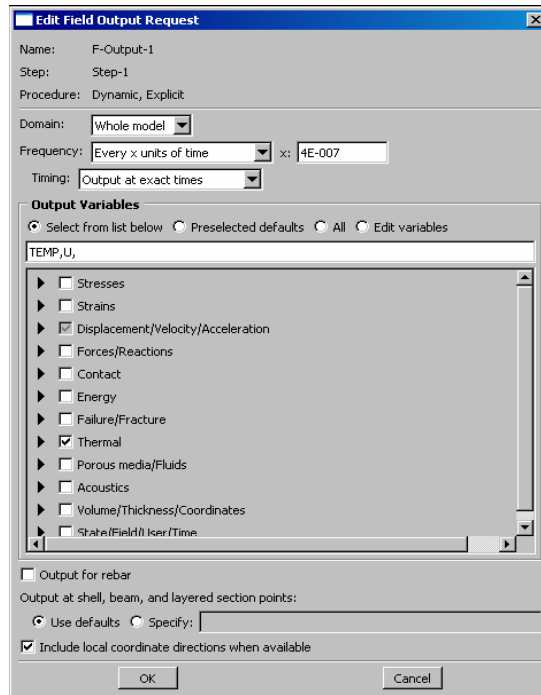
✳ The sensing points(i, i+1, i+2) is decided using node set(Set-1).

3. To control the output database(ODB), do the following:

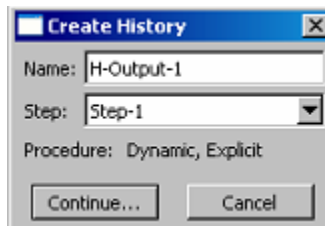
- a) Choose Output > Field Output Requests > Create, give a name for the field output and click “Continue” as shown below.



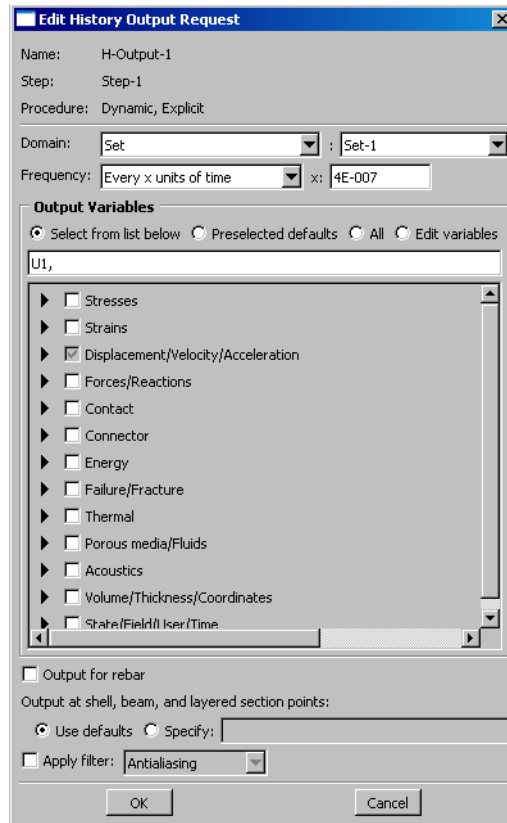
- b) Set as shown below and click “OK”.



- c) Choose Output > History Output Requests > Create, give a name for the history output and click “Continue” as shown below.



d) Set as shown below and click “OK”.



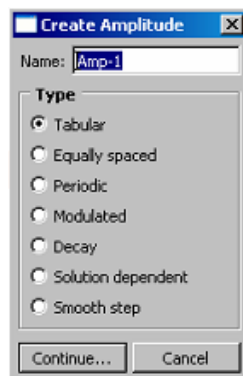
✳ Through this procedure the output data of this simulation will be collected every 0.4μ sec.

L. Module : Load

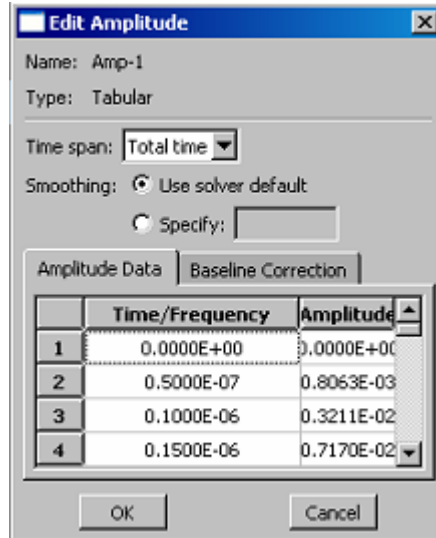
1. To product the excitation signal at the edges of the actuator, do the following:

a) Choose Tools > Amplitude > Create.

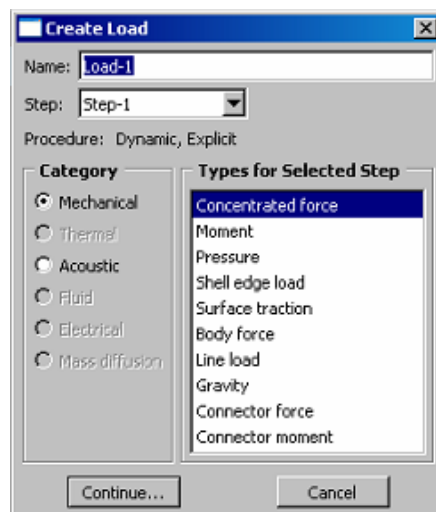
b) Give a name, choose “Tabular” radio button and click “Continue” as shown below.



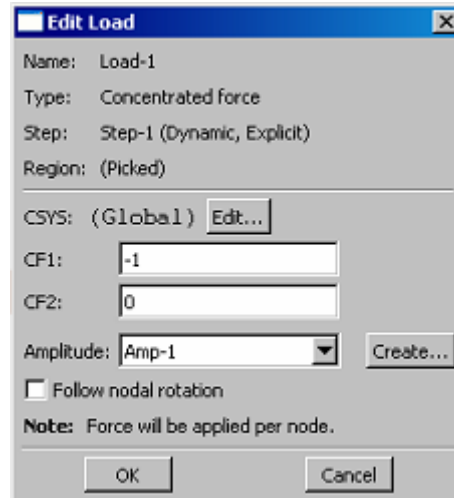
- c) Choose “Total time” in Time span and the amplitude data can be read from the experimental data files(first & second rows).



- d) Click “OK”.
- e) Choose Load > Create
- f) Give a name for load, choose “Mechanical” radio button in Category & “Concentrated force” in Types for Selected Step and click “Continue” as shown below.



g) Choose the CF1 value to be non-zero(left edge of the actuator : -1, right edge of the actuator : +1), CF2 value to be zero. And apply the amplitude which we made and click “OK” as shown below.

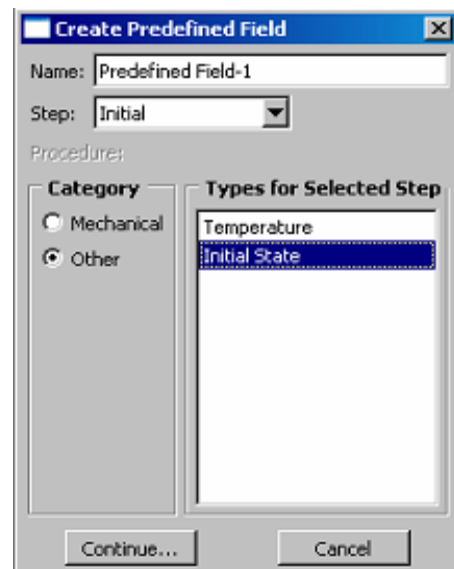


※ Apply two opposite loads at the edges of the actuator.

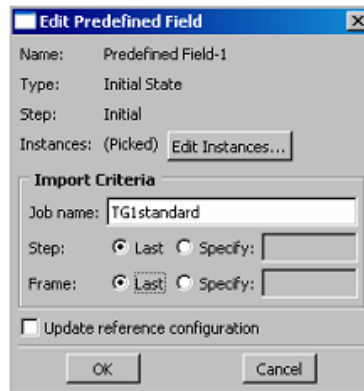
2. To import thermal gradient as an initial state of this analysis, do the following:

a) Choose Predefined Field > Create.

b) Give a name, choose “Other” radio button in Category, Click “Initial State” in Types for Selected Step and click “Continue” as shown below.




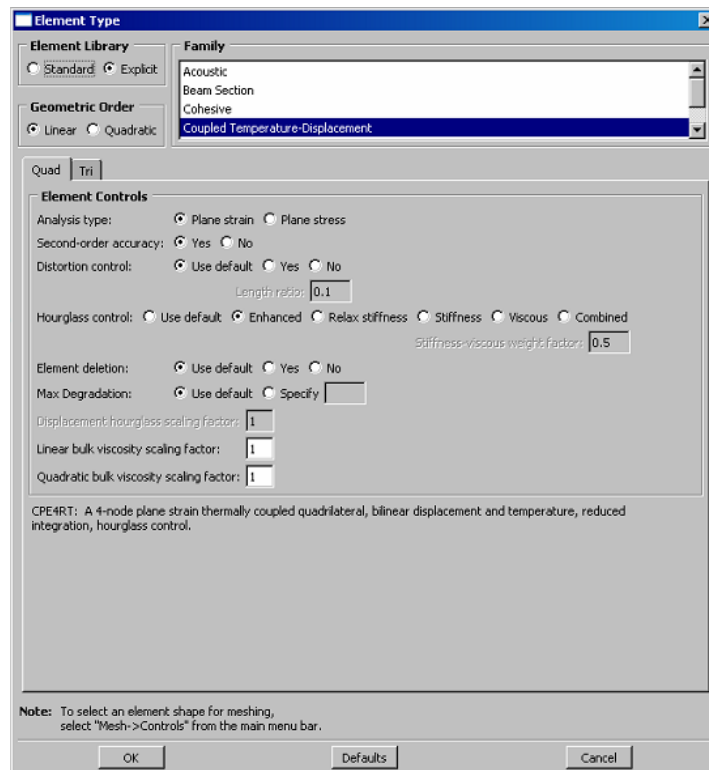
c) Type the name of the Standard ODB in Job name, set as below and click “OK”.



M. Module : Mesh

1. To decide the element type of the model, do the following:

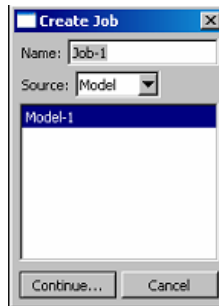
- a) Choose Mesh > Element type or click on the icon  “Assign Element Type”.
- b) Click whole model by using “Shift Key” then click “Done”.
- c) Choose “Explicit” in Element Library , choose “Coupled Temperature Displacement” in Family and click “OK” as shown below.



- ✳ Second-order accuracy and Enhanced Hourglass control are recommended.
- ✳ Element type must be decided before importing Standard ODB.

N. Module : Job

1. To create and submit Job, do the following:
 - a) Choose Job > Create, give a name to the Job(This will also become the name of the ODB file.) and click “Continue” as shown below.

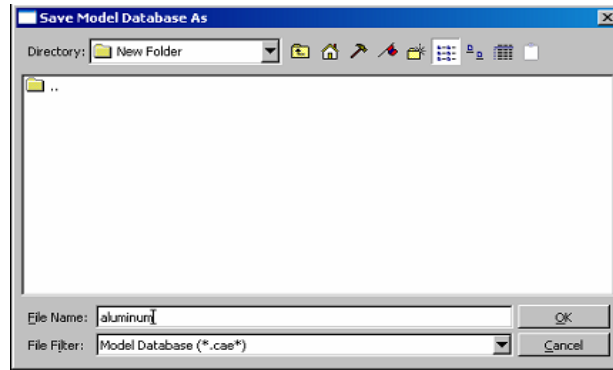


- b) When the Edit Job window pops up, set “Double” in ABAQUS/Explicit precision and “Full” in Nodal output precision under Precision tab and click “OK” as shown below.



- c) Choose Job > Manager, click “Submit”, then click “Monitor” to view the program execution as shown below. When Job is completed click “Dismiss” on the monitor window and click “Results” on the Job Manager window and view result.

d) Save CAE file by clicking File > Save As and giving a file name.

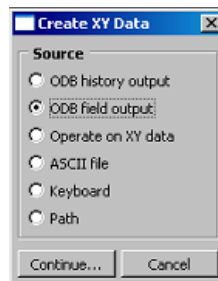


O. Module : Visualization

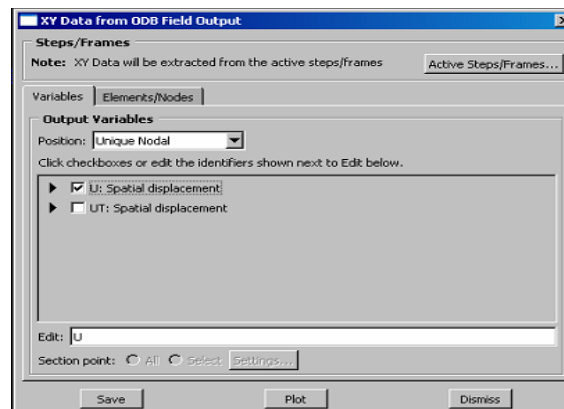
1. To product the rpt(report) file that contains U displacements of the node set, do the following:

a) Choose Tools > XY Data > Create.

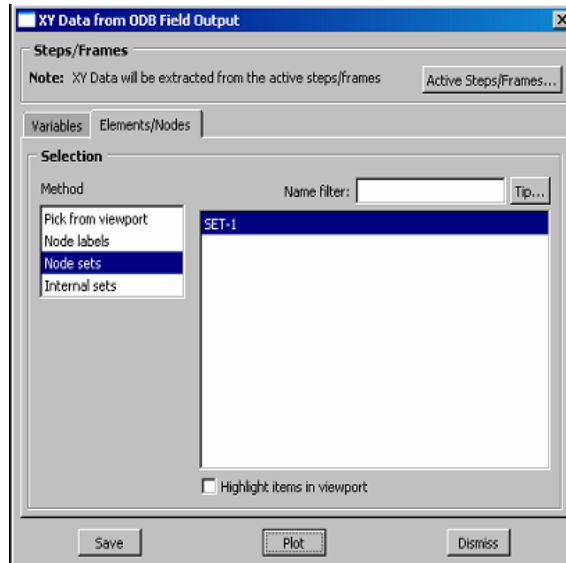
b) Choose ODB field output and click “Continue” as shown below.



c) Under Variables tab, choose “Unique Nodal” and click “U : Spatial displacement” as shown below.

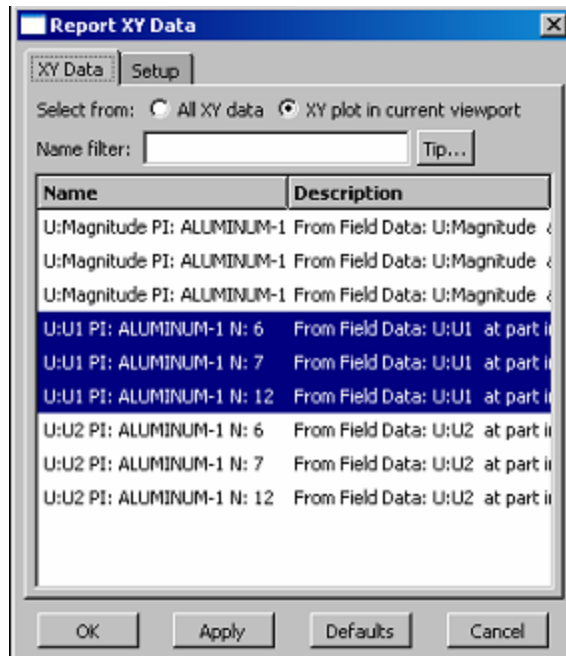


d) Under Elements/Nodes tab, choose “Node sets” in Method and click “Save” as shown below.

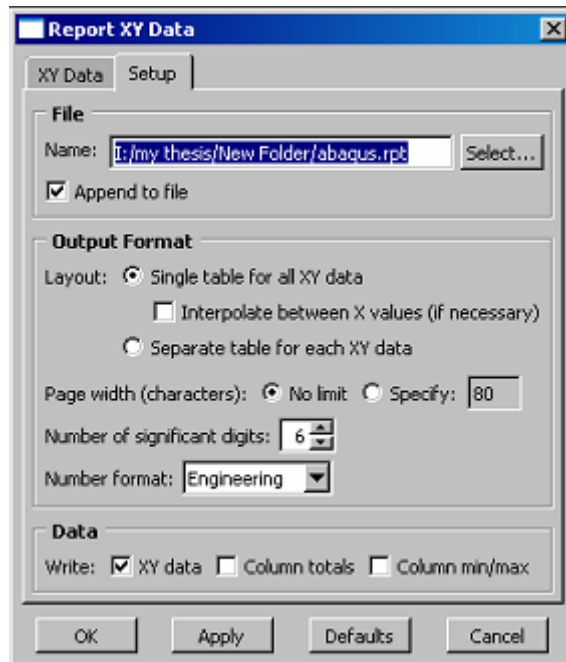


e) Choose Report > XY Data.

f) Under XY Data tab, choose “U:U1” as shown below.



g) Under Setup tab, decide “*.rpt” file name, directory and click “OK” as shown below.



h) “*.rpt” file(i.e., Simulated S_0 response date file) is created in the Work directory.

✳ Reference Table 8 and Appendix D for the formation of the “*.rpt” file.

APPENDIX C: MATLAB® CODE

Simulation vs Theoretical vs Experimental S₀ Response Comparisons

```
% This Thesis Code is provided by Andrews(4), after that...
% Capt SeJin Han modified little bit for his analysis.
% Simulation vs Theoretical vs Experimental S0 Response Wave Propagation Comparisons
% Note: Signal data is normalized w.r.t. the maximum of the absolute value of the
% Note: rpt. files from Appendix A and B will be imported during this analysis.
% Note: This code is execution code which actually carry out plotting three types of results and
following codes are not execution codes. They are used for generating theoretical Hanning-
Window excitation signals and S0 Responses.
% S0 responses
clear all
close all
clc

%% USER INPUTS (A): Temperature and Frequency
TEMP = [0 25 50 75 100 125 150 175 190]; % Choose one of these(°F)
fcset = 1e3*[100]; % Frequency(Hz)
freq = 6;

% 6 ==> 100 kHz
% 26 ==> 300 kHz

if freq == 6
    flip=1;
    END_TIME = 251;
    XEx_END = 65;
    XResp_END = 95;
elseif freq == 26
    flip=1;
    END_TIME = 251;
    XEx_END = 65;
    XResp_END = 60;
else
    'WRONG INPUT'
end

%% Loading Experimental data
load('Exp0Deg100kHz')
E_0deg = Exp0Deg100kHz(:,2);
R_0deg = flip*Exp0Deg100kHz(:,3);
% load('Exp25Deg100kHz')
% E_25deg = Exp25Deg100kHz(:,2);
% R_25deg = flip*Exp25Deg100kHz(:,3);
% load('Exp50Deg100kHz')
% E_50deg = Exp50Deg100kHz(:,2);
% R_50deg = flip*Exp50Deg100kHz(:,3);
```

```

% load('Exp75Deg100kHz')
% E_75deg = Exp75Deg100kHz(:,2);
% R_75deg = flip*Exp75Deg100kHz(:,3);
% load('Exp100Deg100kHz')
% E_100deg = Exp100Deg100kHz(:,2);
% R_100deg = flip*Exp100Deg100kHz(:,3);
% load('Exp125Deg100kHz')
% E_125deg = Exp125Deg100kHz(:,2);
% R_125deg = flip*Exp125Deg100kHz(:,3);
% load('Exp150Deg100kHz')
% E_150deg = Exp150Deg100kHz(:,2);
% R_150deg = flip*Exp150Deg100kHz(:,3);
% load('Exp175Deg100kHz')
% E_175deg = Exp175Deg100kHz(:,2);
% R_175deg = flip*Exp175Deg100kHz(:,3);
% load('Exp190Deg100kHz')
% E_190deg = Exp190Deg100kHz(:,2);
% R_190deg = flip*Exp190Deg100kHz(:,3);

%% Lodaing Simulated data
load('Sim0deg100kHz')
h = 3.2;
a = Sim0deg100kHz(:,2:end);
RR_0deg = flip*( a(:,3) - a(:,1) )./ (2*h)
% load('Sim25deg100kHz')
% b = Sim25deg100kHz(:,2:end);
% RR_25deg = flip*( b(:,3) - b(:,1) )./ (2*h)
% load('Sim50deg100kHz')
% c = Sim50deg100kHz(:,2:end);
% RR_50deg = flip*( c(:,3) - c(:,1) )./ (2*h)
% load('Sim75deg100kHz')
% d = Sim75deg100kHz(:,2:end);
% RR_75deg = flip*( d(:,3) - d(:,1) )./ (2*h)
% load('Sim100deg100kHz')
% e = Sim100deg100kHz(:,2:end);
% RR_100deg = flip*( e(:,3) - e(:,1) )./ (2*h)
% load('Sim125deg100kHz')
% f = Sim125deg100kHz(:,2:end);
% RR_125deg = flip*( f(:,3) - f(:,1) )./ (2*h)
% load('Sim150deg100kHz')
% g = Sim150deg100kHz(:,2:end);
% RR_150deg = flip*( g(:,3) - g(:,1) )./ (2*h)
% load('Sim175deg100kHz')
% j = Sim175deg100kHz(:,2:end);
% RR_175deg = flip*( j(:,3) - j(:,1) )./ (2*h)
% load('Sim190deg100kHz')
% k = Sim190deg100kHz(:,2:end);
% RR_190deg = flip*( k(:,3) - k(:,1) )./ (2*h)

```

```

%% Specimen 1 Parameters
thickness = 1; % Thickness(1 or 0.6 mm)
prop_dist1 = 158; % Propagating distance(158 or 512 mm)
prop_dist = prop_dist1/1000; % mm ==> m

%% Theoretical Code Constants
PadLength = 2048; % Frequency resolution
LambWaveMode = 'S0'; % Wave mode
fsamp = 2.5E6; % Sampling rate
num_cycles = 5.5; % Cycles in excitation signal

%% Experimental Time Vector
N = 1000; % Length of the datafile
delta_t = 1/fsamp; % 4E-7 sec
T = [0:delta_t:(N-1)*delta_t]/1E-6;

%% Theoretical Analysis
for i = 1:length(TEMP)
    Temp = TEMP(i);
    if Temp == 0
        E = E_0deg;
        R = R_0deg;
        RR = RR_0deg;
    elseif Temp == 25
        E = E_25deg;
        R = R_25deg;
        RR = RR_25deg;
    elseif Temp == 50
        E = E_50deg;
        R = R_50deg;
        RR = RR_50deg;
    elseif Temp == 75
        E = E_75deg;
        R = R_75deg;
        RR = RR_75deg;
    elseif Temp == 100
        E = E_100deg;
        R = R_100deg;
        RR = RR_100deg;
    elseif Temp == 125
        E = E_125deg;
        R = R_125deg;
        RR = RR_125deg;
    elseif Temp == 150
        E = E_150deg;
        R = R_150deg;
        RR = RR_150deg;
    elseif Temp == 175
        E = E_175deg;

```

```

R = R_175deg;
RR = RR_175deg;
else
E = E_190deg;
R = R_190deg;
RR = RR_190deg;
end

%% INPUT Signal
nf = length(fcset);
input_signal = zeros(nf,PadLength); %number of input frequency signals
fd = (fcset./1E6)*thickness; %frequency-thickness (MHz-mm)

for k = 1:nf
ip = [WindowedSine(fcset(k),num_cycles,fsamp)];
input_signal(k,1:length(ip)) = ip;
%% Propagated Signal
[prop_sig(k,:), t , prop_sig_norm(k,:) ] = LambFourierDecomp_atk(input_signal(k,:),...
PadLength, ...
LambWaveMode,...
thickness, ...
prop_dist, ...
fsamp,Temp,fd);
end
t = t./1E-6;

%% Excitation Signal: Time Delay between Theoretical and Experimental Results
[C_raw,I_raw] = max((E(1:END_TIME,1)));
[C_theor,I_theor] = max((input_signal));
Input_Time = t(I_theor)
Time_Delay = T(I_raw)-t(I_theor)

%% Simulation & Excitation & Theoretical Response Plots
figure(1)
subplot(length(TEMP),1,i)
plot(T-Time_Delay,E'/max(abs(E(1:END_TIME,1))),'LineWidth',2) %Time Shifted Exp & Sim
Excitation Signal
hold on
plot(t,input_signal,'r','LineWidth',2)
if i == length(TEMP)
xlabel('Time (\musec)','FontWeight','Bold','FontSize',12)
legend('Simulation','Theoretical','Location','SouthEast')
end
xlim([0 XEx_END])
set(gca,'XTick',[0 : 5 : XEx_END])
if i == round(length(TEMP)/2)
ylabel('Normalized Amplitude','FontWeight','Bold','FontSize',12)
end
ylim([-1.1 1.1])

```

```

if i == 1
    title(['Normalized Excitation Signal (' int2str(fcset(1)./1e3) ' kHz): ' int2str(Temp) '\circF'
], 'FontWeight', 'Bold', 'FontSize', 12)
% title(['5 1/2 Cycle Hanning-window Excitation Signal (' int2str(fcset(1)./1e3) ' kHz)
'], 'FontWeight', 'Bold', 'FontSize', 12)
else
    title([int2str(Temp) '\circF: ' ], 'FontWeight', 'Bold', 'FontSize', 12)
end
hold off

figure(2)
subplot(length(TEMP), 1, i)
plot(T-Time_Delay, R./max(abs(R(1:END_TIME, 1))), 'm', 'LineWidth', 2) % Time Shifted
Experimental Response
hold on
plot(T-Time_Delay, RR./max(abs(RR(1:END_TIME, 1))), 'b', 'LineWidth', 2) % Time Shifted
Simulated Response
hold on
plot(t, prop_sig_norm, 'r', 'LineWidth', 2)
if i == length(TEMP)
    xlabel('Time (\musec)', 'FontWeight', 'Bold', 'FontSize', 12)
    legend('Experimental', 'Simulation', 'Theoretical', 'Location', 'SouthWest')
end
xlim([25 XResp_END])
set(gca, 'XTick', [25 : 5 : XResp_END])
if i == round(length(TEMP)/2)
    ylabel('Normalized Amplitude', 'FontWeight', 'Bold', 'FontSize', 12)
end
ylim([-1.1 1.1])
if i == 1
    title(['Normalized S_0 Response at ' int2str(fcset(1)./1e3) ' kHz: Propagated over '
int2str(prop_dist*1000) ' mm ' int2str(Temp) '\circF'], 'FontWeight', 'Bold', 'FontSize', 12)
else
    title([int2str(Temp) '\circF'], 'FontWeight', 'Bold', 'FontSize', 12)
end
hold off

%% TOA calculation...
% [C_raw, I_raw] = max(RR(1:END_TIME, 1));
% [C_theor, I_theor] = max(prop_sig_norm);
% Time_Difference = T(I_raw) - (t(I_theor) + Time_Delay)
% Theoretical_time = t(I_theor)
% Simulation_time = T(I_raw) - Time_Delay
end

```

AFRL/VASA: Primary Function - Generates a Lamb Wave Response Signal

```

% This Thesis Code is provided by Andrews(4).
function [prop_sig, t, prop_sig_norm] = LambFourierDecomp_atk(input_signal, ...

```

```

    PadLength, ...
    LambWaveMode,...
    thickness, ...
    prop_distance, ...
    fsamp,...
    Temp,fd,i);

% INPUTS:
% input signal      % signal to propagate
% PadLength        % specify length of padded signal to avoid time aliasing
% LambWaveMode     % lamb wave mode to simulate; use proper phase velocity curve
% thickness        % thickness of simulated plate (millimeters)
% prop_distance    % distance to propagate input signal (meters)
% delta_distance   % step size of distance (meters )
% fsamp           % sample rate of simulation

% OUTPUTS
% prop_sig = propagated signal
% t = time vector%

% FUNCTIONS CALLED:
% mrc_window
% mrc_spectrum
% fine_phase_velocity

n_in = length(input_signal);
npow2 = ceil(log(n_in)/log(2) );

% pad input signal specified length
tmp = zeros(1,PadLength);
tmp(1:n_in) = input_signal;
input_signal = tmp;

t = [0 : 1: PadLength-1] / fsamp ; % time sampling
nt = length(t);          % number of time samples

% frequency vectors (in Hz and radians/sec)
df = [0: fsamp/PadLength : fsamp/2 - fsamp/PadLength];
omega = df*2*pi;

% initialize output arrays to improve computation speed
s_hat = zeros(nt,PadLength);
s2_hat = zeros(1,nt);
s2_prop = zeros(1,nt);

% DFT of pulse
S = fft(input_signal,PadLength);

% for specified distance, at kth frequency component obtain phase velocity

```

```

% at freq corresponding to kth component and specified plate thickness
for k = 1: PadLength/2
    %fd = thickness*df(k)/1e6;
    v = symm_fine_phase_velocity_temperature(fd,Temp);
    % v = fine_phase_velocity_atk(fd,LambWaveMode);
    s_hat(:,k) = S(k) * ...
    exp(-j*(omega(k)* prop_distance/v * ones(size(t)) - ...
    omega(k)*t));
end

% Synthesize the pulse at specified distance by summing across frequency
prop_sig(1,:) = 2*real(sum(s_hat,2));

% Normalize
prop_sig_norm = prop_sig ./ max(abs(prop_sig)) ;

```

AFRL/VASA: Sub-Function - Generates a Window Function

```

% This Thesis Code is provided by Andrews(4).
function [w] = mrc_window(p,type)

%% This function creates a bartlett, rectangular, hanning, blackman, or hamming
%% window of size. If the type is not specified it is assumed to be a hamming window.
%% Note: It will be very easy to add other types of windows as needed.

% Set hamming window as default

if ( nargin < 2 )
    type = 'hamming';
end

if ( mod(p,2) ~= 0 )
    half = (p+1)/2;
else
    half = p/2;
end

    i = ( 0:(half-1))/(p-1);
if ( strcmp( type, 'hamming' ) )
    w = .54 - .46*cos(2*pi*i);
if ( mod(p,2) ~=0 )
    w = [w w(end-1:-1:1)];
else
    w = [w w(end:-1:1)];
end

elseif ( strcmp( type, 'hanning' ) )
    w = .5 - .5*cos(2*pi*i);
if ( mod(p,2) ~=0 )

```

```

    w = [w w(end-1:-1:1)];
else
    w = [w w(end:-1:1)];
end

elseif ( strcmp( type, 'bartlett' ) )
    w = 2*(0:((p-1)/2))/(p-1);
if ( mod(p,2) ~= 0 )
    w = [w w((p-1)/2:-1:1)];
else
    w = [w w((p/2):-1:1)];
end

elseif ( strcmp( type, 'blackman' ) )
    w = 0.42 - 0.5*cos(2*pi*i) + 0.08*cos(4*pi*i);
if ( mod(p,2) ~=0 )
    w = [w w(end-1:-1:1)];
else
    w = [w w(end:-1:1)];
end

elseif ( strcmp( type, 'rectangle' ) )
    w = ones(p,1);
end
return

```

AFRL/VASA: Sub-Function - Provides a Theoretical S₀ Phase Velocity Value based on a Frequency-thickness Product and a Temperature Value

```

% This Thesis Code is provided by Andrews(4).
function fpv = symm_fine_phase_velocity_temperature( fd, temp );
% fpv = symm_fine_phase_velocity_temperature(fd,temp)
% Returns S0 phase velocity (meters/sec)in aluminum for a given temperature
% INPUT:
% fd = frequency thickness product (MHz-mm); can be a vector of values
% temp = temperature in degrees Fahrenheit, must be one of set:
% = {0, 25, 50, 75, 100, 125, 150, 175, 190, 225, 600}
% OUTPUT:
% fpv = phase velocity (meters/sec)
% fpv/1000 => millimeters/usec

% Polynomial expansion used to fit data from Steve Olson's Root Finding Program
% Use polyfit and polyval; the selected order of polynomials is based on a
% visual fit of actual to approximated curve across fd = [0.01,2];

fd = fd(:); % allows for possible evaluation at multiple points
min_fd = min(fd); max_fd = max(fd);

if min_fd < 0.01 || max_fd > 2

```



```

fpv = - 1;
return
else
switch temp
case 0
coeffs = [-0.05142654709297
0.16993288286982
-0.24100699269294
0.06501025649511
-0.03139299715575
5.33445759520220];

fpv = 1e3 * polyval( coeffs, fd' ); % the 1e3 term converts speed to m/s

case 25
coeffs = [-0.05313655342506
0.17597647815818
-0.24926123503776
0.06938216345670
-0.03236171402414
5.31333398641870 ];
fpv = 1e3 * polyval( coeffs, fd' ); % the 1e3 term converts speed to m/s

case 50
coeffs = [-0.05378413396642
0.17820497231257
-0.25231032456288
0.07105929649346
-0.03279206525247
5.30456449303111 ];
fpv = 1e3 * polyval( coeffs, fd' ); % the 1e3 term converts speed to m/s

case 75
coeffs = [-0.05507959466469
0.18283473780074
-0.25878777906218
0.07466694280557
-0.03365388253713
5.28890170460593 ];
fpv = 1e3 * polyval( coeffs, fd' ); % the 1e3 term converts speed to m/s

case 100
coeffs = [-0.05636949658771
0.18726567362737
-0.26474597824300
0.07779392926725
-0.03437776385729
5.27235220449814 ];
fpv = 1e3 * polyval( coeffs, fd' ); % the 1e3 term converts speed to m/s

```

```
case 125
coeffs = [ -0.05776182834146
           0.19215889069200
           -0.27140615074052
           0.08136089064404
           -0.03521812591011
           5.25635541653454 ];
fpv = 1e3 * polyval( coeffs, fd'); % the 1e3 term converts speed to m/s
```

```
case 150
coeffs = [ -0.06009213310675
           0.20041459643570
           -0.28285321764051
           0.08773695163732
           -0.03676294576454
           5.23012173230380 ];
fpv = 1e3 * polyval( coeffs, fd'); % the 1e3 term converts speed to m/s
```

```
case 175
coeffs = [ -0.06224074229182
           0.20777568402492
           -0.29275654287881
           0.09305453654092
           -0.03808173833658
           5.20484290196241 ];
fpv = 1e3 * polyval( coeffs, fd'); % the 1e3 term converts speed to m/s
```

```
case 190
coeffs = [ -0.06386743863999
           0.21345653682254
           -0.30049681482224
           0.09720554642296
           -0.03900502478225
           5.18692445333935 ];
fpv = 1e3 * polyval( coeffs, fd'); % the 1e3 term converts speed to m/s
```

```
case 225
coeffs = [ 0.01277993922954
           -0.12353223637959
           0.51191653087527
           -1.19397037452427
           1.72202041377808
           -1.59434838933529
           0.94821291882998
           -0.36787658715903
           0.08126191330675
           -0.08799422443185
           0.00060733201852
```

```

5.14209345974537 ];
fpv = 1e3 * polyval( coeffs, fd');

case 600
coeffs = 1e2* [ 0.02608076315068
-0.29095598897656
1.39021437440402
-3.72576781639859
6.16441540312900
-6.53311220622451
4.45289880924999
-1.90827216853626
0.48690552640556
-0.06785420607551
0.00403023304247
0.03748966569755 ];
fpv = 1e3 * polyval( coeffs, fd');

otherwise
disp('Unsupported temperature')
fpv = [];
end
end
return

```

AFRL/VASA: Function - Generates a Hanning-windowed Excitation Signal

```

% This Thesis Code is provided by Andrews(4).
function [ws,t] = WindowedSine(fc,num_cycles,fsamp);
% Creates windowed sinusoid
% INPUTS:
% fc = center frequency of burst (Hz)
% num_cycles = number of cycles, can be non-integer
% fsamp = sample rate of simulation (samples per second)

% compute pulse duration
duration = num_cycles / fc;

t = [0: 1/fsamp : duration ]';
num_samps = length(t);
s = -sin(2*pi*fc*t);
w = mrc_window(num_samps,'hanning');
ws = w .* s ;

```

APPENDIX D: SAMPLES OF THE DATA FILES

Sample of the Experimental Data File

LabVIEW Measurement
Writer_Version 0.92
Reader_Version1
Separator Tab
Multi_HeadingsNo
X_Columns One
Time_Pref Absolute
Operator Administrator
Date 2006/10/26
Time 09:27:04.090963
End_of_Header

Channels 2
Samples 1000 1000
Date 2006/10/26 2006/10/26
Time 09:27:29.186999 09:27:29.186999
Y_Unit_Label Volts Volts
X_Dimension Time Time
X0 2.5086071999999955E+1 2.5086071999999955E+1
Delta_X 4.000000E-7 4.000000E-7
End_of_Header

X_Value	EXCITATION (Filtered)	RESPONCE (Filtered)	Comment
25.096086	2.160402E-22	1.440268E-22	
25.096087	-5.379832E-9	-3.586555E-9	
25.096087	-2.422355E-8	-1.475426E-8	
25.096088	-5.698215E-8	-3.294771E-8	
25.096088	-9.575985E-8	-5.288292E-8	
25.096088	-1.251078E-7	-6.618359E-8	
25.096089	-1.236827E-7	-6.329058E-8	
25.096089	-7.168206E-8	-3.401237E-8	
25.096090	4.071221E-8	3.178824E-8	
25.096090	2.152278E-7	1.419425E-7	
25.096090	4.489589E-7	2.953645E-7	
25.096091	7.289102E-7	4.803435E-7	
25.096091	1.030682E-6	6.707060E-7	
25.096092	1.323448E-6	8.290877E-7	
25.096092	1.578665E-6	9.166565E-7	
25.096092	1.773832E-6	9.001230E-7	
25.096093	1.904495E-6	7.688253E-7	
25.096093	2.001533E-6	5.518928E-7	
25.096094	2.138504E-6	3.268520E-7	
25.096094	2.441866E-6	2.216582E-7	
25.096094	3.098697E-6	4.087820E-7	
25.096095	4.345337E-6	1.089111E-6	
25.096095	6.443843E-6	2.459622E-6	

25.096096	9.646846E-6	4.669565E-6
25.096096	1.415052E-5	7.769362E-6
25.096096	2.003996E-5	1.166837E-5
25.096097	2.722908E-5	1.610611E-5
25.096097	3.540459E-5	2.063144E-5
25.096098	4.397918E-5	2.460977E-5
25.096098	5.206806E-5	2.726408E-5
25.096098	5.849917E-5	2.775026E-5
25.096099	6.185266E-5	2.526292E-5
25.096099	6.053939E-5	1.916204E-5
25.096100	5.293300E-5	9.104388E-6
25.096100	3.753917E-5	-4.835502E-6
25.096100	1.319090E-5	-2.207806E-5
25.096101	-2.074217E-5	-4.151011E-5
25.096101	-6.414663E-5	-6.152037E-5
25.096102	-0.000116	-8.010977E-5
25.096102	-0.000174	-9.506763E-5
25.096102	-0.000235	-0.000104
25.096103	-0.000296	-0.000106
25.096103	-0.000350	-9.818361E-5
25.096104	-0.000391	-8.128009E-5
25.096104	-0.000415	-5.552251E-5
25.096104	-0.000414	-2.253764E-5
25.096105	-0.000384	1.503362E-5
25.096105	-0.000320	5.372116E-5
25.096106	-0.000221	8.953037E-5
25.096106	-8.618173E-5	0.000118
25.096106	8.011230E-5	0.000136
25.096107	0.000272	0.000141
25.096107	0.000480	0.000130
25.096108	0.000691	0.000103
25.096108	0.000891	6.143227E-5
25.096108	0.001064	9.199330E-6
25.096109	0.001190	-4.941374E-5
25.096109	0.001255	-0.000109
25.096110	0.001243	-0.000162
25.096110	0.001143	-0.000203
25.096110	0.000950	-0.000226
25.096111	0.000662	-0.000226
25.096111	0.000288	-0.000200
25.096112	-0.000158	-0.000149
25.096112	-0.000653	-7.383228E-5
25.096112	-0.001167	2.100105E-5
25.096113	-0.001667	0.000129
25.096113	-0.002113	0.000241
25.096114	-0.002467	0.000349

·
·
·

Sample of the Simulated Data File

X U:U1 PI: PART-1-1 N: 8 U:U1 PI: PART-1-1 N: 11 U:U1 PI: PART-1-1 N: 14

0.	0.	0.	0.
400.000005E-09	0.	0.	0.
800.000009E-09	0.	0.	0.
1.20000004E-06	0.	0.	0.
1.60000002E-06	0.	0.	0.
1.99999999E-06	0.	0.	0.
2.40000008E-06	0.	0.	0.
2.79999995E-06	0.	0.	0.
3.20000004E-06	0.	0.	0.
3.60000013E-06	0.	0.	0.
3.99999999E-06	0.	0.	0.
4.39999985E-06	0.	0.	0.
4.80000017E-06	0.	0.	0.
5.20000003E-06	0.	0.	0.
5.59999989E-06	0.	0.	0.
6.00000021E-06	0.	0.	0.
6.40000007E-06	0.	0.	0.
6.79999994E-06	0.	0.	0.
7.20000025E-06	0.	0.	0.
7.60000012E-06	0.	0.	0.
7.99999998E-06	0.	0.	0.
8.4000003E-06	0.	0.	0.
8.7999997E-06	0.	0.	0.
9.20000002E-06	0.	0.	0.
9.60000034E-06	0.	0.	0.
9.99999975E-06	0.	0.	0.
10.4000001E-06	0.	0.	0.
10.8000004E-06	0.	0.	0.
11.1999998E-06	0.	0.	0.
11.6000001E-06	0.	0.	0.
12.0000004E-06	0.	0.	0.
12.3999998E-06	0.	0.	0.
12.8000001E-06	0.	0.	0.
13.2000005E-06	0.	0.	0.
13.5999999E-06	0.	0.	0.
14.0000002E-06	0.	0.	0.
14.4000005E-06	0.	0.	0.
14.7999999E-06	0.	0.	0.
15.2000002E-06	0.	0.	0.
15.6000006E-06	0.	0.	0.
16.E-06	0.	0.	0.
16.3999994E-06	0.	0.	0.
16.8000006E-06	0.	0.	0.
17.2E-06	0.	0.	0.
17.5999994E-06	0.	0.	0.

18.0000006E-06	0.	0.	0.
18.4E-06	0.	0.	0.
18.7999995E-06	0.	0.	0.
19.2000007E-06	0.	0.	0.
19.6000001E-06	0.	0.	0.
19.9999995E-06	0.	0.	0.
20.4000007E-06	0.	0.	0.
20.8000001E-06	0.	0.	0.
21.1999995E-06	0.	0.	0.
21.6000008E-06	0.	0.	0.
22.0000002E-06	0.	0.	0.
22.3999996E-06	0.	0.	0.
22.8000008E-06	0.	0.	0.
23.2000002E-06	0.	0.	0.
23.5999996E-06	0.	0.	0.
24.0000008E-06	0.	0.	0.
24.4000003E-06	0.	0.	0.
24.7999997E-06	0.	0.	0.
25.2000009E-06	0.	0.	0.
25.6000003E-06	0.	-1.83656679E-30	0.
25.9999997E-06	0.	-1.75482108E-27	0.
26.4000009E-06	0.	-614.065155E-27	-89.2398899E-30
26.8000003E-06	-3.93197857E-30	-96.3670967E-24	-43.8284586E-27
27.1999997E-06	-2.77084928E-27	-7.69434116E-21	-9.23832166E-24
27.600001E-06	-791.57863E-27	-341.407347E-21	-960.502296E-24
28.0000004E-06	-107.804646E-24	-8.94826285E-18	-54.334399E-21
28.3999998E-06	-7.79965482E-21	-144.439565E-18	-1.79108239E-18
28.800001E-06	-323.648477E-21	-1.47746612E-15	-36.0758016E-18
29.2000004E-06	-8.12631995E-18	-9.79027193E-15	-458.623289E-18
29.5999998E-06	-128.109882E-18	-43.1470147E-15	-3.76536003E-15
30.0000011E-06	-1.30075451E-15	-132.815661E-15	-20.390182E-15
30.4000005E-06	-8.67491249E-15	-309.597915E-15	-75.2567293E-15
30.8000017E-06	-38.8944485E-15	-576.44151E-15	-201.484567E-15
31.2000011E-06	-122.375078E-15	-793.053936E-15	-423.037961E-15
31.6000005E-06	-290.539457E-15	-617.854075E-15	-698.009304E-15
31.9999999E-06	-550.001993E-15	197.013535E-15	-781.157907E-15
32.3999993E-06	-780.880297E-15	1.80871008E-12	-331.142828E-15
32.7999987E-06	-654.764058E-15	4.38619757E-12	821.834191E-15
33.2000018E-06	101.385202E-15	7.44984109E-12	2.87047621E-12
33.6000012E-06	1.63521432E-12	9.61800344E-12	5.79105774E-12
34.0000006E-06	4.12529472E-12	10.0457836E-12	8.63071073E-12
34.4E-06	7.18560107E-12	7.85142958E-12	10.041537E-12
34.7999994E-06	9.49599427E-12	1.59283361E-12	9.47725492E-12
35.1999988E-06	10.0703491E-12	-7.92116719E-12	5.49261808E-12
35.6000019E-06	8.18122393E-12	-18.933204E-12	-2.42981416E-12
		.	
		.	
		.	

Bibliography

1. ABAQUS Analysis User's Manual, Version 6.6, ABAQUS, Inc., Providence, RI, 2006.
2. Achenbach, J.D., "*Wave propagation in elastic solids*," North-Holland, Amsterdam, Holland, 1980.
3. Alleyne, D., and Cawley, P., "*A two-dimensional Fourier transform method for the measurement of propagating multimode signals*," Journal of the Acoustical Society of America, 89(3), 1991, pp. 1159-1168.
4. Andrews, Jennifer., "*Lamb wave propagation in varying thermal environments*," M.S. Thesis, AFIT/GA/ENY/07-M01, Department of Aeronautics and Astronautics, Air Force Institute of Technology(AU), Wright Patterson, AFB, OH, March 2007.
5. Cawley, P., and Alleyne, D., "*The use of Lamb waves for the long range inspection of large structures*," Ultrasonics 34, 1996, pp. 287-290.
6. Cook, R.D., Malkus, D.S., and Plesha, M.E., "*Concepts and applications of Finite Element Analysis*," 3rd edition, New York, NY: John Wiley & Sons, 1989, pp. 52-234.
7. Department of Defense Handbook, Metallic Materials and Elements for Areospace Vehicle Structures, MIL-HDBK-5J, 2003.
8. Derriso, M.M., Olson, S.E., DeSimio, M.P., and Sanders, B., "*Development of Automated Damage Detection Techniques*," Materials Damage Prognosis, J.M. Larson, et. al., ed., TMS. Warrendale, PA, 2005.
9. Ghosh, T., Kundu, T., and Karpur, P., "*Efficient use of Lamb modes for detecting defects in large plates*," Ultrasonics 36, 1998, pp. 791-801.
10. Giurgiutiu, V., "*Tuned Lamb wave excitation and detection with piezoelectric wafer active sensors for structural health monitoring*," Journal of Intelligent Material Systems and Structures, Vol 16, No 4, 2005, pp. 291-305.
11. Grisso, Benjamin L., "*Considerations of the Impedance Method, Wave Propagation, and Wireless Systems for Structural Health Monitoring*," Master's thesis, Virginia Polytechnic Institute and State University, Blacksburg VA, 2004.
12. Jia, X., "*Model analysis of Lamb wave generation in elastic plates by liquid wedge transducers*," Acoustical Society of America, Vol 101, No 2, February, 1997, pp. 834-842.
13. Krautkramer, "*Emerging Technology - Guided Wave Ultrasonics*," NDTnet, Vol 3, No 6, 1998.
14. Kundu, T., Maji, A., Gosh, T., and Maslov, K., "*Detection of kissing bonds by Lamb waves*," Ultrasonics 35, 1998, pp. 573-580.
15. Kundu, T., Maslov, K., Karpur, P., Matikas, T.E., and Nicolau, P.D., "*A Lamb wave scanning*

- approach for the mapping of defects in [0/90] titanium composites,*” Ultrasonics 34, 1996, pp. 43-49.
16. Lamb, H., “*On Waves in an Elastic Plate,*” Proceedings of the Royal Society of London. Series A, Containing Papers of a Mathematical and Physical Character, Vol 93, No 648, 1917, pp. 114-128.
 17. Lathi, B.P., “*Linear Systems and Signals,*” Oxford University Press: Oxford, NY, 2005, pp. 16-17.
 18. Lempriere, Brian M., “*Ultrasound and Elastic Waves,*” Academic Press, New York, 2002.
 19. Lowe, M.J.S., Alleyne, D.N., and Cawley, P., “*Defect detection in pipes using guided waves,*” Ultrasonics 36, 1998, pp. 147-154.
 20. Mal, Ajit., “*Structural Health Monitoring,*” American Academy of Mechanics, Vol 33, No 11-12, 2004, pp. 1-4.
 21. Moser, F., Jacobs, L.J., and Qu, J., “*Modeling elastic wave propagation in waveguides with the finite element method,*” NDT&E International, 32(4), 1999, pp. 225-234.
 22. Olson, S.E., Derriso, M.M., DeSimio, M.P., and Thomas, D.T., “*Analytical Modeling of Lamb Waves for Structural Health Monitoring,*” in Proceedings of the 3rd European Workshop on Structural Health Monitoring, Granada, Spain. 5-7 July, 2006.
 23. Rose, J.L., “*Ultrasonic Waves in Solid Media,*” Cambridge University Press: Cambridge, MA, 1999.
 24. Saada, Adel S., “*Elasticity Theory and Applications,*” Krieger Publishing Company: Malabar, Florida, 1993.
 25. Timoshenko, S., and Goodier, J., “*Theory of Elasticity,*” McGraw-Hill, New York, N.Y, 1970, pp. 433-441.
 26. Wait, Jeannette R., Park, Gyuhae., and Charles, R. Farrar., “*Integrated Structural Health Assessment Using Piezoelectric Active Sensors,*” Shock and Vibration, 12, 2005, pp. 389-405.
 27. Worlton, D.C., “*Ultrasonic Testing with Lamb Waves,*” Non-destructive Testing, 15, 1957, pp. 218-222.

Vita

Captain SeJin Han graduated from Dae-In private High School in InChon, Korea. He entered undergraduate studies at the Korea Military Academy(KMA) where he graduated with a Bachelor of Science Degree in Weapon Engineering and received a regular commission in March 2001.

He successfully performed various assignments all around Korea for five years. In August 2005, he entered the Graduate School of Aeronautical Engineering, Air Force Institute of Technology.

Upon graduation, he will be assigned to the company commander.

REPORT DOCUMENTATION PAGE			<i>Form Approved OMB No. 074-0188</i>	
<p>The public reporting burden for this collection of information is estimated to average 1 hour per response, including the time for reviewing instructions, searching existing data sources, gathering and maintaining the data needed, and completing and reviewing the collection of information. Send comments regarding this burden estimate or any other aspect of the collection of information, including suggestions for reducing this burden to Department of Defense, Washington Headquarters Services, Directorate for Information Operations and Reports (0704-0188), 1215 Jefferson Davis Highway, Suite 1204, Arlington, VA 22202-4302. Respondents should be aware that notwithstanding any other provision of law, no person shall be subject to a penalty for failing to comply with a collection of information if it does not display a currently valid OMB control number.</p> <p>PLEASE DO NOT RETURN YOUR FORM TO THE ABOVE ADDRESS.</p>				
1. REPORT DATE (DD-MM-YYYY) 13 September 2007		2. REPORT TYPE Master's Thesis		3. DATES COVERED (From - To) Mar 2007 - Sept 2007
4. TITLE AND SUBTITLE Finite Element Analysis of Lamb Waves Acting within a Thin Aluminum Plate			5a. CONTRACT NUMBER	
			5b. GRANT NUMBER	
			5c. PROGRAM ELEMENT NUMBER	
6. AUTHOR(S) Han, SeJin, Captain, ROKA			5d. PROJECT NUMBER	
			5e. TASK NUMBER	
			5f. WORK UNIT NUMBER	
7. PERFORMING ORGANIZATION NAMES(S) AND ADDRESS(S) Air Force Institute of Technology Graduate School of Engineering and Management(AFIT/ENY) 2950 Hobson Way WPAFB OH 45433-7765			8. PERFORMING ORGANIZATION REPORT NUMBER AFIT/GAE/ENY/07-S02	
9. SPONSORING/MONITORING AGENCY NAME(S) AND ADDRESS(ES) AFRL/VASA Attn: Mr. Mark Derriso 2130 8 th Street WPAFB OH 45433-7542			10. SPONSOR/MONITOR'S ACRONYM(S)	
			11. SPONSOR/MONITOR'S REPORT NUMBER(S)	
12. DISTRIBUTION/AVAILABILITY STATEMENT APPROVED FOR PUBLIC RELEASE; DISTRIBUTION UNLIMITED.				
13. SUPPLEMENTARY NOTES				
14. ABSTRACT Structural health monitoring(SHM) is an emerging technology that can be used to identify, locate and quantify structural damages before failure. Among SHM techniques, Lamb waves have become widely used since they can cover large areas from one single location. Due to the development of various structural simulation programs, there is increasing interest in whether SHM data obtained from the simulation can be verified by experimentation. The objective of this thesis is to determine Lamb wave responses using SHM models in ABAQUS CAE(a Finite Element Analysis(FEA) program). These results are then compared to experimental results and theoretical predictions under isothermal and thermal gradient conditions in order to assess the sensitivity of piezo-generated Lamb wave propagation. Simulations of isothermal tests are conducted over a temperature range of 0-190°F with 100kHz and 300kHz excitation signal frequencies. The changes in temperature-dependent material properties are correlated to measurable differences in the response signal's waveform and propagation speed. An analysis of the simulated signal response data demonstrated that elevated temperatures delay wave propagation, although the delays are minimal at the temperatures tested in this study.				
15. SUBJECT TERMS Structural Health Monitoring, Finite Element Analysis, Nondestructive Testing, Piezoelectric Transducer, Rayleigh-Lamb Frequency Equation, Lamb Wave, Time of Arrival, Thermal Stress				
16. SECURITY CLASSIFICATION OF:			17. LIMITATION OF ABSTRACT UU	18. NUMBER OF PAGES 162
a. REPORT U	b. ABSTRACT U	c. THIS PAGE U		
			19a. NAME OF RESPONSIBLE PERSON Dr. Anthony N. Palazotto	
			19b. TELEPHONE NUMBER (Include area code) (937) 255-3636, ext 4599; e-mail: Anthony.Palazotto@afit.af.mil	

**Standard Form 298
(Rev. 8-98)**
Prescribed by ANSI Std. Z39-18
*Form Approved
OMB No. 074-0188*